MEANDER ANTENNAS

by

Jalil-Agha Rashed Mohassel

A dissertation submitted in partial fulfillment
of the requirements for the degree of
Doctor of Philosophy
(Electrical Engineering)
in The University of Michigan
1982

MEANDER ANTENNAS

by

Jalil-Agha Rashed Mohassel

A dissertation submitted in partial fulfillment
of the requirements for the degree of
Doctor of Philosophy
(Electrical Engineering)
in The University of Michigan
1982

Doctoral Committee:

Professor Chen-To Tai, Chairman
Professor Paul G. Federbush
Professor Chiao-Min Chu
Associate Professor Valdis V. Liepa
Associate Professor Dean F. Peterson

ABSTRACT

MEANDER ANTENNAS

by

Jalil-Agha Rashed Mohassel

Chairman: Chen-To Tai

Meander antennas are a new class of wire structures made from meander sections intended to reduce the resonant length of the antenna. Each half section is formed when the wire is folded three times over its course and a complete section is made when two half sections are connected back-to-back. The resonant frequency and other antenna characteristics depend primarily on the number of sections per wavelength N and the separation of the folded arms w. Usually w is kept small in comparison to the length of the antenna and therefore the undesirable radiation due to the horizontal portions are negligible. In this case the reduction in the resonant length depends on N and is typically 25 to 50 percent. The efficiency is affected only by the ohmic losses in the wire and the bandwidth of the antenna is generally less than a conventional monopole but comparable to that of other size reduction techniques such as base loaded antennas. When N increases the resonant resistance increases and so does the resonant frequency (less size reduction) however the bandwidth of the antenna improves. For a constant N, when w is increased the size reduction is enhanced but the bandwidth decreases.

The experimental results on resonant resistance, resonant frequency and the percentage of size reduction are in close agreement with the numerical analysis. The current distribution on the antenna is obtained and compared for several different meander geometries. The current distribution has a marked peak near the feeding point while the phase is relatively constant along the entire antenna. The effect of wire radius on the antenna characteristics and the effect of w on the pattern of the antenna are also investigated.

A log-periodic meander dipole array and a folded meander monopole are studied experimentally with satisfactory results as an illustration of the applications. Many variations of meander structures are also shown to have size reduction potentialities.

ACKNOWLEDGEMENTS

The author wishes to express his grateful appreciations to all of his committee members for their invaluable comments particularly to Professor C. T. Tai, his chairman, who initiated the problem and his continued guidance and encouragement made this study possible.

The author is also indebted to all Radiation Laboratory staff; especially Professors T.B.A. Senior and C. M. Chu for their support and encouragement. He is particularly grateful to Professor V. V. Liepa for his very helpful suggestions during the course of this work.

Special thanks go to Mrs. Wanita Rasey for her outstanding job in typing the manuscript.

Finally the author wishes to thank his wife, Azar, for her support and understanding.

TABLE OF CONTENTS

LIST OF TABLES

LIST OF FIGURES

LIST OF APPENDICES

LIST OF SYMBOLS

a	Radius of a wire.
A	A constant.
$\bar{A}$	Magnetic vector potential.
A_z	z-Component of the magnetic vector potential.
$[A]$	A matrix.
B	A constant.
c	The velocity of light.
C	A constant.
$Cin(x) = \int_0^x$	
$\cdot(1-\cos v)/v\ dv$	Modified cosine integral.
d	A distance.
E	Electric field.
$\bar{E}^i, E^i$	Incident (or impressed) electric field.
$\bar{E}^s$	Scattered electric field.
E_θ	θ-component of the electric field.
E_ϕ	ϕ-component of the electric field.
f	Frequency.
f	A function.
f_{mo}	The resonant frequency of a meander antenna.
f_o	Resonant frequency.
g	A function.
$G = \int_0^{2\pi} 1/2\pi$	Free space Green's function.
$\cdot e^{-jkr}/r\ d\phi$	

$G_o = e^{-jk\|\bar{R}-\bar{R}'\|}/\|\bar{R}-\bar{R}'\|$	Free space Green's function.
$\bar{\bar{G}}_{eo}$	Free space electric dyadic Green's function.
$[G]$	A matrix.
$\bar{H}^s$	Scattered magnetic field.
i	An integer index.
I	Electric current.
I_a	Symmetrical current component.
I_b	Antisymmetrical current component.
I_{in}	Input current.
I_j	Current on the jth segment.
I_m	Maximum current.
$\bar{\bar{I}}$	Unity dyad.
$j = \sqrt{-1}$	Imaginary unit.
j	An integer index.
$\bar{J}$	Electric current density.
$\bar{J}_s$	Surface electric current density.
k	Free space propagation constant.
$\bar{K}$	Magnetic current density.
ℓ	Physical length of a meander antenna.
L	Wire length of a monopole or meander monopole.
L	Length of a curve.
$\mathcal{L}$	An operator.
m	Magnetic charge density.
m	An integer index or a number.
n	An integer index or an integer number.
n	A number.

$\hat{n}$	A normal unit vector.
N	Number of meander sections per wavelength or an integer number.
$N = \iiint_V J(R')^{-jk\hat{R}\cdot\bar{R}'} dv'$	Radiation vector.
N_z	z-component of the radiation vector.
N_θ	θ-component of the radiation vector.
P_{av}	Average radiated power.
R	Radius of a ground plane.
R	A spherical coordinate.
R_o	A resistance level.
R_{rad}	Radiation resistance.
R_{res}	Resonant resistance.
$\bar{R}$	Observation point.
$\bar{R}'$	Source point.
$\hat{R}$	Unit vector in the direction of the observation point, $\bar{R}$.
s	Length parameter on a curve or a wire.
$Si(x)= \int_0^x (\sin v/v)dv$	Sine integral.
$\hat{s}$	A tangent unit vector (observation point).
$\hat{s}'$	A tangent unit vector (source point).
t	Time variable or width of a strip.
u	A variable.
$v = \beta c$	Phase velocity.
v	A variable.
V	A volume.

V_a	Symmetrical voltage component.
V_b	Antisymmetrical voltage component.
V_o	An applied voltage.
V_{in}	Input voltage.
w	Width of each meander section or separation of the two parallel wires.
w	A weighting function.
x	A distance or a variable.
x	A Cartesian coordinate.
$\hat{x}$	Unit vector in the x-direction.
y	A Cartesian coordinate.
$\hat{y}$	Unit vector in the y-direction.
z	A Cartesian coordinate.
$\hat{z}$	Unit vector in the z-direction.
Z_a	A characteristic impedance.
$Z_a = V_a/I_a$	Symmetrical impedance.
$Z_b = V_b/I_b$	Antisymmetrical impedance.
Z_o	Characteristic impedance.
Z_d	Resonant impedance of a dipole or the input impedance of a strip.
Z_{fd}	Resonant resistance of a folded dipole.
Z_{in}	Input impedance.
Z_ℓ	Load impedance.
$Z_o = 50$ ohm	Normalizing impedance
Z_s	Input impedance of a slot.

$[Z]$	A matrix.
α	An angle or a constant.
$\beta = \ell/L$	Reduction factor.
$\delta(s-s_j)$	Dirac's delta function.
Δ	The length of a segment.
Δf	A change in frequency.
ε_o	Permittivity.
η	Efficiency.
$\eta = 120\pi$	Free space characteristic impedance.
θ	A spherical coordinate.
λ	Wavelength.
μ_o	Permeability.
ξ	A variable.
π	A function.
ρ	Electric charge density.
σ	Spacing factor in a LPDA.
$\sigma' = \sigma/\sqrt{\tau}$	Mean spacing factor.
τ	Scaling factor in a LPDA.
ϕ	A spherical coordinate or an angle.
ϕ_m	An angle.
ω	Frequency of the time harmonic field.
$\Omega = 2\ \ell n(2L/a)$	Thickness parameter of a monopole.

CHAPTER I. INTRODUCTION

Great achievements have been reached in antenna engineering since the pioneer work of Hertz and Marconi in demonstrating the existence of radio waves (and their utilization). Nowadays utilization of antennas with different electrical and non-electrical requirements in diverse applications is being complicated due to their physical size. In broadcast engineering the existing antennas normally have a height of several hundred feet. They are hazardous for airplanes and costly to install. Shipboard antennas are limited by the available space on board. The same limitation exists for vehicle and satellite antennas. The enormous size of log-periodic antennas, mostly designed for wideband applications, is also a limiting factor at lower frequencies. Any scheme which can reduce the size of these and other existing antennas can be utilized in the now exceedingly increased applications. In this work, the objective is to present and study a new class of antennas called meander antennas as possible elements for size reduction.

1.1 Background

While the theoretical investigation of linear antennas was of paramount interest in the early decades of antenna engineering development, many pioneers were involved in practical aspects of this area. The inevitable huge size of broadcasting antennas due

to their operating frequency range and the outbreak of their application launched the search for innovative techniques to reduce the size of these and many low frequency antennas.

The idea of reducing the physical size especially for resonant antennas has been considered by many engineers. In broadcasting, according to Brown [1], for heights of the order of a half wavelength a straight vertical wire is difficult to be replaced by any reduced size version. His review included broadcasting antennas of a reduced size such as top loaded, sectionalized and uniformly loaded (slow wave) antennas. These studies show that this reduction is at most 25 percent for the anti-fade top loaded antennas. This enables one to reduce the tower height from 0.53λ to 0.4λ. In this range the vertical pattern does not change significantly. The sectionalized antenna has reportedly similar characteristic variation but with a total height limited to 0.4λ because of the drop in the antenna efficiency for further reductions. Top loaded antennas have frequently been considered as possible alternatives to vertical radiators [2,3], but a considerable size reduction by those structures deteriorates the vertical polar pattern. In fact, the unwanted radiation from the horizontal top part should be limited if similar characteristics to a vertical radiator is desired.

Not only broadcasting antennas were under intensive study but meanwhile resonant antennas were subject to similar investigations as well. A resonant monopole is inherently a simple and efficient

antenna and perhaps is the most utilized in handling radiation problems. In general, any attempt to reduce the size of a monopole while preserving the same resonant frequency, leads to deficiencies such as bandwidth deterioration, pattern distortion and reduction in efficiency. A variety of methods such as top loading and base loading have been frequently invoked in the past to secure resonance at a lower frequency. These antennas have been analyzed by many investigators [4 through 15]. In general, size reduction methods in resonant antennas can be categorized into three wide classes:

(a) The geometrical deformation of the antenna.

(b) The insertion of various types of lumped loads.

(c) The use of different coating materials.

Although a drastic change in the physical size of an antenna may be contemplated, it turns out that in most cases a considerable size reduction, can be achieved only at the expense of cross polarization, bandwidth deterioration, losses and other undesirable side effects.

Examples of the first group are the open folded monopoles [5], helical antennas and top loaded (capacitive loaded) antennas such as "T" antennas or inverted "L" wires. In many of these antennas the reduction is generally associated with a lateral expansion of the structure. In these structures, the undesirable radiation from the nonvertical portions, if significant, leads to a distorted pattern.

In the second class, the antennas suffer from losses and therefore have low efficiency. In this group, most of the previous works basically include various types of inductive loading intended to cancel the reactive component of the input impedance at a frequency lower than the resonant frequency of the unloaded antenna. Lumped elements contribute mainly in efficiency reduction due to losses either in tuning coils or in the resistor itself, in the case of resistive loading. The loaded folded dipole presented by Williams [2] is one example with an efficiency barely reaching 40 percent at its best according to Josephson [5]. Even with well designed coils of high quality factor Q, inductive loaded monopoles such as base loaded or center loaded antennas have the same problem [9,16]. The reason lies in the necessity to insert a large coil to annihilate the capacitive reactance of the antenna input impedance. The ohmic resistance of this coil is usually an appreciable part of the total resonant resistance decreasing the antenna efficiency drastically. This reduction in efficiency is not necessarily limited to the reduced size antennas, but it is also present in other cases of resistive loading as well [17,18,19].

Despite the lossy nature of coating materials, their use as the third group have been sought to bring about resonance in a monopole with a height less than one quarter of the free space wavelength. A partial sleeve from a ferrite material has been used by Grimes [20] as a surrounding medium in which a dipole was assumed to be embedded and reductions of 10 percent and 40 percent

in length are reported. For this ferrite sleeve dipole, a failure in the production of the necessary material for a desired reduction factor seriously affects the applicability of the antenna. Recently this idea has received attention to reduce even further the length of resonant monopoles [21,22,23]. Studies of James and Henderson [24] show that although considerable size reduction can be achieved by these methods, there are also obvious drawbacks such as the unavailability of the suitable material and the excessive weight of the antenna especially at lower frequencies. According to these studies a test antenna with a sample of such a material showed it to be heavily lossy with a narrow bandwidth of 1.2 percent with respect to the resonant frequency. As a better alternative they introduced two new types of helical antennas (and hence belonging to the first group) namely counter wound and double wound helical antennas. The former is narrow in bandwidth and has lower input impedance with a better reduction factor while the latter is much more lossy in exchange for a rather improved input impedance and bandwidth. However, in both cases improved performance over the well known helical antenna is reported. The conventional helical antenna and its application as a resonant element is not a new idea. Examples are whip antennas with a helical portion [25] or tapered helical versions [26] and helices with small diameters [27,28,29,30]. Moore and Beam used helices in Yagi-Uda arrays [31]. Other applications include using helices or conical helices rather than dipoles in log-periodic arrays in order to achieve a lateral

size reduction [32,33,34]. Log-periodic antennas with other size reduced dipoles have also been considered in the past [35,36,37]. Finally, attention should be drawn to the fact that size reduction techniques are not restricted to the previously mentioned antennas or their applications only, but they have been applied to other radiators such as flat log-spiral antennas [38] and conical log-spiral antennas [39,40].

In the present work we try to rejuvenate the idea of a reduced resonant length. The new antenna is simple in geometry and unlike most of other size reduction schemes losses are not appreciable. This structure can be used to reduce the size of the existing wire antennas such as Yagi-Uda antennas and log-periodic dipole arrays.

1.2 Outline of the Work

An experimental as well as theoretical investigation is conducted to study meander antennas during the course of this work. A familiarization with the parameters and geometry of the antenna is contained in this introductory chapter. Chapter II gives an approximate analysis along with various experimental results to understand the general characteristics of meander antennas. In Chapter III the numerical results for the current distribution using the method of moments will be presented. This analysis will be carried out for different geometries to verify the experimental results. Samples of meander antenna applications and some new structures are brought forth in Chapter IV and Chapter V, respectively. A summary and conclusion is provided in Chapter VI.

1.3 Preliminary Considerations

Meander antennas are made from a continuously folded wire (Fig. 1.1) intended to reduce the resonant length. Since the wire is folded three times over its course on each half section, the length ℓ, of the meander monopole is only one-third of the length of a monopole made from the same wire. We define a quantity $\beta(<1)$ as the reduction factor for a meander antenna. If a conventional monopole of length L and a meander monopole of length ℓ have the same resonant frequency, $\beta = \ell/L$ is designated as the reduction factor. Equivalently, the resonant frequency of a meander monopole, f_{mo}, is β times the resonant frequency, f_o, of a monopole with the same length. Preliminary experiments show that the reduction factor is of the order of 0.6 rather than one-third, the ideal value for a threefold meander antenna. This factor depends primarily on the number of sections per wavelength (N) and the width of the rectangular loops (w).

Figure 1.2 shows some meander monopoles with different values of N. In this figure, N = 2 corresponds to half of a meander section while N = 4 constitutes a complete section. The former, while being categorized as a meander antenna can be considered separately. It satisfies the general characteristics of meander antennas however, and has similar properties. Comparing this special case with a loaded folded monopole, which is normally terminated in a lumped element, we can treat the N = 2 case as a folded monopole terminated by a monopole. Here the difference is in the existence of the

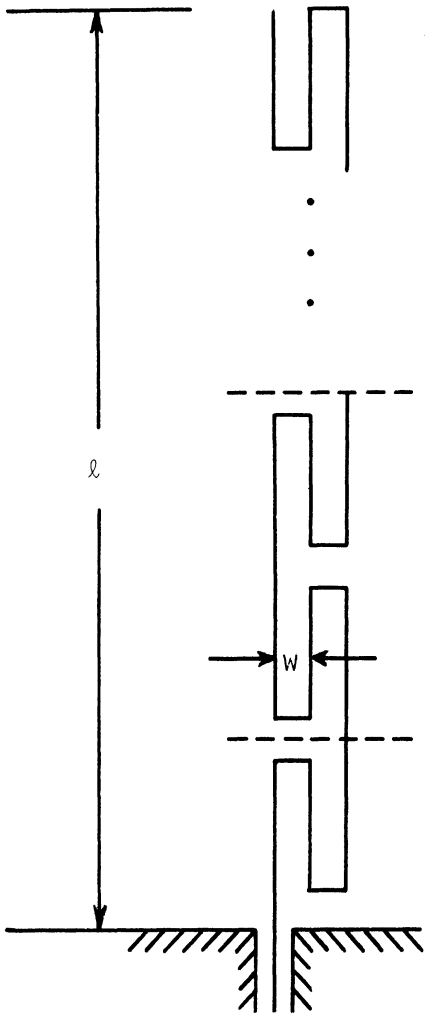

Fig. 1.1: A meander monopole with many sections.

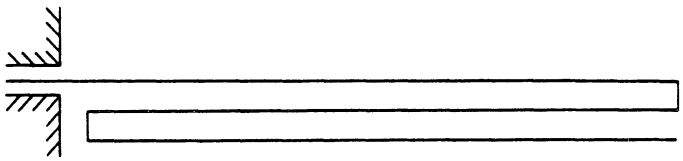

(a) N = 2

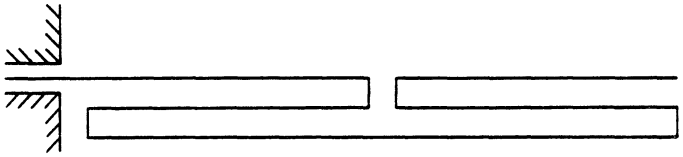

(b) N = 4

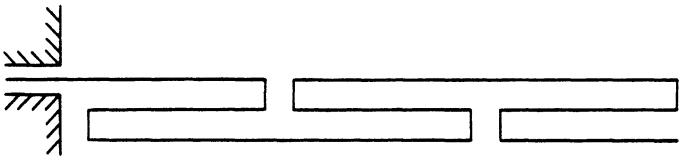

(c) N = 6

Fig. 1.2: Some special cases of meander antennas, N = 2,4,6.

coupling between the elements within the structure and the load itself.

This coupling signifies the main difference between this antenna and the conventional loaded folded monopole. Because of this coupling, the resulting current distribution differs from that of a monopole. Hence a rather simple analysis, similar to the one used for folded monopoles cannot be employed for this special case, nor can one be developed for meander antennas in general. A more precise formualtion is therefore needed.

CHAPTER II. CHARACTERISTICS OF MEANDER ANTENNAS

The two basic parameters associated with the geometry of meander antennas, namely, N and w, were introduced in the preceding chapter. The effect of these parameters on the reduction factor, β, and other antenna characteristics will be explored in this chapter.

2.1 Impedance Measurements

To understand the characteristics of meander antennas, some impedance measurements were first performed. The experimental setup using sweep frequency technique is shown in Fig. 2.1. A circular aluminum ground plane with a radius of R = 60 cm and a thickness of 6 mm is used with the antenna erected from the center of the plane.

Each of the antennas were soldered to a threaded base which permitted screw attachment to the center conductor of a UG-58/U flange connector through the center of the ground plane. The base had a diameter of 3 mm and due to mechanical limitations, slightly higher than the surface of the ground plane. The height of the meander antennas measured from the surface of the ground plane corresponds to ℓ = 4.5 cm with a small separation w less than 0.3 cm ($w/\ell \simeq 0.06$).

A monopole with a length of L = 13 cm was also used as a reference. The diameter of the enamelled copper wire used in the experiments is 0.8 mm (= 2a). Hence the thickness parameter for the monopole is

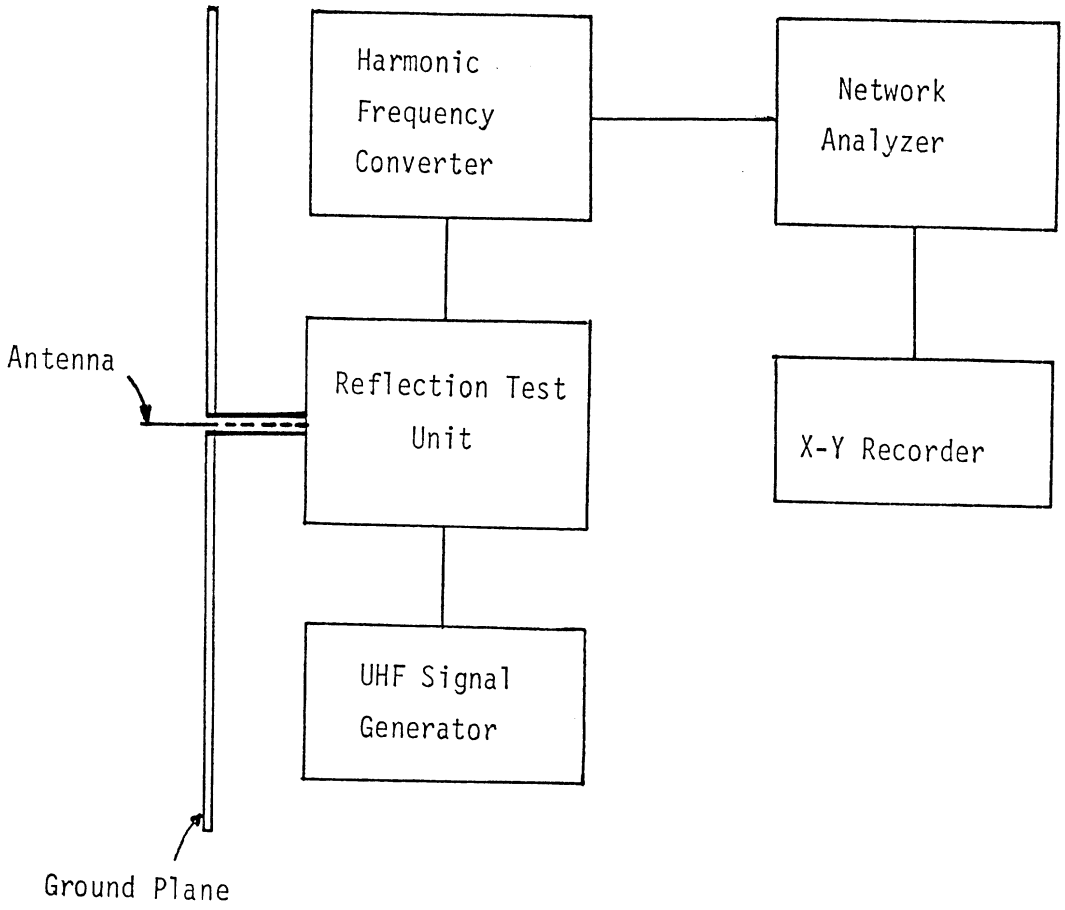

Fig. 2.1: Antenna Impedance Measurement Setup.

$$\Omega = 2\,\ell n(2L/a) \simeq 12.9 \quad .$$

The impedance curves for some meander monopoles with N as a variable are shown in Fig. 2.2. The impedances are normalized to Z_o = 50 ohms. These plots show that the resonant frequency increases as the number of sections per wavelength, N, increases. By the definition of reduction factor, β, given in Chapter I, the increase in resonant frequency, f_o, means a higher reduction factor, i.e., less size reduction. The experimental data for resonant frequency and the calculated β corresponding to the curves of Fig. 2.2 are given in Table 2.1. In addition to β, the experimental resonant resistance, R_{res}, is provided in the same table along with the calculated radiation resistance, R_{rad}, based on an approximate analysis. This calculation will be presented later in this chapter.

The bandwidth, as a percentage of the resonant frequency is also tabulated. To determine the bandwidth, the impedance curves are normalized to their resonant resistance values and hence they pass the center of the chart. Then a VSWR = 2 circle is used to find the upper and lower frequencies.

2.2 Effect of N on Antenna Characteristics

From Table 2.1 the effect of different values of N on the antenna characteristics can now be explained. For a small constant w, an increasing N means an increase in the reduction

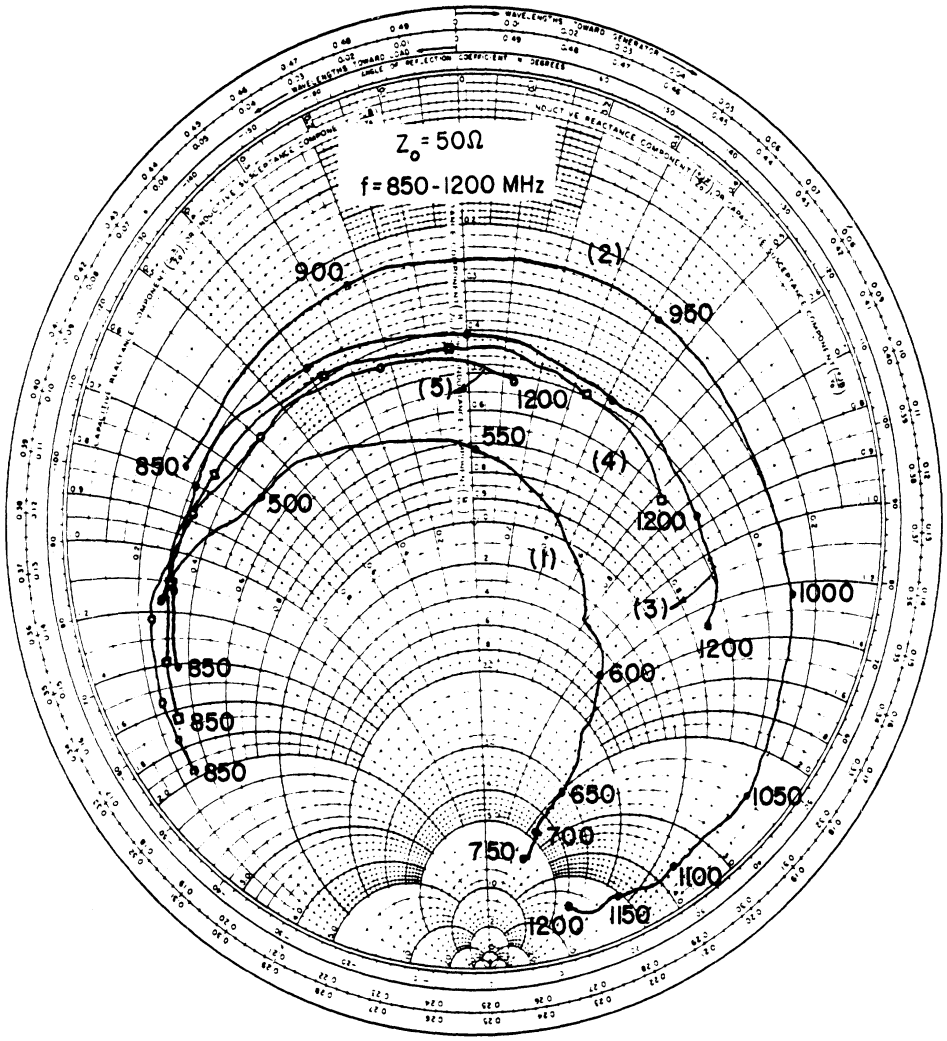

Fig. 2.2: Impedance of meander antennas: N = 2,6,10,14 and the reference monopole.

Table 2.1

Data table for meander antennas with small w and ℓ = 4.5 cm. The reference monopole has a length of L ≃ 13 cm

Antenna type	N	f_o(MHz)	$(\Delta f/f_o)$ %	β	Experimental $R_{res}(\Omega)$	Calculated $R_{rad}(\Omega)$ (Approx.)
Monopole (1)	-	545	9.5	1.0	36.0	36.5
Meander: (2)	2	922	3.0	0.59	13.0	13.5
(3)	6	1050	7.0	0.67	20.5	17.0
(4)	10	1110	7.5	0.71	22.0	19.0
(5)	14	1180	8.0*	0.75	23.5	21.5

*Rough approximation using extended impedance curve.

factor typically ranging from 0.6 for N = 2 to 0.7 for N = 10. However, one can decrease β even further by increasing w as far as cross polarization constraint is not exceeded. This aspect of size reduction will be investigated later.

In general the lower the N, the better the reduction property. But meanwhile the resonant resistance and the bandwidth decrease as β decreases. For the lowest values of N, i.e., N = 2, the reduction factor is about 0.6 which corresponds to 40 percent reduction in size. In this case, R_{res} is about 13 ohms, much lower than that of a conventional monopole. The bandwidth is also diminished as a result of the shortening. These are common characteristics of size reduction methods. Some techniques are needed for improvement. Other meanders, however, do not suffer frequency sensitivity to this extent.

While the resonant resistance can readily be compensated by a matching system, little can be done about the bandwidth of the antenna with a fixed reduction factor. One remedy is to compromise on size reduction by choosing higher values of N such as N = 4, 6, 10 or even more to obtain a much improved bandwidth in exchange for a slight sacrifice in the amount of size reduction. This is evident from Table 2.1 which indicates the apparent increase in the bandwidth and resonant resistance as N increases.

For bandwidth consideration of meander antennas, we compare them to an equivalent base loaded monopole, i.e., the one with

the same resonant frequency and the same length. Consider the impedance curves of two meander antennas (N = 4,8, w ≃ 0.2 cm) and a reference monopole all having the same length, $\ell \simeq 4.5$ cm (Fig. 2.3). Since the monopole is also of the same length, the impedance of the equivalent base loaded monopole can be found by adding, in series, the proper value of reactance to secure resonance at the resonant frequency of it's meander counterpart. This reactance is inductive and approximately equal in magnitude to the capacitive component of the input impedance at the desired frequency [16]. The bandwidth is defined as previously explained.

From Fig. 2.3, the following two cases can be distinguished:

a) N = 4, $f_o \simeq 1050$ MHz, $R_{res} = 20\ \Omega$, $\Delta f/f\ \% \simeq 6$

The required normalized reactance to warrant resonance for the monopole at f = 1050 MHz is, $x_L \simeq 2.83$ which results in a bandwidth of 5 percent compared to the 6 percent bandwidth of N = 4 meander antenna.

b) N = 8, $f_o \simeq 1100$ MHz, $R_{res} = 22\ \Omega$, $\Delta f/f\ \% \simeq 7$

A normalized reactance of $x_L \simeq 2.48$ is needed for resonance to take place resulting in a bandwidth of 7 percent, the same as the meander antenna. In both cases, if a pure reactance is assumed, the resulting resonant resistance in the base loaded antenna is seen to be lower than the corresponding meander value.

Although meander antennas are comparable to the widely used base loaded antennas from a bandwidth point of view but the most

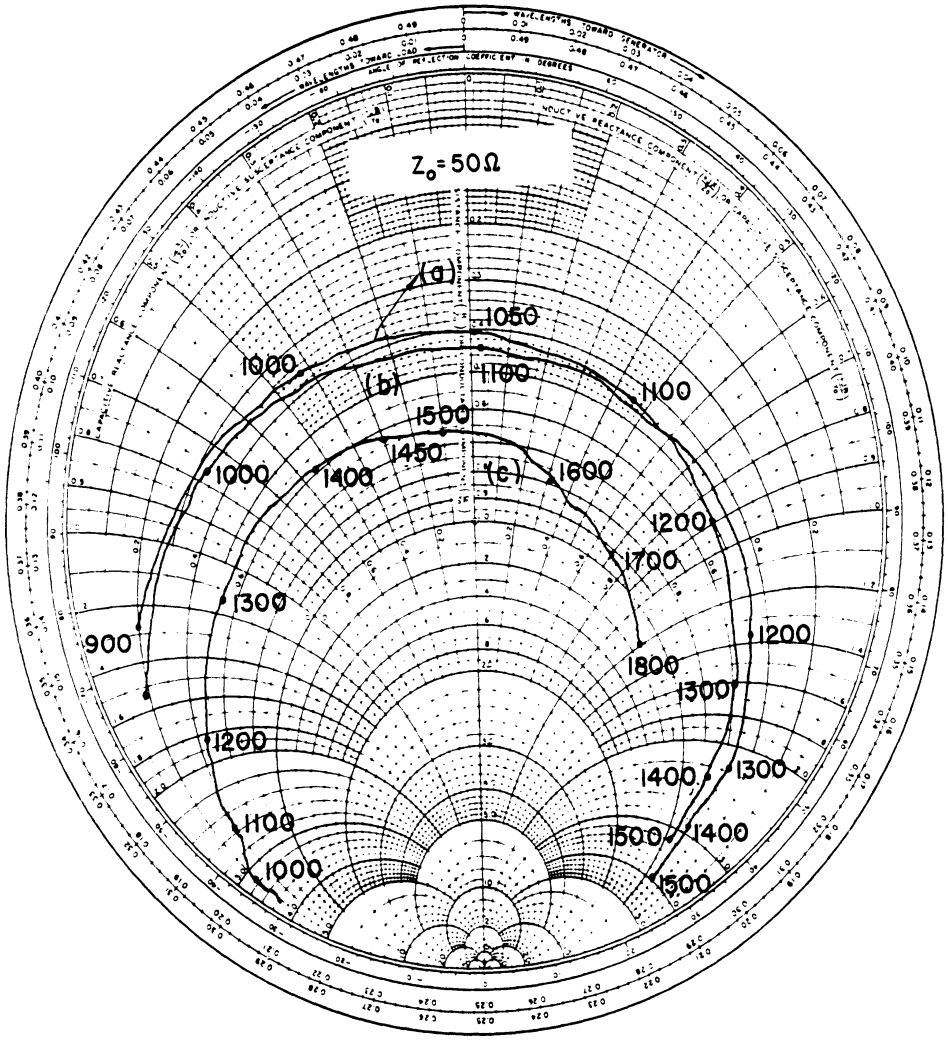

Fig. 2.3: Impedance of meander antennas, N = 4 and 8 and a reference monopole of the same length.

promising feature has not yet been considered. Unlike most of the size reduction techniques such as lumped loadings and use of dielectric materials, the efficiency is comparable to an unfolded monopole in the meander geometry. Many of these methods including base loaded antennas have poor efficiency due to their losses. The efficiency consideration should be underlined by the fact that when the resonant resistance is decreased, any additional loss may aggravate the efficiency. This should always be considered as one of the prime concerns in shortened antennas. In view of the efficiency advantage meander elements provide a suitable solution to the efficiency problem of inductive loaded antennas. A small fine tuning coil can be added at the base of a meander antenna. Since the shortening has already been achieved, the coil is a rather small inductance and this does not affect the efficiency to any degree.

Since meander dipoles have a resonant length less than half of a wavelength, and the separation w is negligibly small, they have essentially a figure eight pattern. The only difference with a conventional dipole is a slight decrease in the directivity due to the shortening of the antenna. With an increase in N, the resonant length increases and the directivity improves accordingly.

As long as w is relatively small in comparison to the length of the antenna, ℓ, which is normally the case, a change in the circular H plane pattern is not eminent. This property is in

contrast with some of the size reduction techniques in which the problem is aggravated by the fact that size reduction is attributed to the lateral expansion of the structure which is also responsible for the pattern distortion.

2.3 Approximate Analysis

Consider a meander antenna with length ℓ, negligible w, and a large number of sections per wavelength, N. Based on a slow wave structure model, if the phase velocity is taken into account, we have, at resonance,

$$\frac{\omega}{v} \cdot \ell = \frac{\pi}{2} \quad \text{or} \quad \frac{k\ell}{\beta} = \frac{\pi}{2} \ ,$$

where we write, $v = \beta c$, the phase velocity and $k = \omega/c$, the free space propagation constant.

Using the approximate effective current distribution,

$$I(z) \simeq I_m \sin \frac{k}{\beta} (\ell - |z|) \ , \quad 0 \leq z \leq \ell \qquad (2.1)$$

and the experimental data for β, we can determine the fields and the impedance of the antenna at resonance. The Poynting vector method can be used to calculate the value of the radiation resistance, R_{rad}. This value is very close to the resonant resistance R_{res}, viz, the input resistance when the monopole is slightly shorter than a quarter of a wavelength.

For a volume current distribution $\bar{J}(\bar{R}')$, the radiation vector, $\bar{N}(\theta,\phi)$ is expressed by

$$\bar{N}(\theta,\phi) = \iiint_V \bar{J}(\bar{R}') \cdot e^{-jk\hat{R}\cdot\bar{R}'} \, dv' \quad . \tag{2.2}$$

where the position vectors $\bar{R}$ and $\bar{R}'$ correspond to the observation point and source point, respectively, and $\hat{R}$ is the unit vector in the direction $\bar{R}$.

In a z-directed dipole of length 2ℓ and an effective current distribution given by equation (2.1), the radiation vector is expressed as:

$$\bar{N}(\theta,\phi) = N_z \cdot \hat{z}$$

with

$$N_z = \int_{-\ell}^{+\ell} I_m \sin\frac{k}{\beta}(\ell - |z'|)e^{jkz'\cos\theta}dz' \tag{2.3}$$

or

$$N_z = \frac{2\beta}{k} I_m \left[\frac{\cos(k\ell\cos\theta) - \cos(\frac{k\ell}{\beta})}{1 - \beta^2\cos^2\theta}\right] \tag{2.4}$$

At resonance,

$$\frac{k\ell}{\beta} = \frac{\pi}{2} \quad .$$

Hence

$$N_z = \frac{2\beta}{k} I_m \left[\frac{\cos\left(\frac{\pi}{2}\beta\cos\theta\right)}{1-\beta^2\cos^2\theta} \right] . \qquad (2.5)$$

Since $N_\theta = -N_z \sin\theta$ and

$$E_\theta = -\frac{j\eta k}{4\pi} \frac{e^{-jkR}}{R} N_\theta ,$$

we find,

$$E_\theta = \frac{I_m \eta}{j 2\pi R} e^{-jkR} \left[\beta \frac{\cos\left(\frac{\pi}{2}\beta\cos\theta\right)}{1-\beta^2\cos^2\theta} \right] \sin\theta \qquad (2.6)$$

For the meander monopole, the average radiated power is:

$$P_{av} = \frac{1}{2\eta} \int_0^{2\pi} \int_0^{\pi/2} |E_\theta|^2 R^2 \, d\theta \, d\phi .$$

Using

$$P_{av} = \frac{1}{2} R_{rad} \cdot I_m^2 ,$$

one finds

$$R_{rad} = 60\, I , \qquad (2.7)$$

where

$$I = \int_0^{\pi/2} \frac{\beta^2}{2} \frac{1+\cos(\pi\beta\cos\theta)}{(1-\beta^2\cos^2\theta)^2} \sin^3\theta \, d\theta \qquad (2.8)$$

To find I, we set $u = \cos\theta$ and use

$$\frac{1 - u^2}{(1 - \beta^2 u^2)^2} \equiv \frac{1}{4\beta}\left[\frac{2\beta + (1 + \beta^2)u}{(1 + \beta u)^2} + \frac{2\beta - (1 + \beta^2)u}{(1 - \beta u)^2}\right]$$

to obtain

$$I = \frac{\beta}{8}\int_{-1}^{+1}\left[\frac{2\beta + (1 + \beta^2)u}{(1 + \beta u)^2}\right][1 + \cos(\pi\beta u)]\ du$$

in which symmetry has been used.

Setting $v = \pi(1 + \beta u)$ and integrating by parts, the integral I can be expressed in a closed form:

$$I = -\frac{1 + \cos(\pi\beta)}{4} + \frac{1}{8\beta}\left\{(1 + \beta^2)[\mathrm{cin}(x_2) - \mathrm{cin}(x_1)] - \pi(1 - \beta^2)[\mathrm{Si}(x_2) - \mathrm{Si}(x_1)]\right\} \tag{2.8}$$

where

$$\mathrm{cin}(x) = \int_0^x \frac{1 - \cos v}{v}\ dv \quad ; \quad \mathrm{Si}(v) = \int_0^x \frac{\sin v}{v}\ dv$$

$$x_2 = \pi(1 + \beta) \quad ; \quad x_1 = \pi(1 - \beta) \ .$$

Once the integral is known, one can calculate R_{rad} from Eq. (2.7).

Table 2.1 shows the acceptable agreement between the experimental results and the approximate analysis, however this analysis is not an independent confirmation of the experimental data.

2.4 Effect of w on Antenna Characteristics

Some measurements were made on the antenna with the separation of the wires, w, as a variable. The impedance curves corresponding to N = 2 are shown in Fig. 2.4 and the data is tabulated in Table 2.2. These experiments show that when w increases, β decreases, but the resonant resistance drops drastically. These effects are also accompanied by a narrower bandwidth. Furthermore, for an increasing w, cross polarization appears in the plane xz while in the yz plane, linear polarization is still preserved. This asymmetry also produces nonradiating balanced current components in the antenna-image system. In fact, for large w and small ℓ the N = 2 antenna approaches the limiting case of an open quarterwave transmission line with a very small radiation resistance at resonance [41], which justifies the apparent shift of the impedance curves to the outer circle of the chart. This behavior supports our earlier statement that to maintain a linear polarization, one must choose w to be small compared to ℓ. Under this condition one can obtain a reduction factor typically in the neighborhood of 0.6.

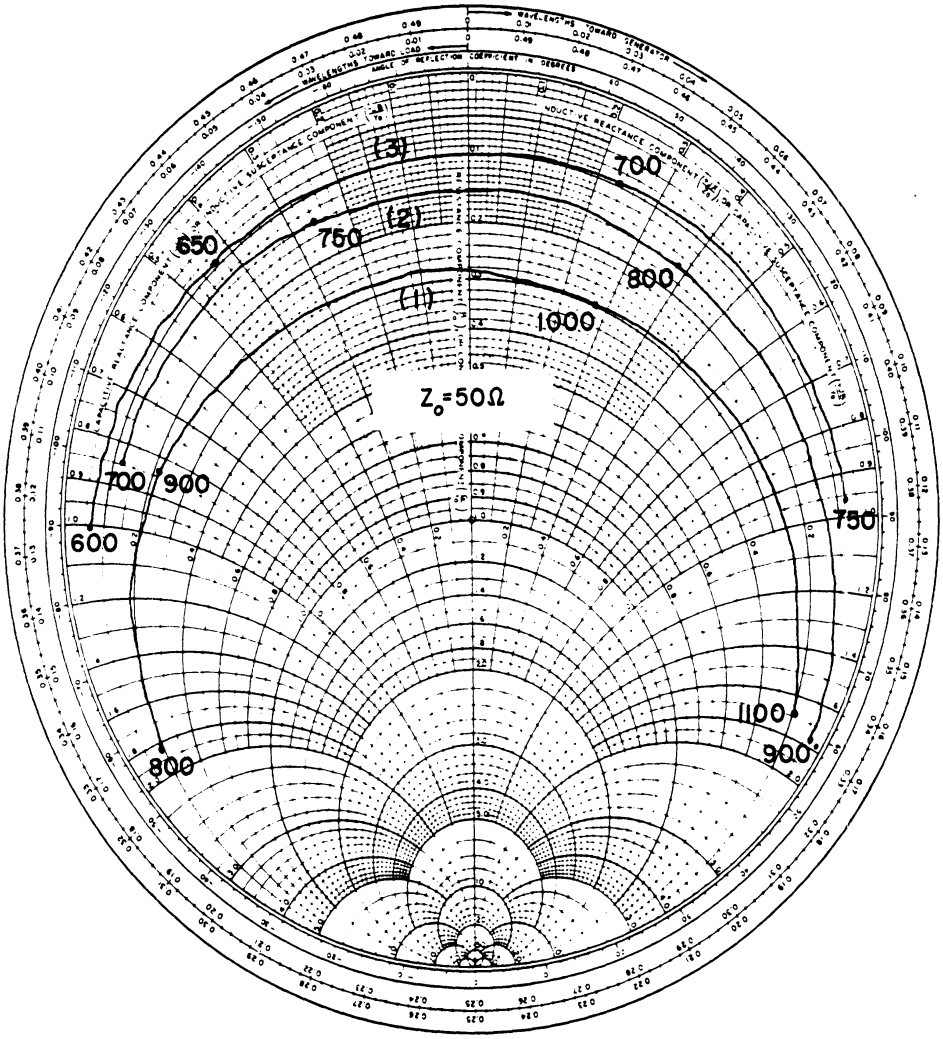

Fig. 2.4: Impedance curves for N = 2 meander antennas with w as a variable.

Table 2.2

Data table for N = 2 meander monopole, with total length, L ≃ 13.5 cm and w as a variable

Antenna	w(cm) (Approx.)	f_o(MHz)	$(\Delta f/f_o)$ %	$R_{res}(\Omega)$	β
(1)	~ 0.25	976	3.6	14.0	0.64
(2)	0.5	770	2.1	7.5	0.5
(3)	1.0	684	1.5	5.0	0.45

The effects of an increasing w are valid for other meander antennas as well. A substantial size reduction by further increasing w is accompanied by similar side effects. Experiments with N = 4 show that when w increases to a value comparable to ℓ, the drop in both resonant resistance and bandwidth become eminent. A typical reduction factor of 0.65 can be achieved without significant side effects in this antenna, however, when w is kept small compared to ℓ.

2.5 Sleeve Version of Meander Antennas

As we showed earlier, meander antennas have lower input impedance in comparison to a conventional monopole. A method is used here to increase the input resistance at resonance. The most stringent case, i.e., N = 2 was selected for matching purposes. This antenna, while having a reduction factor of $\beta \simeq 0.6$ for small w, has a low input resistance of about 13 ohms at resonance (Table 2.1). This, creates the mismatch problem if it is fed by a 50-ohm line. To overcome this difficulty, one can use a sleeve version of the antenna. By removing the outer conductor and the dielectric of a coaxial cable at a distance x from the end, one can shift the feeding point (Fig. 2.5).

If one assumes a sinusoidal current distribution along the wire, and the antenna is fed at a point other than at the base, the input resistance at resonance will be increased. This technique was suggested by Josephson [5]. By changing the value of x in Fig. 2.5, we can adjust for any value of the input

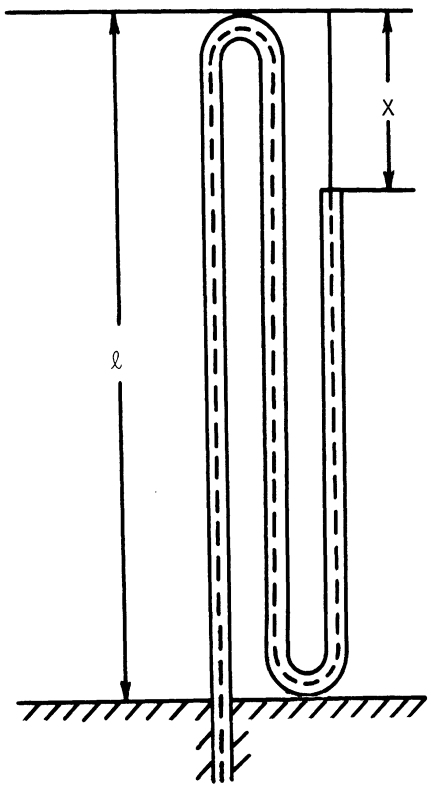

Fig. 2.5: Sleeve version of the N = 2 meander antenna.

resistance, hence, a matching with the feeding system with certain designated output resistance.

Josephson applied this technique to change the input impedance of an open folded monopole. However, in his analysis, he has overlooked the proper decomposition of the antisymmetrical components of current and voltage as has been observed by Tai [42]. This mechanism of Josephson's technique can be explained by treating the sleeve as part of the transmission line and as part of the antenna proper. This combination acts as an impedance converter by shifting the feeding point away from the base. Impedance measurements were carried out for some different values of x as given in Table 2.3.

The antenna has a height of $\ell \simeq 8.5$ cm with a total wire length of $L \simeq 26.5$ cm and a separation $w \simeq 0.9$ cm between the arms. The 50-ohm coaxial cable has outer and inner diameters of $2b = 0.22$ cm and $2a = 0.51$ mm, respectively. The square aluminum ground plane is 91.5 cm x 91.5 cm, with the antenna erected from the center of the plane. The other end of the coaxial cable is connected to the feeding system through the center of the ground plane. From the impedance curves of Fig. 2.6, a value of $x \simeq 74$ mm is seen to be the proper value to establish the matching. The reduction factor of this antenna ($w/\ell \simeq 0.1$) is found to be $\beta \simeq 0.5$.

The effect of the dielectric presence on the exposed part of the antenna may now be considered. If the dielectric of the

Table 2.3

Data table for a sleeve version of the N = 2 meander antenna with x as a variable

Antenna No.	x (cm)	x/L	f_o (MHz)	R_{res} (Ω)
(1)	4.2	0.16	433	164.0
(2)	6.5	0.25	440	68.5
(3)	7.4	0.28	437	50.0

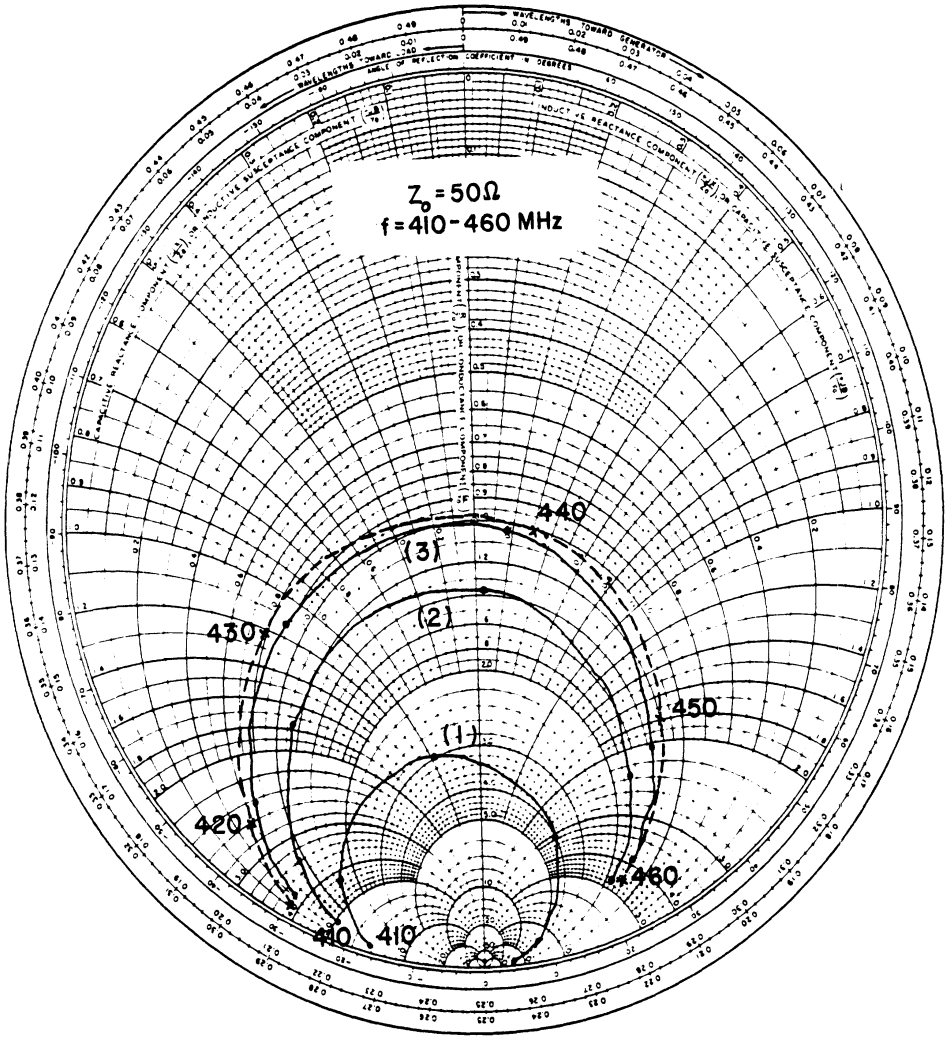

Fig. 2.6: Impedance of the sleeve antenna with x as a variable.

coaxial line is not removed from the exposed part of the antenna for any purpose such as protection, the required x for a matching condition will be slightly different. While x = 74 mm is adequate for matching with the dielectric removed, the value x = 65 mm has the desired matching effect in the presence of the dielectric. The impedance, in this case is shown by the dashed curve in Fig. 2.6, with a resonant frequency of f_o = 437 MHz. The thickness of the dielectric for this partially coated antenna is not sufficient for a marked change in the reduction factor. In general, a significant decrease in the reduction factor by means of coating materials can be obtained using a thick layer. The result is, however, increases losses and less efficiency.

CHAPTER III. MEANDER ANTENNA ANALYSIS

Since most of the antenna characteristics are fundamentally related to the current distribution, a solution to the current of an antenna is of primary interest. The lack of rigorous analytical approaches for practical problems on one hand, and the shortcomings of approximate solutions for accurate interpretations on the other hand, result in the inevitable use of numerical techniques in electromagnetic problems. This chapter is devoted primarily to the numerical solutions of meander antennas with different geometries.

3.1 Integral Equation Formulation

The scattered field due to induced sources distributed throughout a volume V, can be expressed as [43]:

$$\bar{E}^s(\bar{R}) = -\frac{1}{4\pi}\iiint_V \left(j\omega\mu_o \bar{J}G_o + \bar{K} \times \nabla' G_o - \frac{\rho}{\varepsilon_o}\nabla' G_o\right) dV' \quad (3.1)$$

$$\bar{H}^s(\bar{R}) = \frac{1}{4\pi}\iiint_V \left(-j\omega\varepsilon_o \bar{K}G_o + \bar{J} \times \nabla' G_o + \frac{m}{\mu_o}\nabla' G_o\right) dV' \quad (3.2)$$

where, $\bar{E}^s(\bar{R})$ and $\bar{H}^s(\bar{R})$ are the field quantities at the observation point. $\bar{J}$ and $\bar{K}$ are the electric and magnetic current densities and ρ and m are the electric and magnetic charge densities.

G_o is the Green's function pertaining to free space wave propagation given by

$$G_o(\bar{R},\bar{R}') = \frac{e^{-jk|\bar{R}-\bar{R}'|}}{|\bar{R} - \bar{R}'|} \tag{3.3}$$

in which a positive $j\omega t$ convention is used.

For the special case when only the electric current density, $\bar{J}(\bar{R}')$ is present, the integral representation for the electric, $\bar{E}(\bar{R})$ is

$$\bar{E}(\bar{R}) = \frac{-j\omega\mu_o}{4\pi} \iiint_V \bar{J}(\bar{R}') \cdot \bar{\bar{G}}_{eo}(\bar{R},\bar{R}')\, dV' \quad , \tag{3.4}$$

where $\bar{\bar{G}}_{eo}(\bar{R},\bar{R}')$ is the free space electric dyadic Green's function and given by the relationship [44]

$$\bar{\bar{G}}_{eo}(\bar{R},\bar{R}') = (\bar{\bar{I}} + \frac{1}{k^2}\nabla\nabla)G_o(\bar{R},\bar{R}') \tag{3.5}$$

where $\bar{\bar{I}} = \hat{x}\hat{x} + \hat{y}\hat{y} + \hat{z}\hat{z}$ is the identity dyad.

Equation (3.4), when applied over the surface S of a perfect conductor, yields the integral equation for the current induced on the surface by an incident (or impressed) field, $\bar{E}^i$. On the surface of a perfect conductor, the boundary condition is

$$\hat{n} \times [\bar{E}^i(\bar{R}) + \bar{E}^s(\bar{R})] = 0 \quad , \qquad (3.6)$$

where $\hat{n}$ is the normal unit vector of the surface at $\bar{R}$ and $\bar{E}^s(\bar{R})$ is the scattered field due to the induced current. If the electric field $\bar{E}(\bar{R})$ in Eq. (3.4) is assumed to be the scattered field due to a surface current distribution, enforcement of the boundary condition (3.6), yields the integral equation for the surface current density $\bar{J}_s(\bar{R})$, with the incident (or impressed) field $\bar{E}^i$ as a given function. For wire antennas, thin wire approximation can be employed to reduce the integral equation for the surface current density $\bar{J}_s(\bar{R})$ to a line integral with the current distribution as an unknown.

Consider a thin wire of circular cross section with radius a, much less than the wavelength λ. Thin wire approximation neglects the transverse currents and assumes that the circumferential variations in the axial current are not present [6,45]. Therefore, the surface current density $\bar{J}_s(\bar{R})$ on the wire and the equivalent axial current I(s) are related:

$$I(s)\hat{s} = 2\pi a \, \bar{J}_s(\bar{R}) \quad ,$$

where $\hat{s}$ is the unit vector tangent to the wire axis at s.

In view of the negligible azimuthally directed currents, the boundary condition is only applied parallel to the wire axis:

$$\hat{s} \cdot (\bar{E}^i(\bar{R}) + \bar{E}^s(R)) = 0 \quad .$$

This condition, when applied to the equation for surface current density, $\bar{J}_s(\bar{R})$, gives the following integral equation for the current distribution:

$$\hat{s} \cdot \bar{E}^i(\bar{R}) = \frac{j\omega\mu_o}{4\pi} \int_{\ell} I(s') \left[\hat{s}\cdot\hat{s}' - \frac{1}{k^2} \frac{\partial^2}{\partial s \partial s'}\right] G_o(\bar{R},\bar{R}') \, ds' \, , \tag{3.7}$$

where the integral is taken along the length of the wire and $\hat{s}'$ is the tangent unit vector at the source point. The integral is no longer singular since the filamentary current I(s) is assumed to be on the axis of the wire and $\bar{R} \neq \bar{R}'$.

In the case of a z-directed center driven dipole with length 2ℓ,

$$\hat{s} = \hat{s}' = \hat{z}$$

and the integral equation for the current distribution simplifies to:

$$E^i(z) = \frac{j\omega\mu_o}{4\pi} \int_{-\ell}^{+\ell} I(z') \left[1 + \frac{1}{k^2} \frac{\partial^2}{\partial z^2} \right] G(z,z')\, dz' \quad , \qquad (3.8)$$

where

$$G(z,z') = \int_0^{2\pi} \frac{1}{2\pi} \frac{e^{-jkr}}{r} d\phi \qquad (3.9)$$

with

$$r = |\bar{R} - \bar{R}'| = \left[(z - z')^2 + (2a \sin \frac{\phi}{2})^2 \right]^{1/2} .$$

In this expression for r, both the source and field points are on the surface of the wire. Since $a << \lambda$, the thin wire approximation for r is defined as:

$$r = [(z - z')^2 + a^2]^{1/2} . \qquad (3.10)$$

This approximation assumes a current flow on the axis of the wire, whereas the observation point is on the surface of the wire. The singularity of the free space Green's function is not included in this approximate thin wire kernel representation. This final step, which was used in the Hallen's integral equation for many years, was subject to criticism until an interpretation was given by Tai [46] based on a variational method. The

approximate kernel is now widely used to represent the effect of wire radius for sufficiently thin wire antennas. Substituting for r from (3.10) in (3.9) yields the free space Green's function for this approximation. Equation (3.8) with the thin wire kernel is an integral equation of the first kind and is called Pocklington's integral equation [47] and is the one which is used in many computer software today.

One other widely used equation is the Hallen's integral equation [45] sometimes referred to as the vector potential type. For a dipole the magnetic vector potential $\bar{A}$ is z-directed and can be found from the wave equation:

$$\left(\frac{\partial^2}{\partial z^2} + k^2 \right) A_z = 0 \quad . \tag{3.11}$$

On the other hand, for a volume current distribution,

$$\bar{A} = \frac{\mu_o}{4\pi} \iiint_V \bar{J}(\bar{R}')G_o(\bar{R},\bar{R}') \, dV$$

and therefore for a perfectly conducting thin dipole of length 2ℓ, we have,

$$A_z(z) = \frac{\mu_o}{4\pi} \int_{-\ell}^{+\ell} I(z')G(z,z') \, dz' \quad . \tag{3.12}$$

Combining the solution to (3.11) and the equation (3.12), the Hallen's form of the integral equation for current is obtained, i.e.,

$$\int_{-\ell}^{+\ell} I(z')G_0(z,z')\,dz' = B\cos kz - \frac{jV_0}{2\eta}\sin k|z| \quad , \qquad (3.13)$$

where V_0 is the terminal voltage of the antenna, η is the free space characteristic impedance and B is a constant.

The difference between this integral equation and the Pocklington's integral equation can be seen from the comparison of the two equations. In Pocklington's form, the boundary condition is already embedded in the formula while in Hallen's equation the constant B is evaluated from the boundary condition for the current distribution, i.e., $I(\pm L) = 0$. Furthermore, in Pocklington's method the source is represented by $\bar{E}^i$ and can be modeled in different ways but in Hallen's method a delta-gap (slice) generator has already been imposed in Eq. (3.13). The source model is important, particularly for the imaginary part of the input impedance. Hallen's equation, like the Pocklington's equation, was also the subject of study by many investigators [48]. Mei has generalized Hallen's equation to wire antennas of arbitrary geometry [49]. This equation is expressed as:

$$\int_L J(s')\pi(s,s')ds' = B\cos ks - \frac{j}{\eta}\int_0^S E_\xi^i(\xi)\sin k(s-\xi)\,d\xi \qquad (3.14)$$

where B is a constant and

$$\pi(s,s') = G(s,s')\hat{s}\cdot\hat{s}' - \int_0^S \left[\frac{\partial G(\xi,s')}{\partial \xi} \hat{\xi}\cdot\hat{s}' + \frac{\partial G(\xi,s')}{\partial s'} + G(\xi,s') \frac{\partial(\hat{\xi}\cdot\hat{s}')}{\partial \xi} \right] \cos k(s - \xi)\, d\xi \qquad (3.15)$$

with

$$G(s,s') = \frac{e^{-jk|\bar{R}-\bar{R}'|}}{|\bar{R} - \bar{R}'|} .$$

For a delta-gap generator, Eq. (3.14) simplifies to

$$\int_L J(s')\pi(s,s')\, ds' = B \cos ks - \frac{jV_o}{2\eta} \sin ks \quad , \qquad (3.16)$$

which is the general form of Eq. (3.13).

The method of Harrington is different from that of Hallen in that both scalar and vector potentials are used in the derivation of the matrix equation for finding the antenna current distribution [50,51].

All of the above integral equations can be solved by a now widely used numerical method called the method of moments [50], in which an integral equation is transformed into a pertinent set of algebraic equations. This method represents a numerical solution to the integral equations in field problems. The analytical solution of these problems are normally difficult to obtain if not impossible. The moment method is capable of solving a wide range of integral equations with high accuracy pending on the appropriate choices.

3.2 Method of Moments

3.2.1 General Procedure.

The current distribution along wire antennas usually involve certain types of integral equations which are not generally tractable analytically and therefore require numerical treatment. A thorough discussion on the method of moments is given by Harrington [50,51]. A brief review of the method is given here. If $\mathcal{L}$ is assumed to be a linear operator, then an inhomogeneous equation can be expressed in the operational form:

$$\mathcal{L}f = g \quad , \tag{3.17}$$

where f is the unknown response to be determined and g is a given function related to the excitation.

Let $f=\sum_n \alpha_n f_n$, where the basis functions (expansion functions), $f_1, f_2, \ldots$, are defined in the domain of the operator $\mathcal{L}$. We can write,

$$\sum_n \alpha_n \mathcal{L} f_n = g \quad . \tag{3.18}$$

Now a set of weighting functions (testing functions), w_m, $m = 1,2,\ldots$, are chosen in the range of $\mathcal{L}$. Defining a suitable inner product for the problem, we take the inner product of both sides of Eq. (3.18) with w_m and find:

$$\sum_n \alpha_n \langle w_m, \mathcal{L} f_n \rangle = \langle w_m, g \rangle \quad , \qquad m = 1,2,\ldots . \tag{3.19}$$

If the series $f = \sum_n \alpha_n f_n$ is truncated at $n = N$ and the sequence of testing functions, $w_1, w_2, \ldots$, is chosen to have M terms, then for $N = M$, Eqs. (3.15) constitute N equations with N unknowns. In the matrix notation, we have

$$[Z]\,[A] = [G] \quad , \tag{3.20}$$

from which

$$A = \begin{bmatrix} \alpha_1 \\ \alpha_2 \\ \vdots \\ \alpha_N \end{bmatrix}$$

and therefore

$$f = \sum_N \alpha_n f_n$$

can be determined.

Since we often seek an approximate solution to the integral equation, this method does not necessarily require the choice of a complete set of basis functions nor does it imply the need for an infinite series. In fact, the exact solution to many equations related to problems of practical interest simply cannot be obtained. An exact solution may be obtained in some special cases depending on the operator $\mathcal{L}$ and the appropriate choice of basis and weighting functions.

3.2.2 Selection of f_n and w_n. The choice of a suitable basis function, f_n, is of fundamental importance in both accuracy and convergence of the solution. In general, the greater the resemblance of the expansion function to the actual solution, the better is the convergence and possibly, stability as well.

Two commonly used functions for w_n are the Dirac delta function (collocation method) and f_n itself (Galerkin's method). The collocation method is also called the pointmatching method. In general, two numerical integrations are necessary for each element of the [Z] matrix in Eq. (3.20); one due to the integral operator $\mathcal{L}$ and the other due to the inner product involved. However, the collocation method via the delta function definition reduces the number of these integral computations to one for each matrix element.

Galerkins' method is equivalent to the Rayleigh-Ritz method provided that appropriate bases are used in both approximations. It can, therefore be considered as a variational method [52].

Basically, the expansion functions can be chosen from both entire-domain or sub-domain bases. Entire-domain bases are applied over the entire operator domain, i.e., the entire structure. In contrast, the subdomain bases are zero on part of the operator domain. One example of an entire domain basis function is the Fourier series representation of the current. A table of some of the entire domain bases is given by Richmond where other bases with faster convergence such as Legendre or Chebyshev polynomials are introduced [47].

In general for a structure of complex geometry it may be impossible to perform $\mathcal{L}f_n$ over the entire operator domain and therefore subsectional basis are often used. Examples of subdomain bases are constant, linear, quadratic and sinusoidal functions, which have support on some subdomain and are zero otherwise. A criteria for the choice of polynomial basis functions is given by Anders [53]. The simplest of all the polynomial basis functions is the piecewise constant function (stairstep) when applied in conjunction with the collocation method. These functions, although simple, are efficient when carefully treated [54].

Yeh and Mei [55] have developed a sinusoidal current interpolation which assumes a current distribution of the form,

$$I_j(s) = A_j + B_j \sin k(s - s_j) + C_j \cos k(s - s_j) \qquad (3.21)$$

on the jth segment of a wire antenna. Because of the oscillatory nature of the solutions to many integral equations for wire

antennas, the above current distribution gives a fast convergence [55,56,57].

The number of unknowns in the matrix equation resulting from an integral equation depends on the number of segments and the form of the basis functions. For example, for a wire divided in N segments, a simple pulse function has N equations and N unknowns while the sinusoidal interpolation has 3N unknowns. However, in these types of basis functions, the number of unknowns can be reduced by local conditions on the segment junctions and the antenna free ends. These local conditions are often dictated by the nature of the operator and usually take the form of some certain continuities, the lack of which may result in poor convergence.

3.3 Numerical Solution to Meander Antennas

3.3.1 Current Distribution Along the Antenna Wire.

As was pointed out in Chapter II, the approximate analysis based on the effective current distribution

$$I = I_m \sin \frac{k}{\beta} (\ell - |z|) , 0 \leq z \leq \ell \qquad (3.22)$$

is neither adequate nor accurate for a complete determination of the antenna characteristics. This is true for two reasons:

1. Equation (3.22) is not an analytical solution but rather an empirical one, because the reduction factor is deduced from the experimental data.

2. The coupling between the adjacent wire elements comprising the antenna proper has a crucial role in the current distribution and is implicitly included in the reduction factor.

These basic limitations underline the necessity to elaborate on the problem by a numerical study. The program used in this study is the Numerical Electromagnetic Code (NEC) [58]. This program employs sinusoidal interpolation given by Eq. (3.21) in conjunction with the collocation method. The Dirac delta function $\delta(s - s_j)$ is used as the weighting function where s_j corresponds to the center of the jth segment.

Each basis function, $I_j(s)$ is assumed to have its maximum on segment j, and extended on the two adjacent segments approaching zero on their outer ends. Therefore, segment j, is covered by three currents; $I_j(s)$, $I_{j-1}(s)$ and $I_{j+1}(s)$ to form one effective current [58]. For n segments, we have 3n unknowns where 2n unknowns are eliminated by using the end condition and applying the continuity of current and charge at each junction of two segments. The source model used in the analysis is a current-slope-discontinuity type. The field of this model is more localized in the source region than that of a delta gap generator model [58,59].

Among the possible values of the two geometrical parameters associated with meander antennas, namely N and w, a small w with different values of N is of particular interest. The antennas under study (N = 2, 6 and 10) have the following specifications:

Total length, L = 13.5 cm

Wire radius, a = 0.4 mm.

These values were used for the experimental studies of Chapter II with the data given in Table 2.1. The antennas have a separation, w = 0.3 cm and a physical length, ℓ = 4.5 cm and are divided into 45 segments of equal length, each having a length, Δ = 0.3 cm. This segmentation is shown in Fig. 3.1. For equal segments, there is an upper limit, w, for the length of each segment. If the segments have a length Δ, less than w, it cannot be chosen arbitrarily small since at some point the thin wire approximation will be invalidated.

Two factors, namely Δ/λ and Δ/a have a profound effect on the accuracy of the solution in wire antennas. For a better resolution in the current distribution, Δ/λ should be kept small (corresponding to a higher number of segments on the antenna) while at the same time Δ/a should be large enough to guarantee the validity of the thin wire approximation in the kernal of the pertinent integral equation. In the frequency range of these meander antennas, the largest value of Δ/λ belongs to N = 10 (Table 2.1) and is approximately equal to 1.1×10^{-2} resulting in a high resolution for the current distribution. The value of Δ/a is 7.5 for all antennas which warrants the validity of thin wire approximation with errors of the order of one percent [58,60].

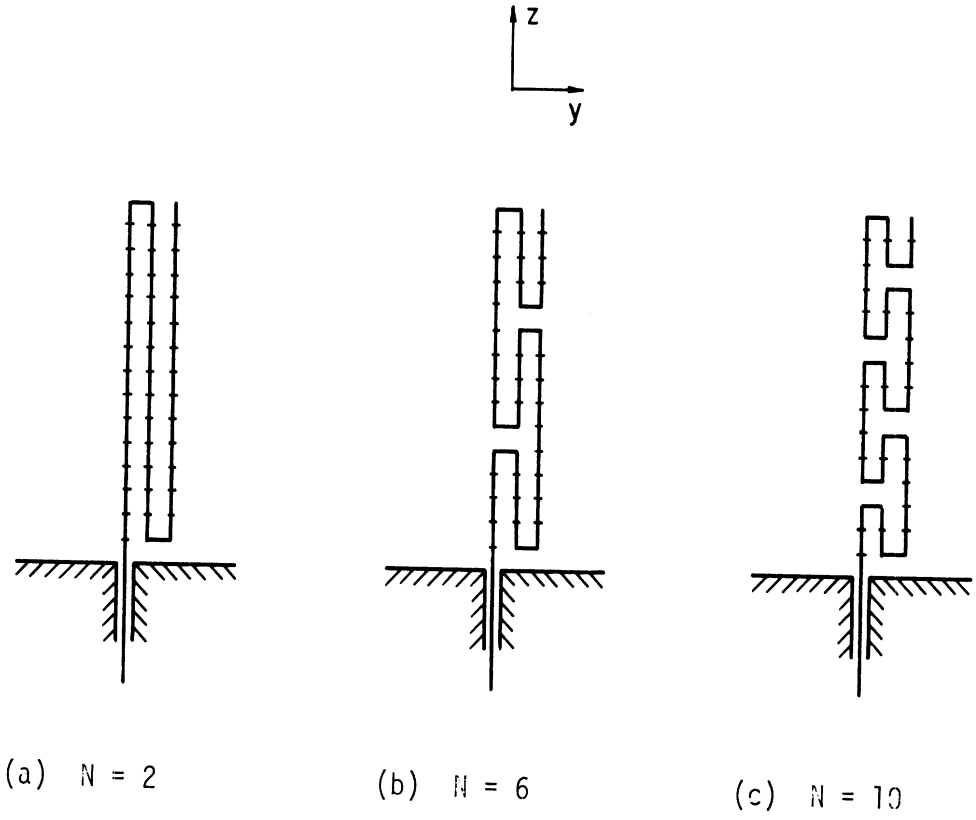

Fig. 3.1: Meander antenna segmentation.

The current distribution at resonance due to a one-volt source is shown in Fig. 3.2. The current on a resonant monopole (f_o = 540 MHz) with the same wire length is also shown on the same plot as a reference. The horizontal axis, s/L, is the normalized length from the antenna base. It is observed that for the same input voltage and for an increasing number of sections per wavelength, N, the input current is diminished, indicating an increase in the input resistance at resonance. The monopole, having the least input current of all, has the highest resonant resistance. The meander current has its maximum magnitude shifted from the excitation point, approaching zero at the free end of the antenna. This shift is greatest for N = 2 and decreases as N is increased. The phase is seen to be relatively constant especially for lower values of N corresponding to higher size reduction. These gradual changes signify the expected increased deviation from a conventional monopole behavior as the resonant length is decreased. Table 3.1 compares the theoretical results and the experimental data for the reduction factor β and the resonant resistance, R_{res}. In two cases, the results for w = 0.25 cm are also included for a better comparison. The theoretical reduction factor is calculated using a monopole with length, ℓ = 4.5 cm and wire radius, a = 0.4 mm. The resonant frequency of this monopole is 1559 MHz. Close agreement is observed between experimental and theoretical results.

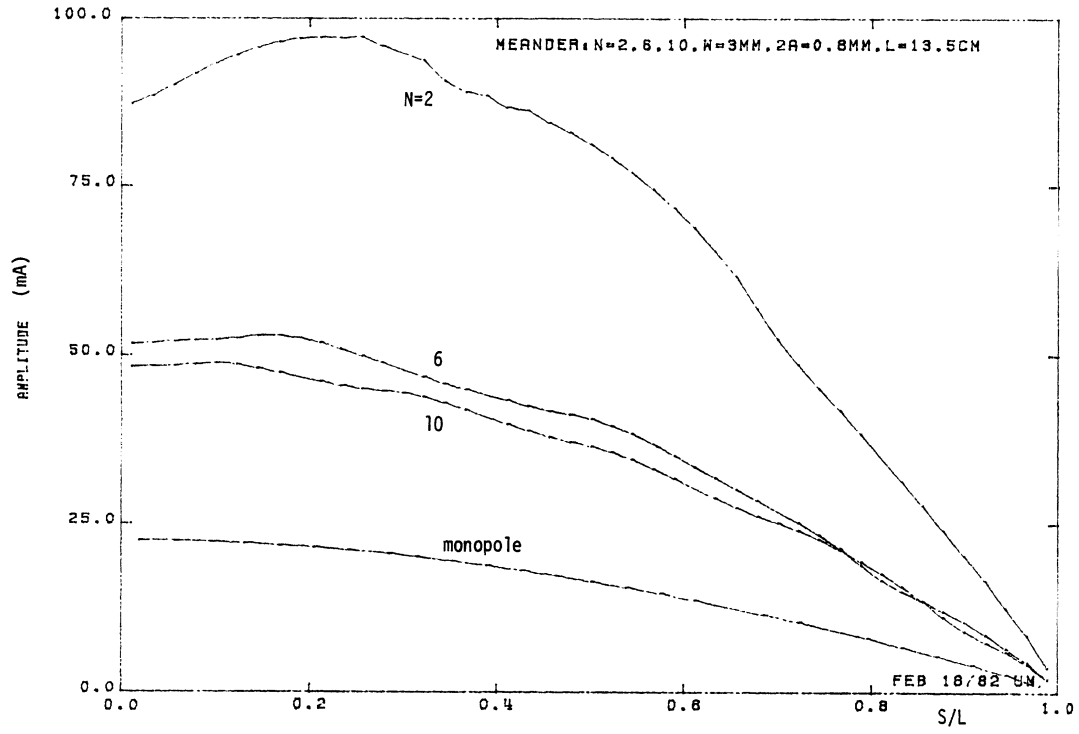

(a) Amplitude

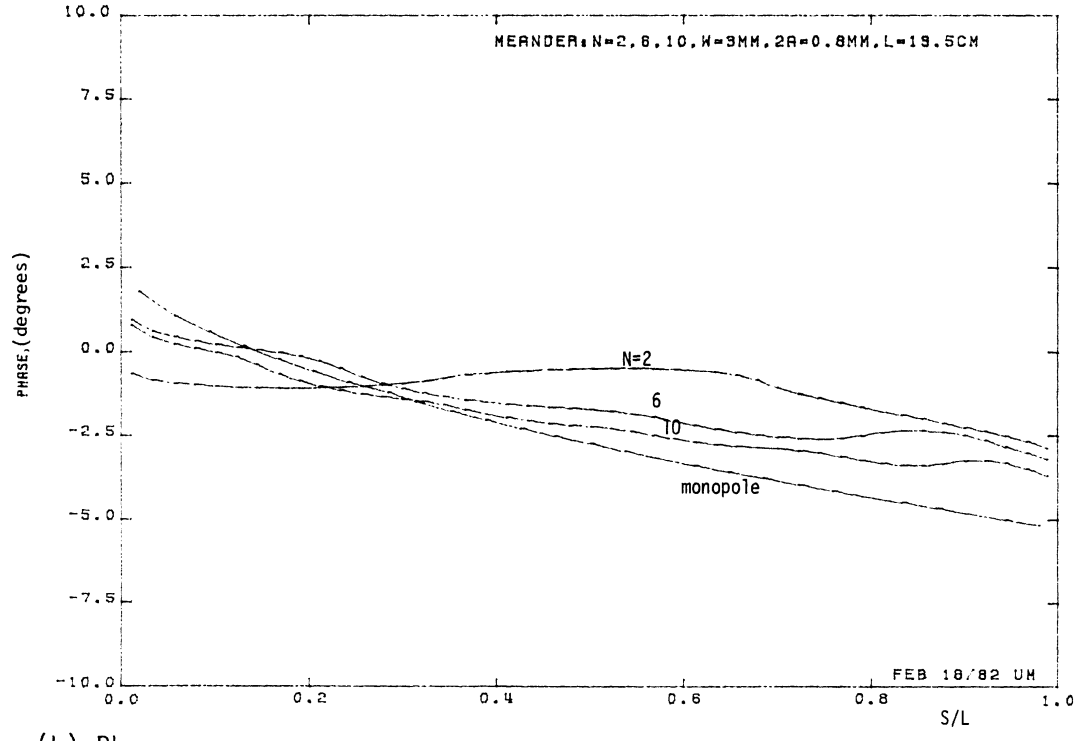

(b) Phase

Fig. 3.2: Current distribution on meander antennas.

Table 3.1

Comparison of theoretical results and experimental data for some meander antennas with ℓ = 4.5 cm and a = 0.4 mm

Meander Antenna	f_o (MHz)		β (Numerical)		β (Exp.)	$R_{res}(\Omega)$ (Numerical)		$R_{res}(\Omega)$ (Exp.)
	w=0.25cm	w=0.3cm	w=0.25cm	w=0.3cm	0.25cm<w<0.3cm	w=0.25cm	w=0.3cm	0.25<w< 0.3cm
N = 2	962	918	0.62	0.59	0.59	12.7	11.5	13
N = 6	1051	981	0.67	0.63	0.67	22.2	19.3	21
N = 10	---	1005	---	0.64	0.71	---	20.7	22

3.3.2 Effective Current in Meander Structures. Consider the three currents passing through a perpendicular plane at an arbitrary point on a meander antenna. For a negligible w these three currents can be considered as one effective current, the net current, in the interval $0 \leq z \leq \ell$. The net current can be readily obtained using the previous numerical results for the current distribution. It is the phasor sum of three components at each cross section. This effective current determines both the antenna impedance and its field. It is a more precise version of the approximate current distribution discussed in Chapter II, since the interaction effects are already embedded in the numerical solution. The smaller the w, the better the net current represents the effect of the actual current distribution along the meander wire. Figure 3.3 shows the effective current corresponding to the current distributions in Fig. 3.2. The horizontal axis is the normalized distance from the feeding point, z/ℓ. w is assumed to be 0.3 cm with N = 2, 6 and 10. The current of a resonant monopole with ℓ = 4.5 cm (and f_o = 1559 MHz) is also shown for comparison. It is observed that although the current along the meander wire has its maximum shifted from the antenna base (Fig. 3.2), the net current has its greatest magnitude at the feeding point itself. Furthermore, unlike the phase of the actual current along the meander wire, the phase, in the net current exhibits more similarity to that of a resonant monopole.

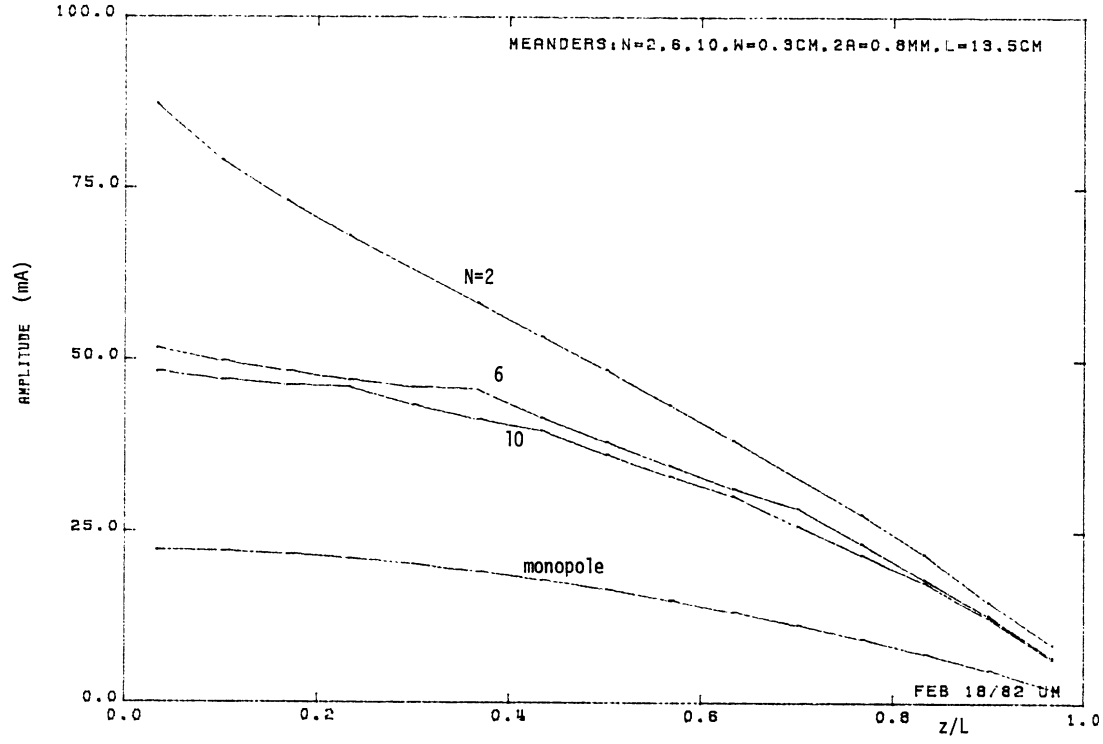

(a) Amplitude

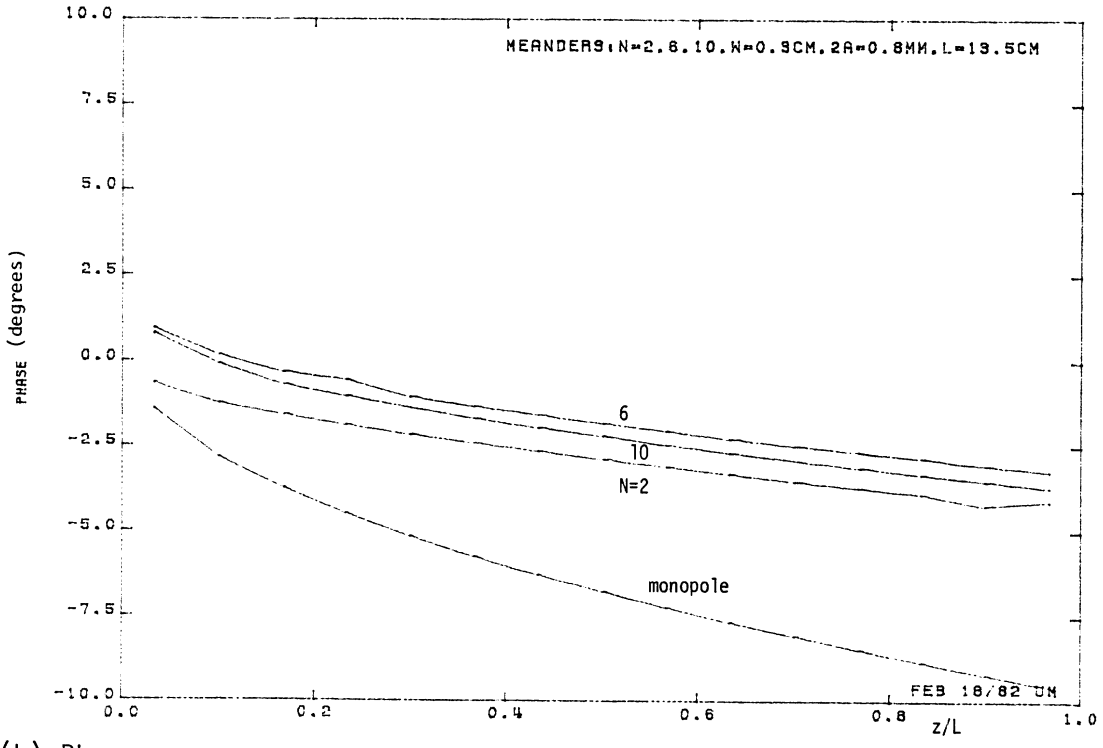

(b) Phase

Fig. 3.3: The effective current distribution for meander antennas (N = 2,6, and 10) at resonance.

In Fig. 3.4, the effective currents for w = 0.25 cm are compared to the effective currents with w = 0.3 cm. In each antenna (N = 2 or 6) the small difference in the separation w slightly changes the resonant resistance. The input current is therefore slightly different but the general shape of the effective current is preserved.

3.3.3 Transfer of the Excitation Point. In Section 2.5, we showed than meander antennas can be matched by means of a sleeve. The idea was based on feeding the antenna at some point with a distance x from the free end of the antenna (Fig. 2.5). Since the amplitude of the antenna current diminishes, as the free end is approached, the input impedance at resonance will increase accordingly. This method is indeed true, not only for open folded monopoles [5], but for meander antennas as well. Generally speaking, it can be used in any wire structure since the input impedance is regarded as a general circuit relation and can be determined by the equation

$$Z_{in} = \frac{V_{in}}{I_{in}} \quad . \tag{3.23}$$

When x/L is properly chosen, the antenna can be matched to any desirable impedance level. For meander antennas, when x is increased, the resonant resistance decreases until a matched condition is achieved. An impedance level of 50 ohms was chosen and it was found that meander antennas with N = 2, 6 and 10

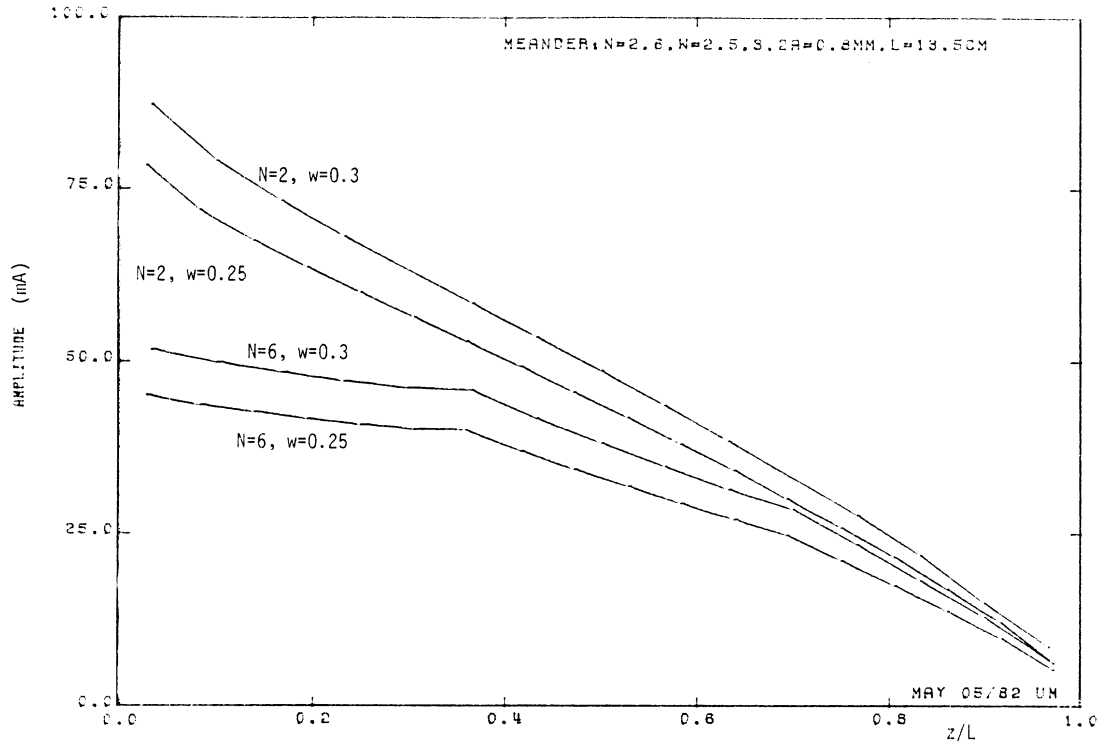

(a) Amplitude

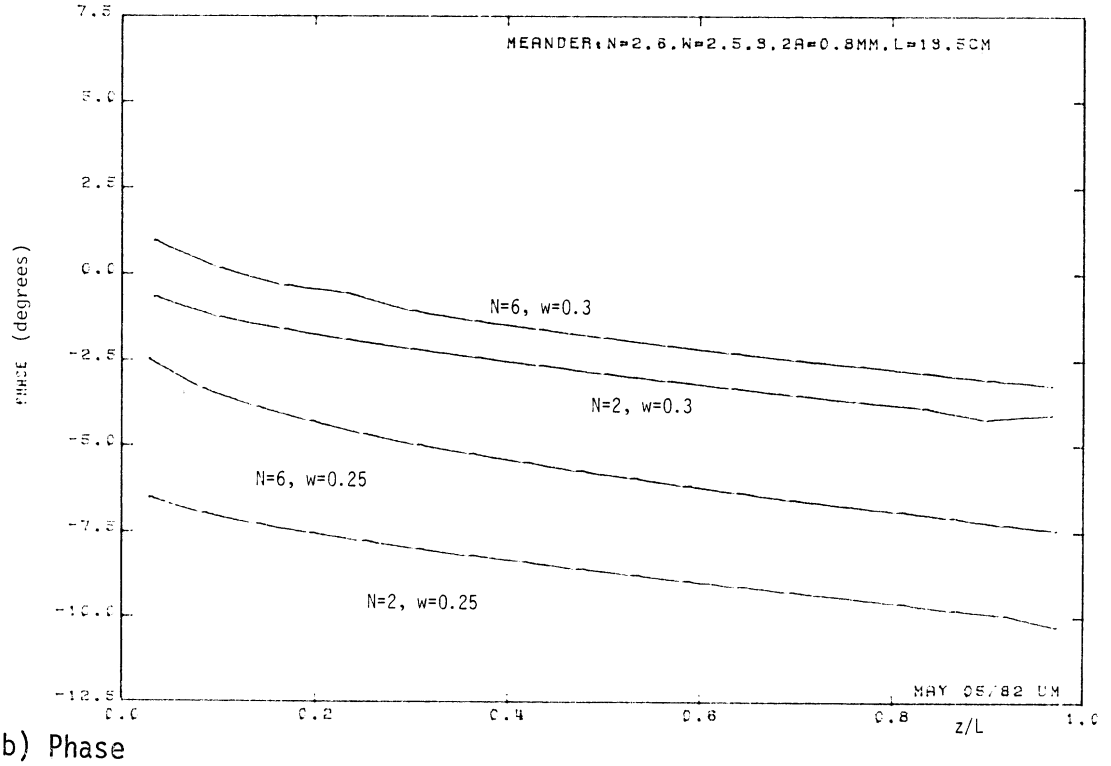

(b) Phase

Fig. 3.4: The effective current for two meander antennas (N = 2,6) with w = 0.25 cm and w = 0.3 cm.

(w = 0.3 cm, a = 0.4 mm), can be matched for x/L = 0.222, 0.356 and 0.4, respectively. It was also verified that by transferring the input from the base to some point on the antenna, the resonant frequency remains unchanged.

For a 50-ohm matched condition, x/L is seen to be greater for a higher N. This is evident from the current plots in Fig. 3.1. For a fixed value of x/L, the current amplitude is higher for lower values of N. Therefore, a horizontal line, corresponding to a required current for a certain impedance level, intersects the current plots at the appropriate point yielding the desirable value of x/L for proper matching in each antenna. This process supports the earlier statement that meander antennas with lower N's need lower values of x/L.

3.4 Other Factors Affecting the Antenna Characteristics

3.4.1 Effect of Width, w.

In Chapter II, we observed that if w is increased to an appreciable value in comparison to the length of the antenna, the reduction factor decreases but the undesirable radiation due to the lateral parts of the antenna is increased. Another related disadvantage with an increased w is a decreased bandwidth and a lower resonant resistance. To understand the behavior of the antenna under these circumstances, one can study the gradual transformation of the current and the possible changes in the antenna properties when separation is increased. On the other hand, the values of w up to one tenth of ℓ, are acceptable for reduction purposes without significant deterioration of the antenna performance.

Figure 3.5 shows the current distribution at resonance along the antenna wire for N = 2 and with w as a variable (w = 0.25, 0.3, 0.5 and 1.0 cm). The total wire length L, and wire radius a, of each antenna is 13.5 cm and 0.4 mm, respectively. Since L is constant in all antennas, the height ℓ, of the antenna for w = 0.5 and w = 1 cm is less than 4.5 cm because of the increased separation between the wires. The input currents in Fig. 3.5 indicate the dependence of the resonant resistance on the separation of the wires. The magnitude of the current demonstrates a maximum near the feeding terminals and diminishes towards the antenna end. The phase however remains relatively constant. Figure 3.6 shows the current distribution for two meander antennas, N = 2,6 (L = 13.5 cm, a = 0.4 mm) with small separations, w = 0.25 cm and w = 0.3 cm. These separations correspond to $w/a \simeq 6.0$ and 7.5 respectively. The shape of the current is seen to be unchanged except for an amplitude factor of approximately 0.9 which is attributed to the slight change in the resonant resistance.

Table 3.2 summarizes the numerical results of the analysis. The experimental data from Chapter II is included for comparison. According to these analytical results, supported by experimental evidence, when the radius is constant, an increased w produces an improved reduction factor. However, in view of the reduced bandwidth and resonant resistance, it is emphasized that unless specific applications are projected, w should be kept small in comparison to the physical length ℓ of the antenna. Under these

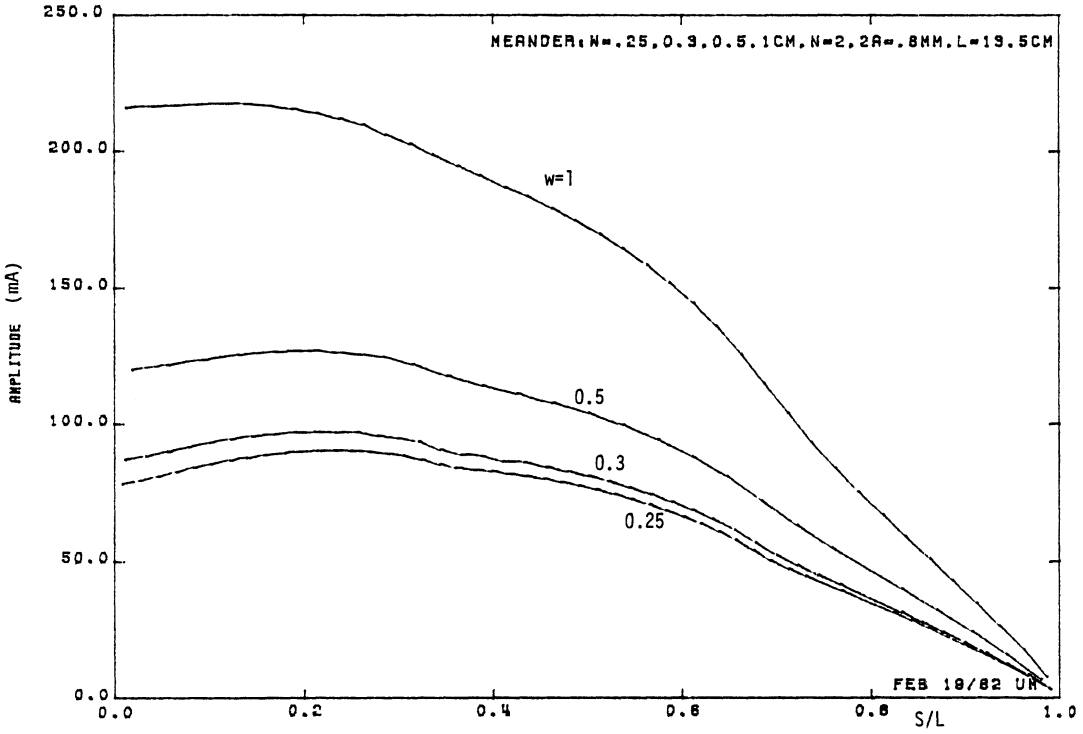

(a) Amplitude

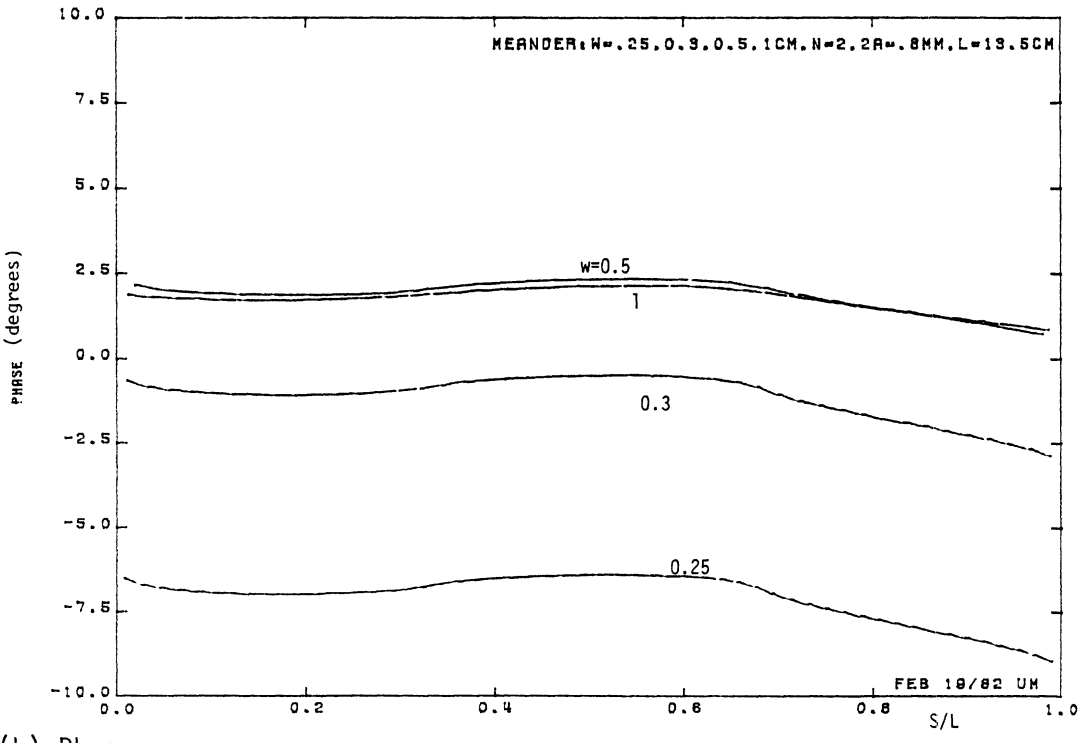

(b) Phase

Fig. 3.5: Current distribution for N = 2 with w as a variable.

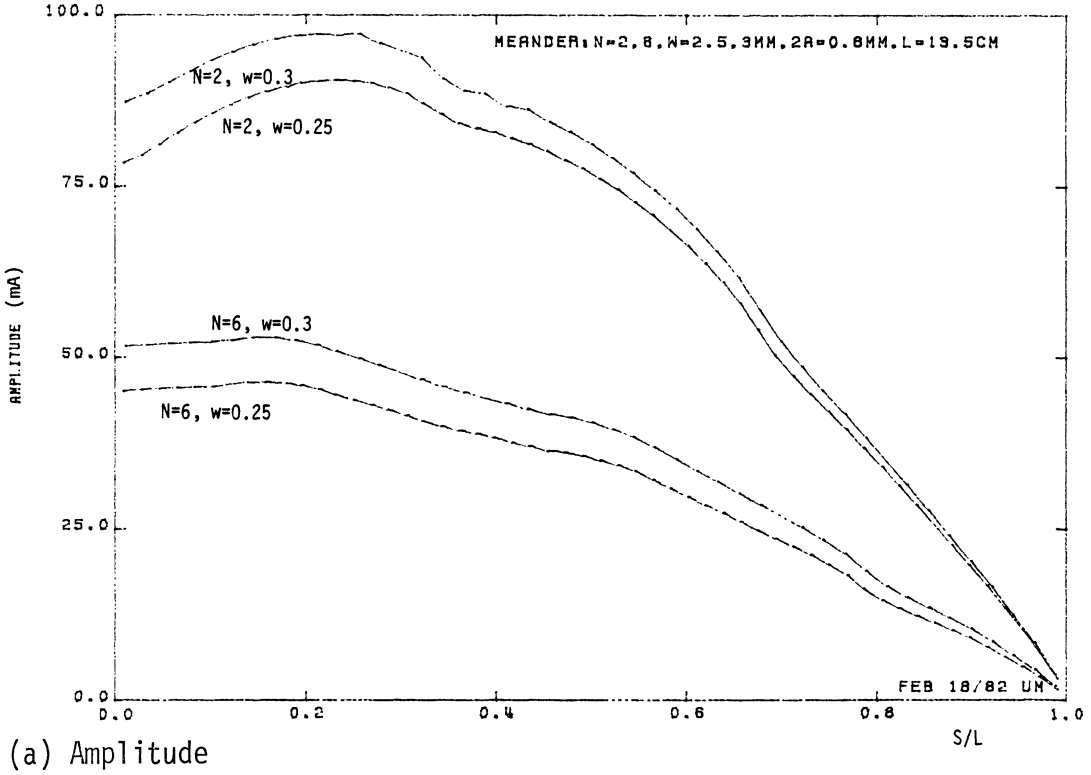

(a) Amplitude

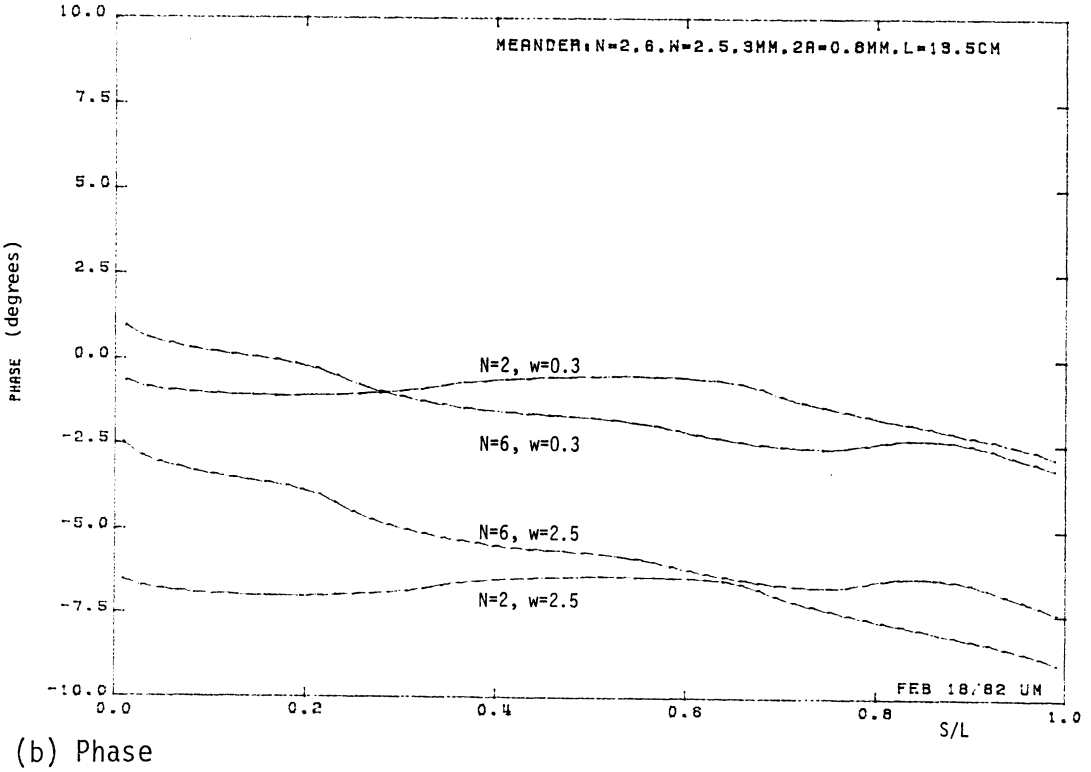

(b) Phase

Fig. 3.6: Current distribution for N = 2,6 with w = 0.25 cm and w = 0.3 cm.

Table 3.2

Numerical results for N = 2 with L = 13.5 cm and a = 0.4 mm, w is variable. Experimental data are provided as a reference.

	Numerical			Experimental		
w (cm)	f_o (MHz)	β	R_{res} (Ω)	f_o (MHz)	β	R_{res} (Ω)
0.25	962	0.62	12.7	976	0.64	14.0
0.3	918	0.59	11.5	($w \simeq 0.25$)	($w \simeq 0.25$)	($w \simeq 0.25$)
0.5	787	0.50	8.3	770	0.50	7.5
1.0	712	0.46	4.6	684	0.45	5.0

circumstances, no marked change is expected in the antenna characteristics.

3.4.2 Effect of Wire Radius. Although all the antennas under consideration are sufficiently thin, the effect of radius change should not be ignored. It is presumably true that a change of the radius does not significantly affect the resonant frequency of thin wire monopoles, but the validity of such a hypothesis for meander antennas cannot be postulated without further investigation. In fact such an assumption is not justified due to the presence of the extra parameter, w, associated with the meander geometry. The ratio w/a is doubled if a is reduced to one half of its value. This ratio can be increased by the same factor, however, if a is kept constant and w is doubled. In view of the foregoing discussion and the dependence of the antenna characteristics on the separation of the wires, one can anticipate that a change in radius will, indeed, affect the meander antenna characteristics. A reduced wire radius is expected to similarly affect the reduction factor as does an increased w, but not to the same degree.

To study the effects of change of radius, three different radii corresponding to a = 0.1 mm, a = 0.2 mm and a = 0.4 mm are considered. Generally speaking, a smaller value of the radius yields a more accurate numerical solution since the increased dominance of the axially directed currents will be more prominent. However, the analysis of thin wire antennas with a sufficiently high number of segments and the use of basis function with fast convergence,

adequately incorporates the effect of radius and gives the solution within a few percent of the exact value. Therefore, as far as thin wire antennas are concerned, any possible inadequacy resulting from thin wire kernel approximation will not undermine the accuracy of a numerical solution for different radii.

Table 3.3 compares the numerical results for meander antennas (L = 13.5 cm, w = 0.3 cm and ℓ = 4.5 cm) with different radii. In each case, the reduction factor is calculated using the resonant frequency of a monopole with the same length, ℓ, and the same radius. It is seen that the resonant frequency decreases for smaller radii as does the resonant resistance. In other words, the size reduction is increased by decreasing the wire radius. The same behavior was previously observed when the separation of wires, w, was increased. One can therefore reach the conclusion that for a constant wire length a greater reduction in size is possible by increasing w/a, either by increasing the separation of the wires or decreasing their radius. When w/a is to be increased, one should recognize that there is an upper limit for the value of w due to the increased lateral expansion of the structure (increased w/ℓ) while a decrease in radius a, improves the accuracy of a numerical solution. The latter is limited by the minimum thickness requirement for a self-supporting structure in practical problems. It is therefore recommended that for a size reduction, by increasing w/a, a decrease in the wire radius be considered before any attempt is made to increase the separation.

Table 3.3

Effect of radius change in meander antennas. L = 13.5 cm, w = 0.3 cm and ℓ = 4.5 cm for all antennas

	$\simeq f_o$ (MHz)			R_{res} (Ω)			β		
N	a=0.4 mm	a=0.2mm	a=0.1mm	0.4mm	0.2 mm	0.1 mm	0.4 mm	0.2 mm	0.1 mm
2	918	851	805.5	11.5	8.9	7.5	0.59	0.54	0.51
6	981	915	855	19.3	15.6	12.9	0.63	0.58	0.54
10	1005	940	877	20.7	17.1	13.9	0.64	0.60	0.55

Figures 3.7 through 3.9 show the current distribution of resonant meander monopoles with different radii. The input resistance is different for each radius as it is reflected by the different input currents. These plots illustrate the dependence of the current distribution on the radius of the wire in meander antennas.

3.5 Pattern and Polarization

The question of whether the undesirable radiation from the horizontal protions of a meander antenna is appreciable for a specific wire separation, must also be answered particularly when the separation w increases. In other words, we strive to determine if and when the lateral expansion of the structure affects the pattern of the antenna.

We assume a z-directed meander monopole in the yz plane with the origin as the feeding point and the 'xy' plane as the ground. Two principal planes, namely $\phi = 0°$ and $\phi = 90°$ in a conventional spherical coordinate system, are selected for calculating the far zone electric field for R = 1 meter. $|E_\theta|$ is present on both planes, while $|E_\phi|$ is zero on the $\phi = 90°$ plane.

Figures 3.10(a), 3.10(b) and 3.11(a), show the magnitude of the electric field components, $|E_\theta|$ and $|E_\phi|$, corresponding to meander antennas with N = 10, 6 and 2 respectively. All the antennas have a total wire length, L = 13.5 cm (ℓ = 4.5 cm) with a = 0.4 mm and w = 0.3 cm ($w/\ell \simeq 0.07$). It is recognized that for small values of

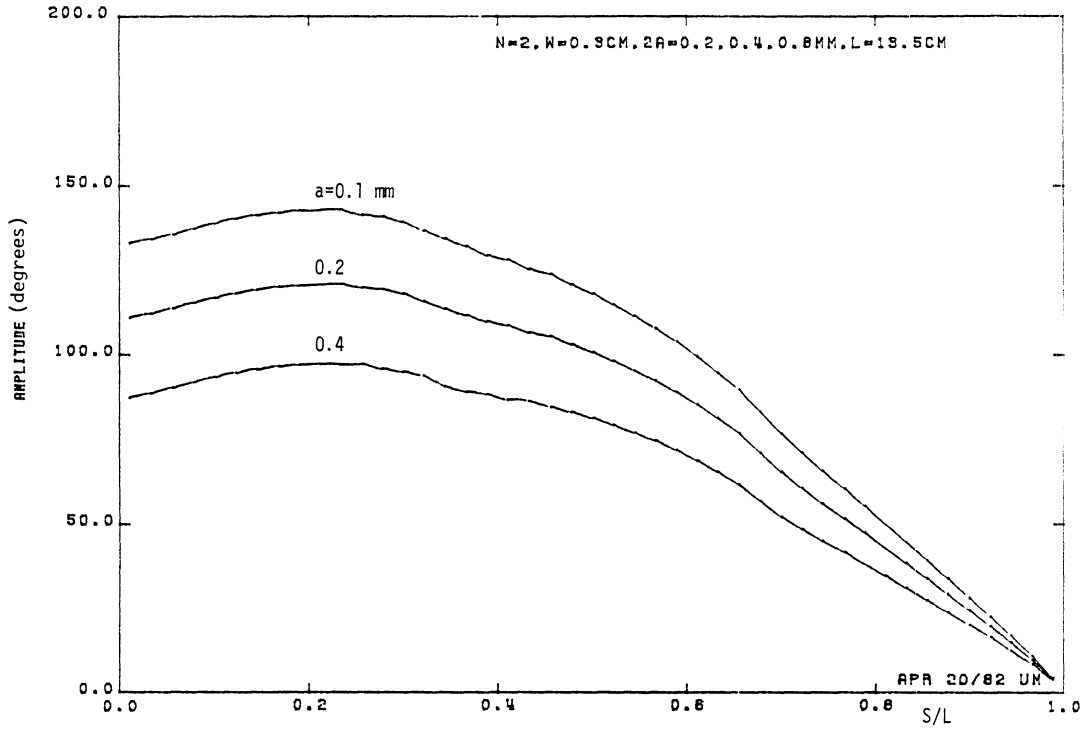

(a) Amplitude

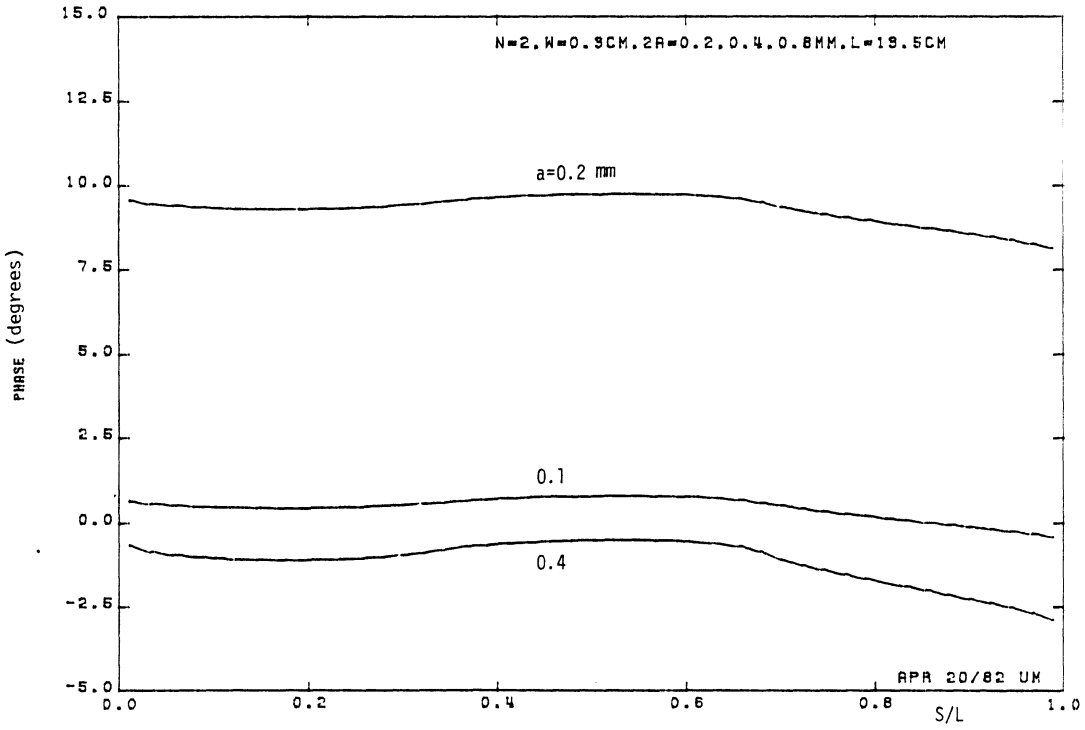

(b) Phase

Fig. 3.7: Current distribution for N = 2 with different radii.

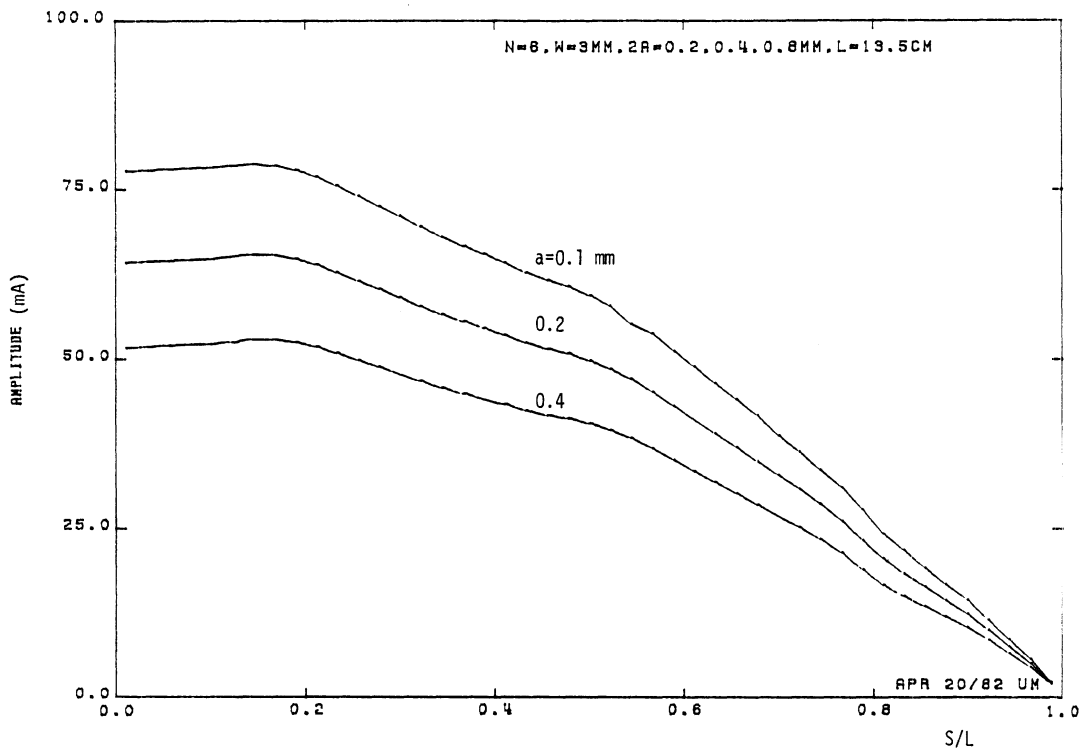

(a) Amplitude

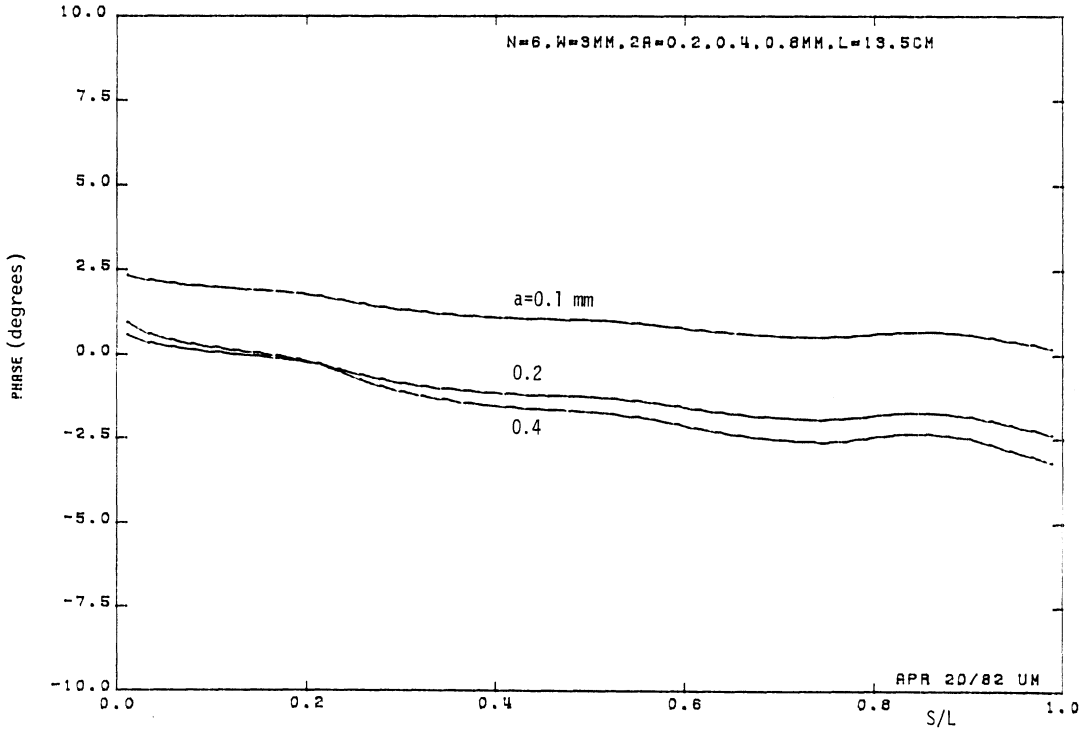

(b) Phase

Fig. 3.8: Current distribution for N = 6 with different radii.

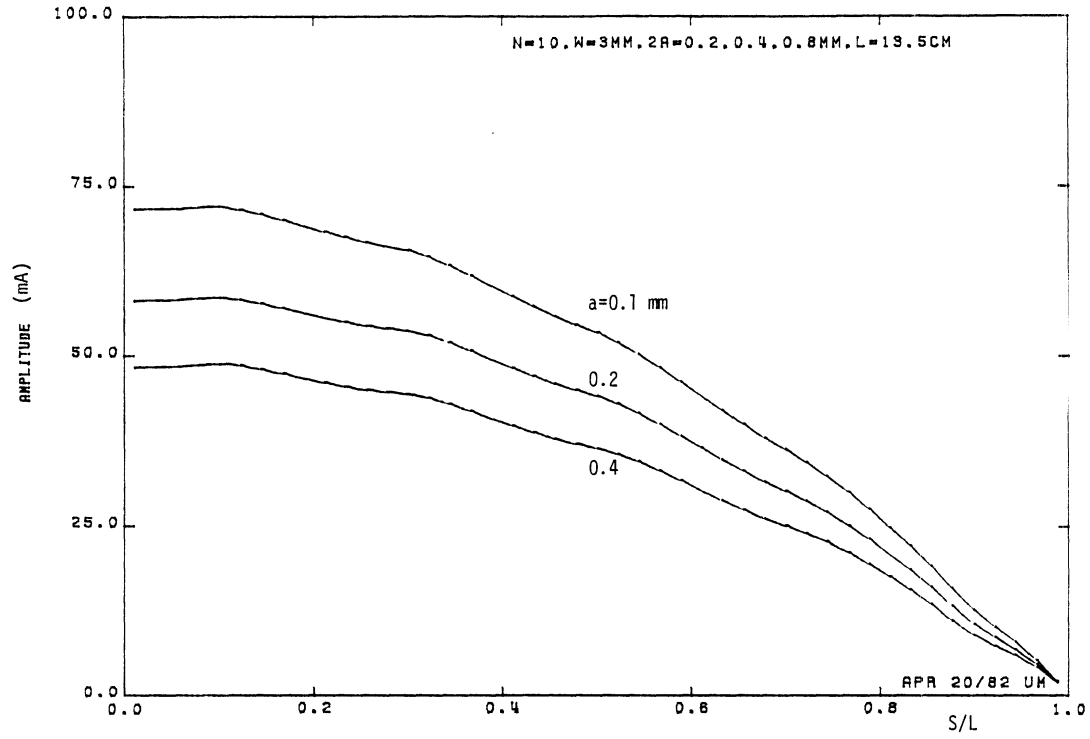

(a) Amplitude

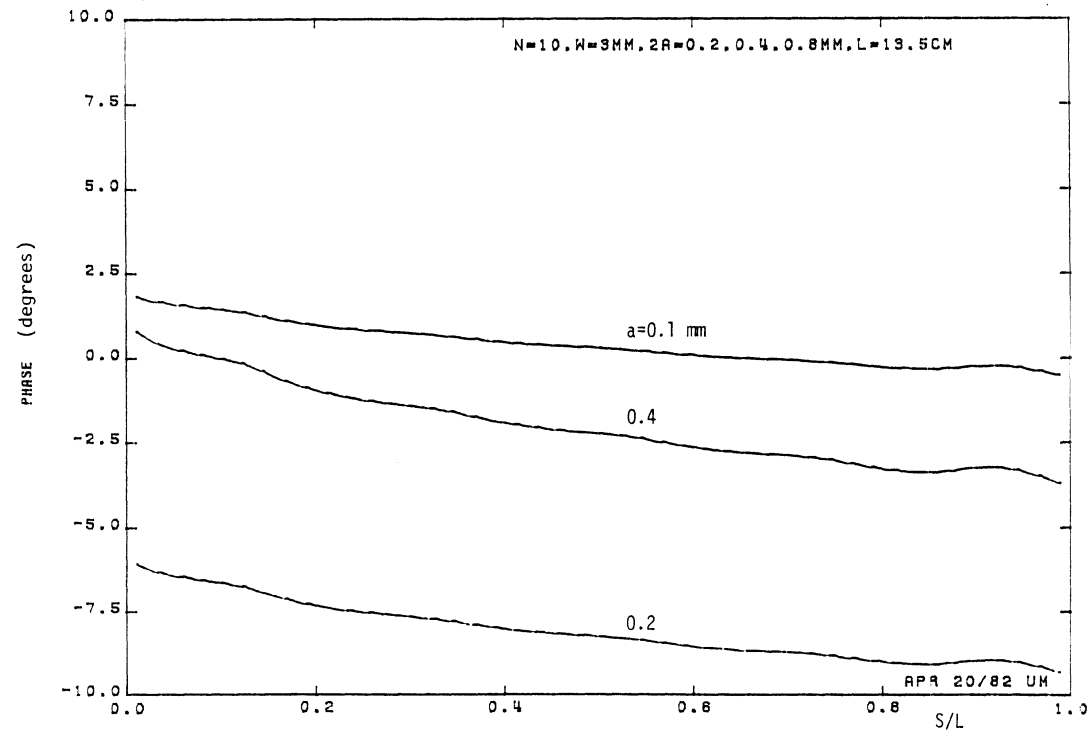

(b) Phase

Fig. 3.9: Current distribution for N = 10 with different radii.

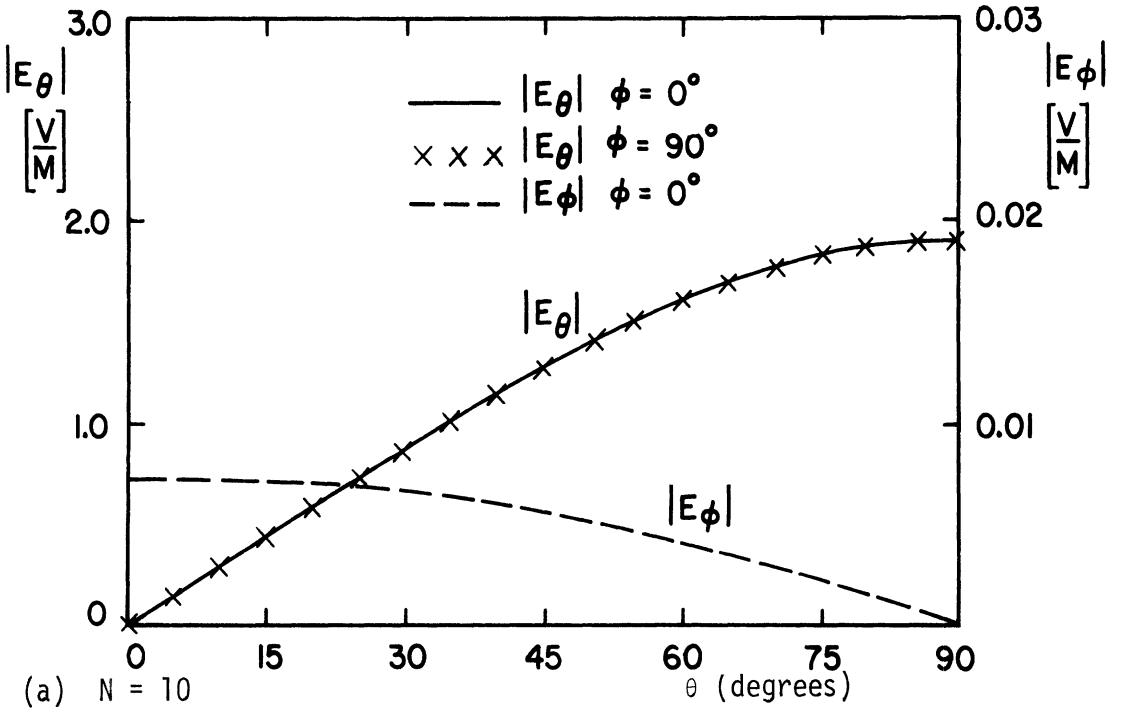

(a) N = 10

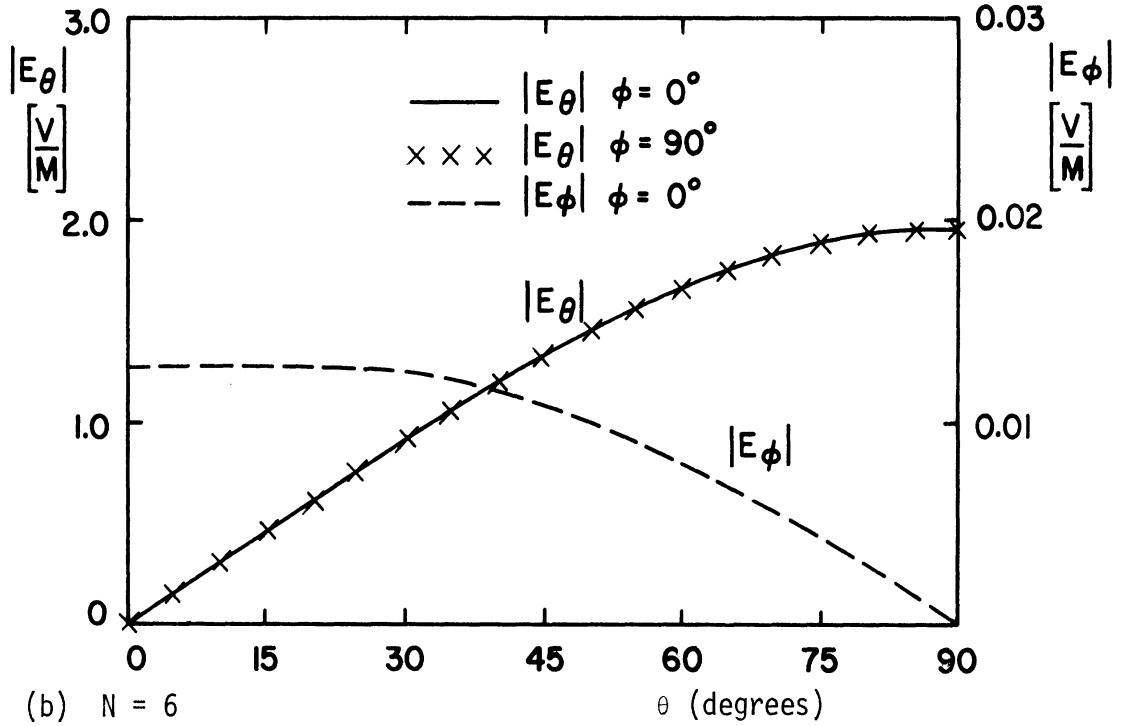

(b) N = 6

Fig. 3.10: Electric field components for meander antennas, L = 13.5 cm, w = 0.3 cm ($w/\ell \simeq 0.07$), a = 0.4 mm.

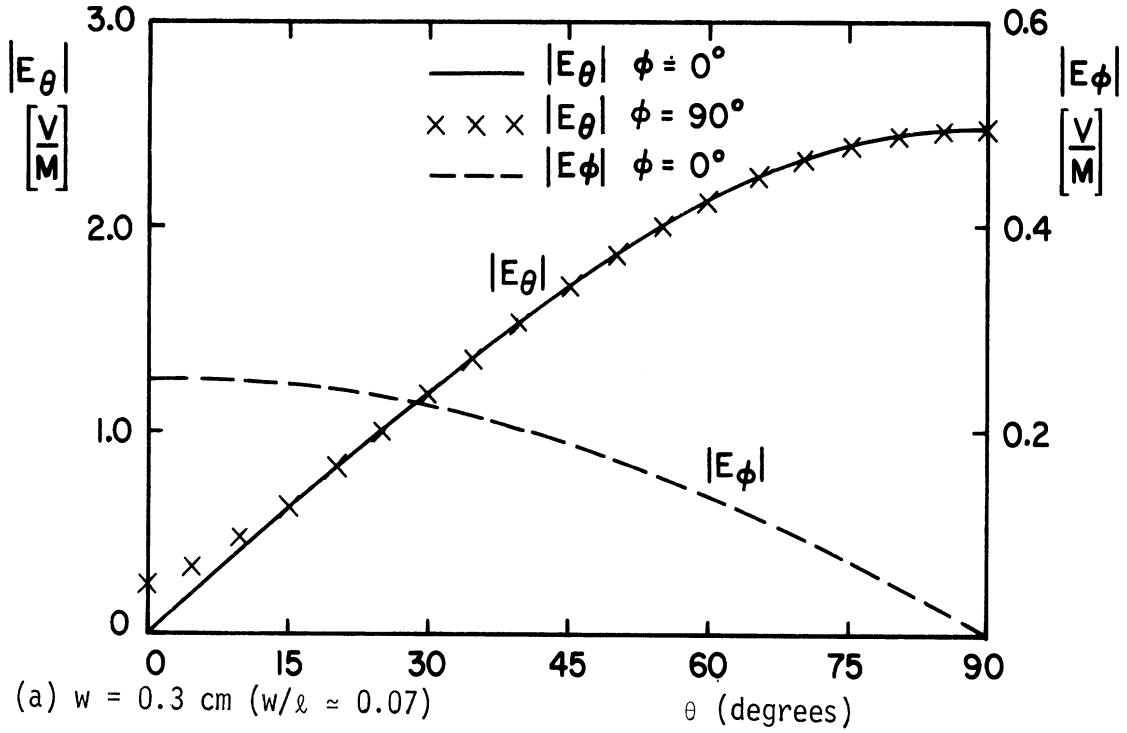

(a) w = 0.3 cm (w/ℓ ≃ 0.07)

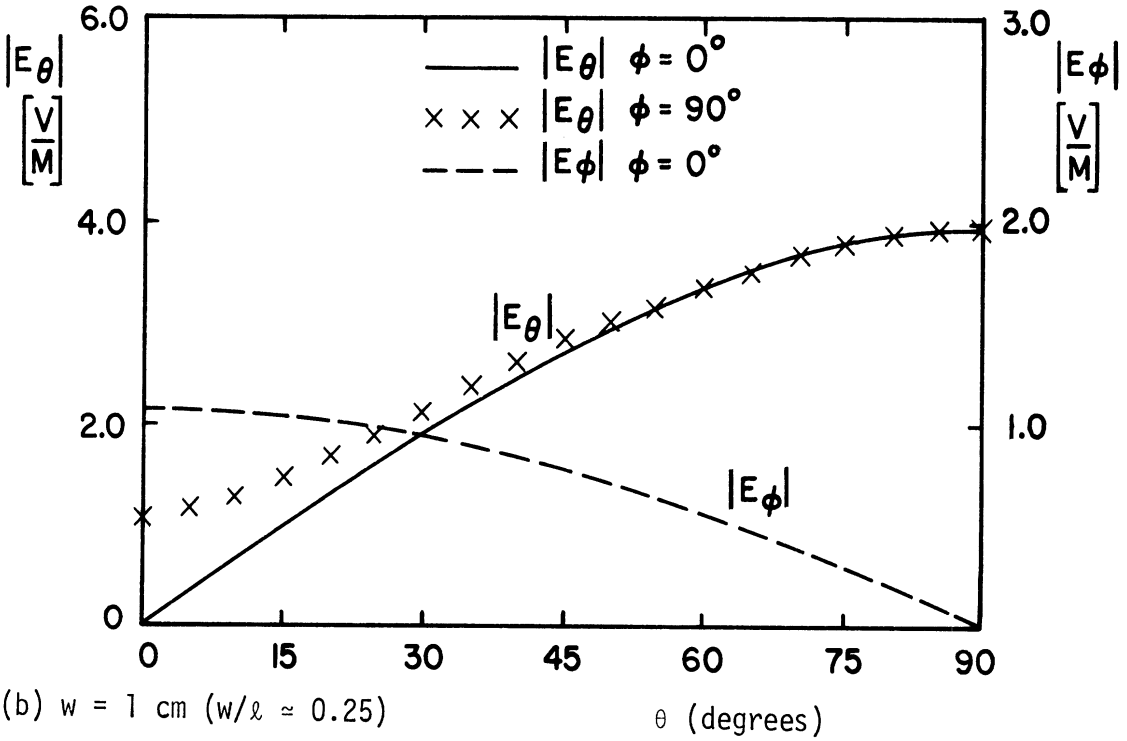

(b) w = 1 cm (w/ℓ ≃ 0.25)

Fig. 3.11: Electric field components for N = 2 meander antenna, with L = 13.5 cm, a = 0.4 mm.

w/ℓ, $|E_\phi|$ is negligible on the $\phi = 0$ plane and the θ component of the electric field is the same on the two major planes. In the most stringent case, i.e., $N = 2$, and for small angles of θ, a slight difference between $|E_\theta|$ on the two planes is observed. The negligible difference between $|E_\theta|$ on the two major planes and the diminishing $|E_\phi|$ in the $\phi = 0$ plane for an increasing N, is attributed to the partial cancellation of the oppositely directed currents in neighboring meander cells. This cancellation increases when N is increased.

The extent to which the lateral expansion of meander antennas contributes to the asymmetry of the pattern can be seen from the comparison of Fig. 3.11(a) and Fig. 3.11(b). The latter shows the fields of $N = 2$ meander antenna where the separation w is increased to 1.0 cm ($w/\ell \simeq 0.25$).

Generally speaking, as w/ℓ increases, $|E_\phi|$ on the $\phi = 0$ plane increases as does the difference between $|E_\theta|$ in the two principal planes. This deviation in the field components, if significant, results in a nonuniform pattern. Therefore, the improvement of β by increasing w/ℓ, if necessary, is acceptable only to the extent to which the resultant cross polarization can be tolerated. This is in fact one limitation on reduction techniques obtained by the geometrical deformation with excessive lateral expansion of the structure. In many cases, however, the bandwidth requirement is of primary concern in the design of size reduced antennas.

CHAPTER IV. APPLICATIONS OF MEANDER ANTENNAS

In the foregoing chapters we have discussed the basic characteristics of meander antennas as resonant elements. Some examples incorporating meander elements will be presented in this chapter.

4.1 Log-Periodic Meander Antennas

4.1.1 Size Reduction in log periodic dipole arrays (LPDA).

Log-periodic dipole arrays [61] are one of the most versatile and widely used broadband antennas. They have moderate directivity typically in the neighborhood of 10 dB for a single array. Operation of these antennas as a special case of a wider class of antennas known as log-periodic structures is based on a novel concept introduced by DuHamel and Isbell [6]. As the frequency is changed these structures scale to themselves in a log-periodic manner before a significant change is observed in their characteristics, hence they show broadband properties within a certain bandwidth limit which depends on the geometry of the structure. Ideally, in an LPDA, not only the length of the elements and their spacing should be scaled, but all other dimensions, such as wire radii, the spacing and the diameters of the feeder conductors should be scaled as well. However, in some practical cases, a relaxation of this rigorous scaling does not markedly affect the performance of the antenna and only the length of the elements and their spacing need to be scaled.

Factors such as the operating frequency, bandwidth and directivity determine the size of an LPDA. At low frequencies, the length of the elements become enormous since they have to be approximately half a wavelength long for the antenna to operate efficiently. Bandwidth requirements and increased directivity result in a longer antenna with more elements.

The problem of reducing the size of an LPDA has been challenged by many investigators. Because of the directivity requirements, it is difficult to reduce the boom length of an LPDA. A lateral size reduction of the antenna requires the shortening of each individual element. Since the shortened dipoles have lower resonant resistance and may suffer efficiency reduction, cross polarization and narrower bandwidth pending on their method of size reduction, one would anticipate a deterioration in the overall characteristics of a shortened LPDA. A qualitative discussion on the effects of size reduction is given by Stephenson and Mayes [32]. They showed that a log-periodic array with helical dipoles has lower directivity and higher VSWR in comparison with an LPDA. For a reduction factor of 0.54 a VSWR of 4.85 and a directivity of 6.3 dB is reported in contrast to the corresponding values of 1.5 and 9 dB for an LPDA over the same frequency range. For better performance, they suggested a mixed LPDA with helical elements for the low frequency part. However, as frequency decreases and the helical dipoles become effective, the patterns become broader introducing less and less front-to-back ratio and an increased VSWR. This hybrid version

does not affect the overall size reduction of the antenna, but rather it improves, slightly, the gain and directivity of the antenna at the high frequency side. It is also helpful in arrays where the proper fabrication of small elements corresponding to high frequencies are not readily achieved [33].

In the helical versions of LPDA, polarization is not completely linear and the axial ratio has to be controlled. Furthermore, the construction of helices with low pitch angles especially at the high frequency band is difficult to facilitate.

Two new log-periodic dipole arrays, with conical helical and multiple dipole elements have been suggested as better alternatives for helical log-periodic dipole arrays [34]. Other techniques for LPDA shortening such as different loading methods have also been tried in the past. An inductive loading for low frequency elements is discussed by Elfving [35]. In this version, more inductive loading is needed as the lower frequency elements become active. In addition to the overall gain reduction due to element shortening, the losses in the loading coils reduce the efficiency of the antenna.

Loading techniques including various typs of capacitive loadings have been discussed by DiFonzo [36]. Kuo [37] has suggested a so-called double ridged waveguide shaped dipole as elements to be used for size reduction. A 35 percent size reduction for LPDA using these elements is reported to have the expected properties with approximately 1.5 dB loss in gain and wider beamwidths in both

vertical and horizontal planes. A mixed version with ordinary dipoles at high frequency side is also reported with better performance.

4.1.2 Log-Periodic Meander Dipole Arrays (LPMDA). In this section, an LPDA is compared with its meander version. The feeding system is maintained the same in both antennas and only the elements are replaced with their counterparts. The arrays are constructed with only the length of the elements and their spacing scaled. Other dimensions such as radius of the dipoles or spacing of the feeder conductors are held constant. In the meander version the additional parameter, w, was also not scaled. A 5:3 bandwidth (2.25 GHz to 3.75 GHz) is selected with a directivity of 9 dB and an arbitrarily chosen minimum E-plane beamwidth of 50 degrees. The design specifications are given in Appendix A. A meander version of the above LPDA, with N = 4 and an assumed average reduction factor of 0.65 was built. All other specifications such as wire diameters and the feeding system were the same in both arrays. Figure 4.1 shows the impedance plots of the LPDA and LPMDA over a 2 to 4 GHz frequency range. According to these curves in both LPDA and LPMDA, a deterioration of VSWR on and beyond the high frequency side of the band is evident. In an ideal log-periodic design all the dimensions including the diameter of the elements should be scaled. If the diameters are not scaled, then the VSWR will not remain constant over the frequency range. In light of Eq. (A.6), these variations become more severe for lower values of Z_a or equivalently, smaller thickness parameter Ω which corresponds to the high frequency side of

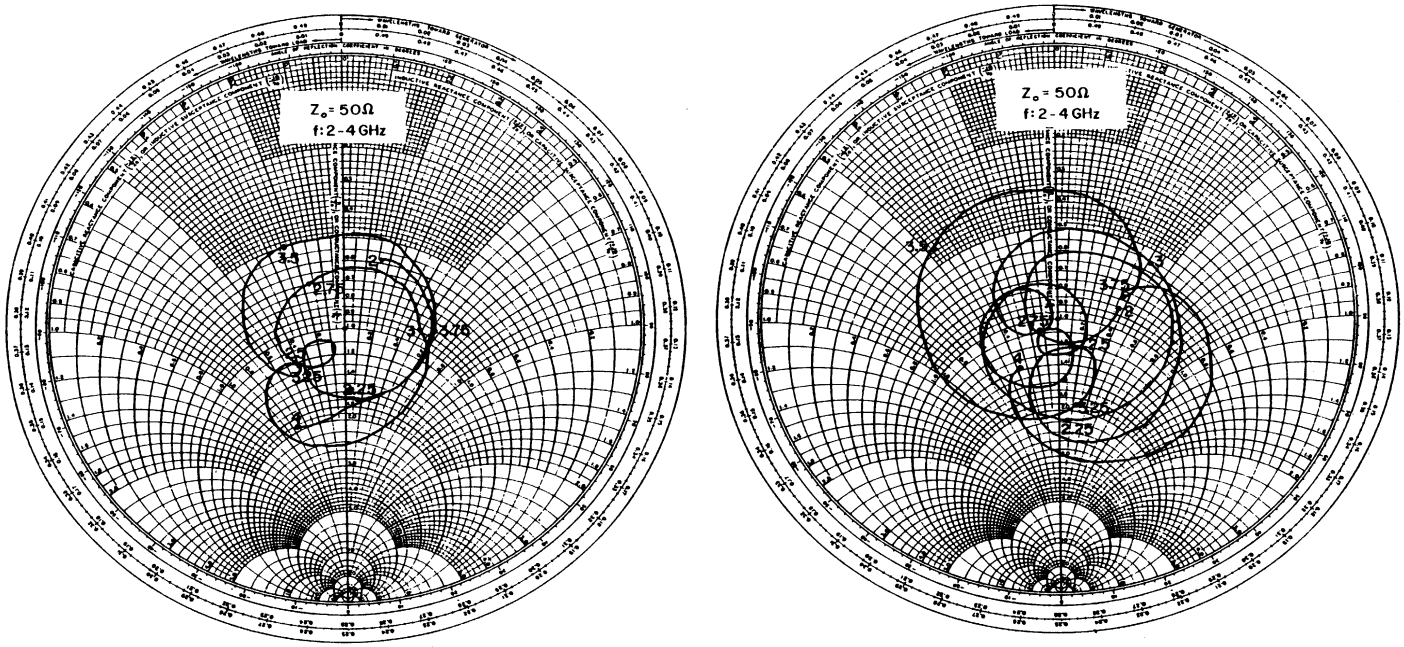

(a) LPDA (b) LPMDA

Fig. 4.1: Normalized impedance of the log-periodic dipole arrays.

the band. One remedy for this problem is a partial diameter scaling in which the elements are made from groups of wires with different diameters [63]. In LPMDA, in addition to the diameter of the wires, the separation w also was not scaled resulting in a further increase in VSWR. The VSWR of the antennas with respect to their mean resistance level, R_o over 2.25 to 3.75 GHz frequency range are

LPDA : VSWR = 2.33 , R_o = 55.86 Ω

LPMDA : VSWR = 2.85 , R_o = 49.1 Ω

The VSWR is increased from 2.33 to 2.85 in the LPMDA in return for a reduction factor of 0.65. The reported VSWR increase of a helical version [32] is from 1.5 to 4.85 for a reduction factor of 0.54. The VSWR of the LPDA and LPMDA obtained from the impedance curves at discrete frequencies is shown in Fig. 4.2(a). An increase in the overall VSWR of the antenna is noted. In Fig. 4.2(b) the gain of the two antennas and in Fig. 4.3 through Fig. 4.6 their patterns are compared. The pattern measurements were performed in a 6 ft x 28 ft x 12.5 ft room with part of the walls around the turntable covered by absorbers. From the pattern plots it is seen that the front-to-back ratio is less in LPMDA and the beamwidth is increased in both planes. Therefore the directivity decreases which brings about an average loss of about 2.5 dB in the overall gain in the LPMDA. The reduction in directivity is common in all reduced LPDA versions and is fundamentally related to the compact distribution of the current on a shortened antenna.

The mixed version of a reduced LPDA in which the high frequency elements are replaced by the corresponding dipoles is

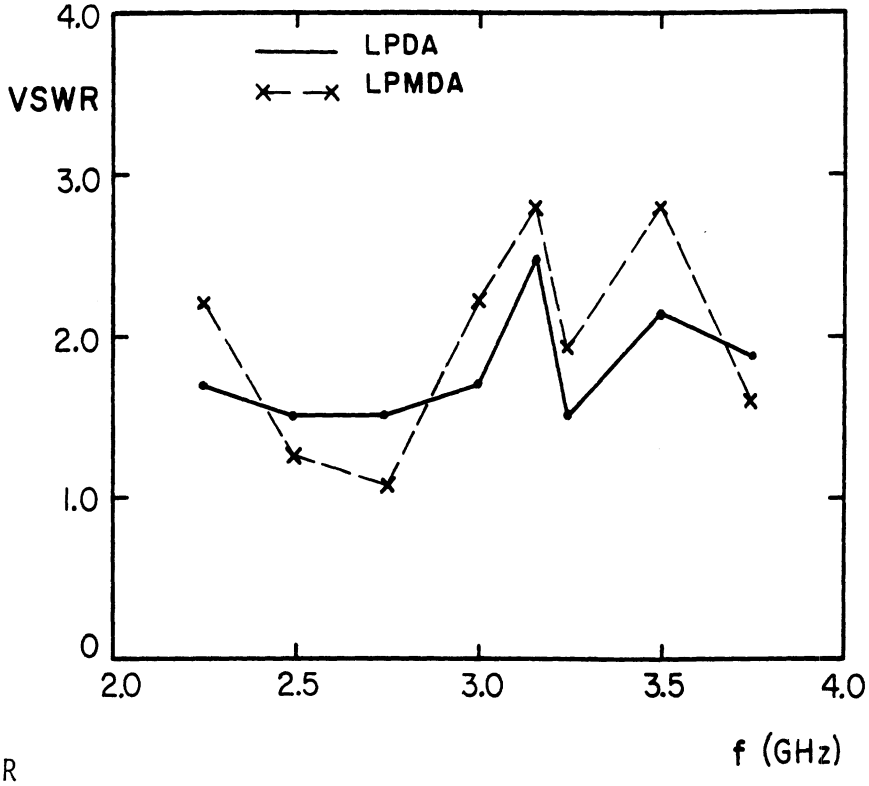

(a) VSWR

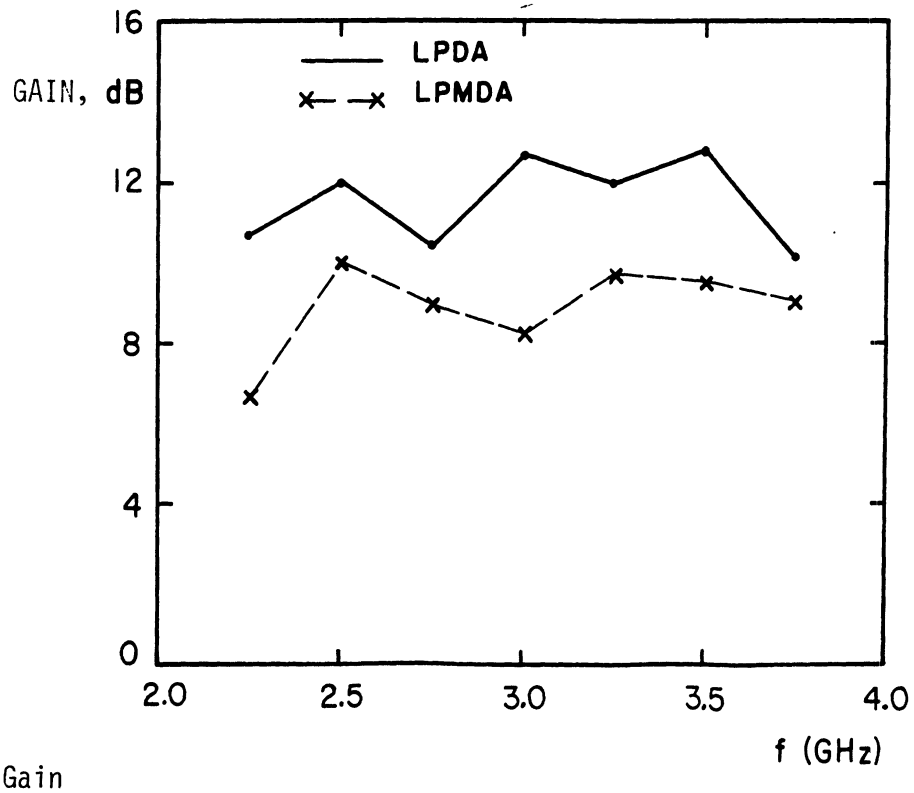

(b) Gain

Fig. 4.2 Comparison of VSWR and gain of the antennas.

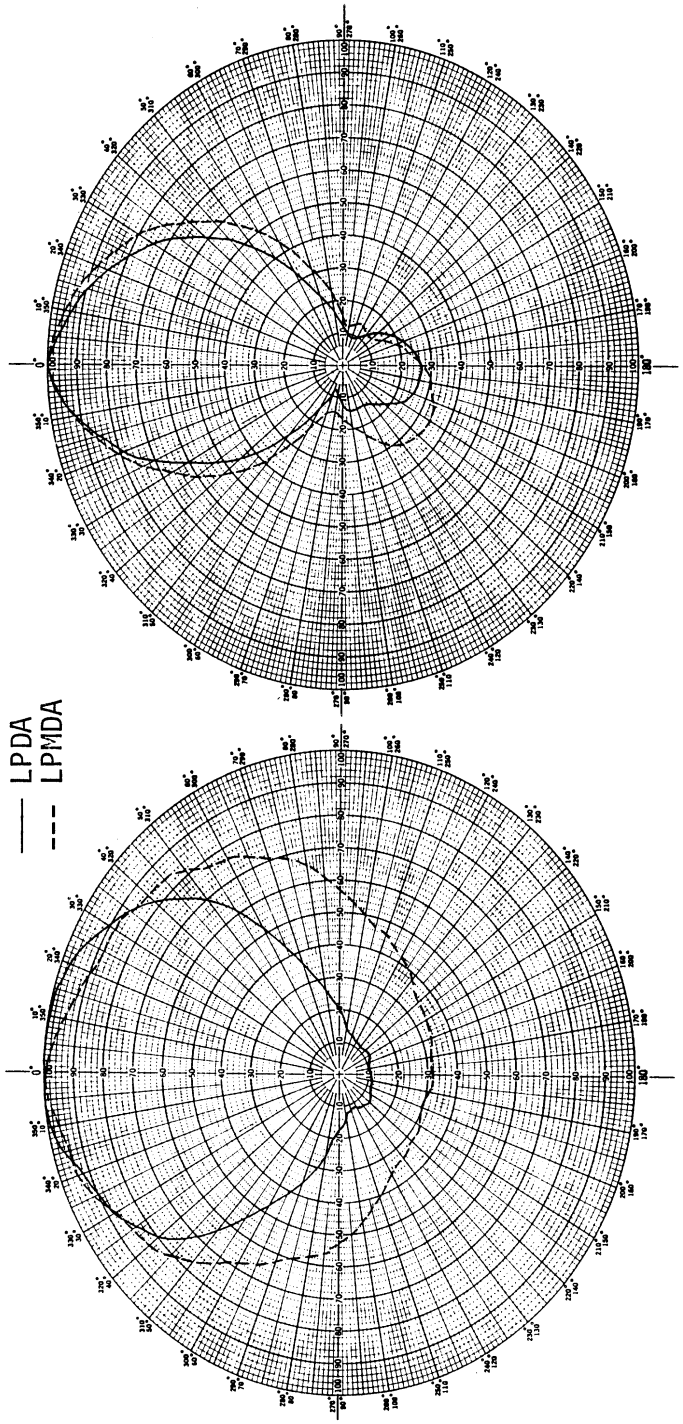

Fig. 4.3: Patterns of LPDA and LPMDA at f = 2 GHz.

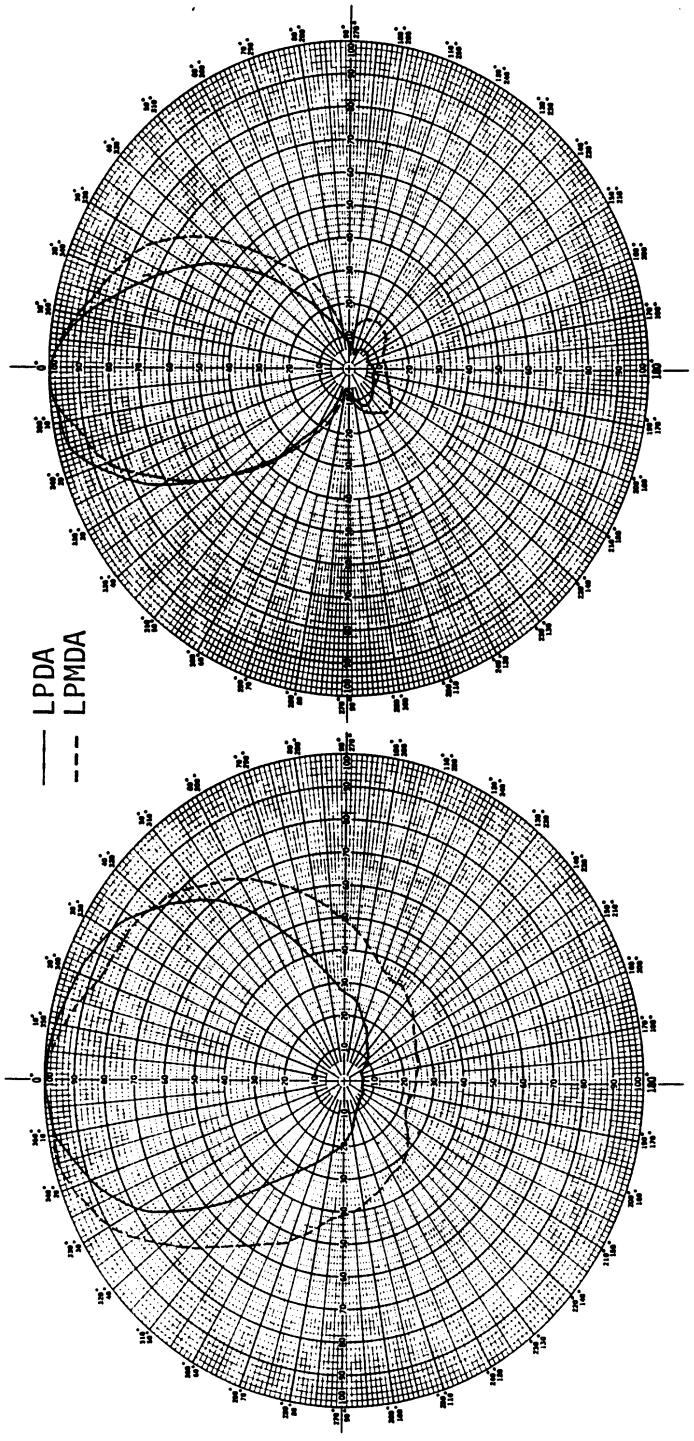

Fig. 4.4: Patterns of LPDA and LPMDA at f = 2.75 GHz.

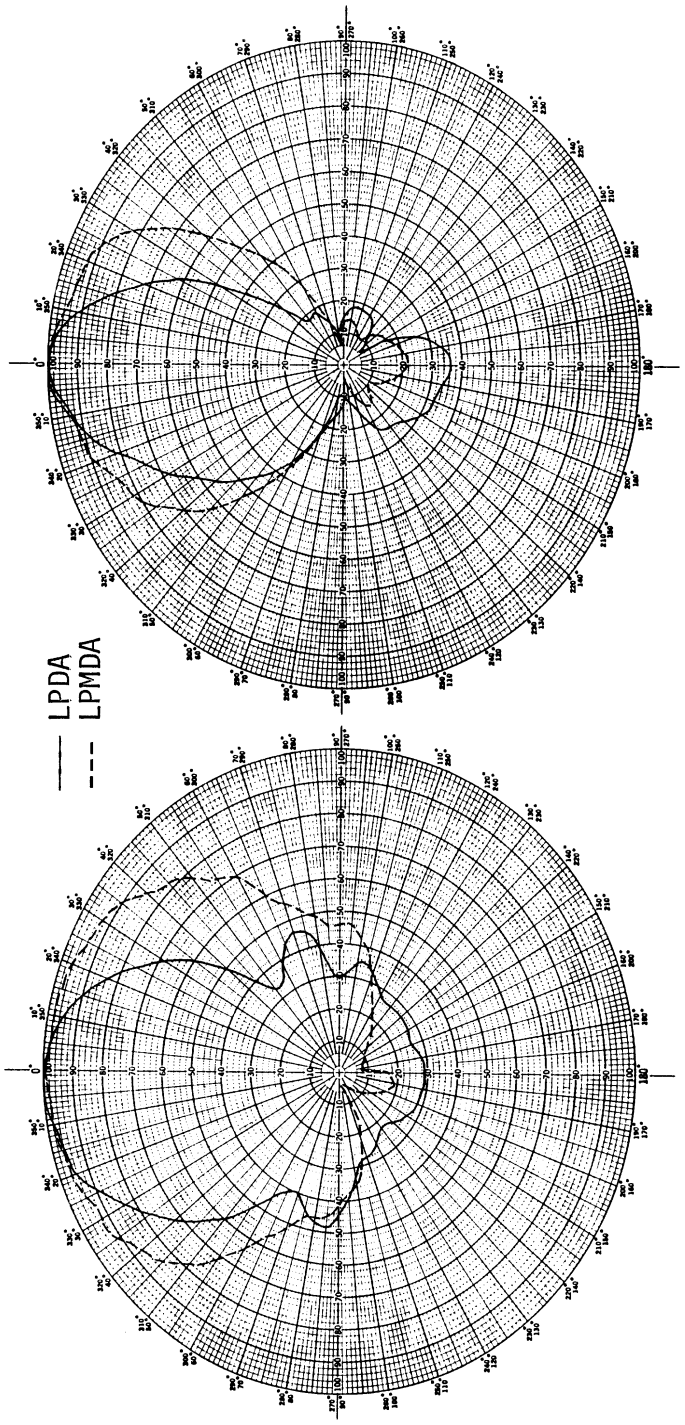

(a) H-plane (b) E-plane

Fig. 4.5: Patterns of LPDA and LPMDA at f = 3.25 GHz.

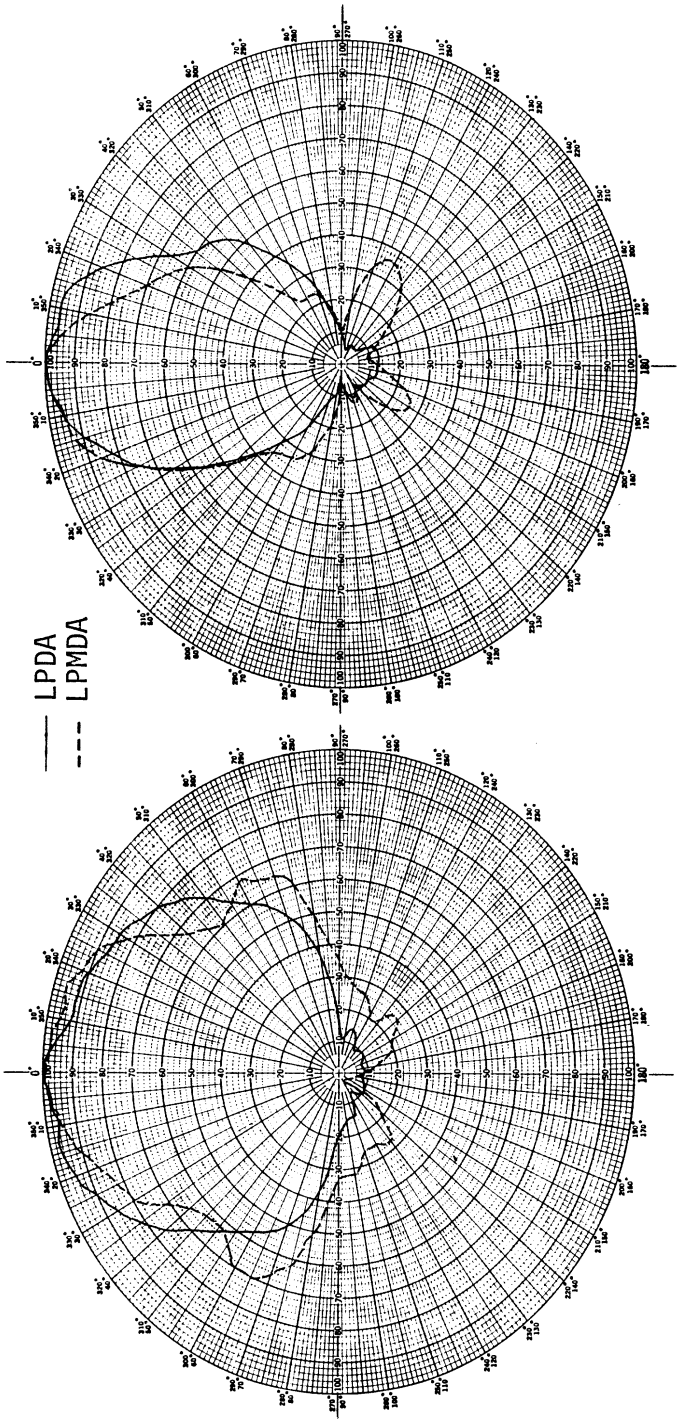

Fig. 4.6: Patterns of LPDA and LPMDA at f = 3.75 GHz.

similarly applicable for the LPMDA versions, improving the performance of the antenna at the high frequency end.

From Chapter I, we learned that resonant elements with a reduced size have a narrower bandwidth. Since in LPDA the 'active region' is responsible for radiation, a substantial change in the overall bandwidth may be expected for low reduction factors (N = 2 in the case of meander antennas). For a considerable size reduction, an increase in the number of elements may be necessary for certain requirements such as a minimum prescribed directivity. This increases the boom length of the antenna since one or more periods may be added to the structure.

4.2 Meander Folded Monopoles

Folded monopoles and folded dipoles are commonly used antennas. Their high input impedance makes them favorable for many applications. They are widely used as the active elements in the Yagi-Uda arrays and TV antennas.

The input impedance for a multiple folded dipole at resonance is approximately n^2 times the impedance of a single resonant dipole where n, is the number of arms in the folded dipole. For a conventional folded dipole, n = 2, we have, at resonance,

$$Z_{fd} \simeq 4Z_d \quad , \tag{4.1}$$

where Z_{fd} and Z_d are the resonant resistance of the folded dipole and the ordinary dipole respectively. As was pointed out in Chapter I,

loaded folded monopoles or dipoles have been used from time to time for size reduction purposes [2,5,8].

To study the behavior of the meander version of folded monopoles, a meander monopole with N = 4, w ≃ 0.2 cm and ℓ = 4.5 cm and the corresponding folded meander monopole have been built. The experimental reduction factor is $\beta \simeq 0.69$, when compared to a monopole of the same length with $f_0 \simeq 1525$ MHz. The wire from which the antennas are made has a diameter of 2a = 0.8 mm. Figure 4.7(a) shows the meander monopoles with the input impedance curves given in Fig. 4.7(b). The corresponding data is tabulated in Table 4.1. The impedance measurements and the bandwidth calculations were carried out by the same method as that given in Chapter II.

An inspection of Table 4.1 shows close agreement between the experimental results and the expected values. The resonant frequency is approximately the same for both antennas (within five percent) and the folded version has an expected resonant resistance four times the meander monopole with an error of about six percent. This shows that a folded meander version can be used in increasing the resonant resistance of a meander monopole in the same manner as a conventional folded monopole increases the resonant impedance of the ordinary monopoles. The bandwidth improves considerably when a meander folded version is made from a meander monopole.

For other meander monopoles with different numbers of sections per wavelength, the input impedance will increase accordingly. This input impedance is approximately four times the values given in Table 2.1 for the ordinary meander monopoles. The bandwidth also increases substantially for the folded versions. This example shows

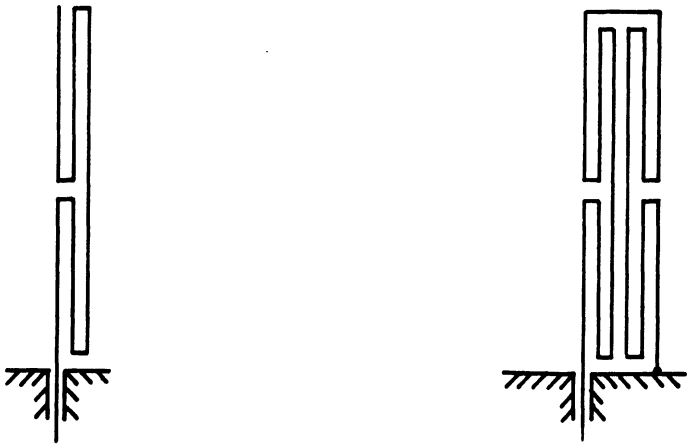

(a) A meander monopole and the corresponding folded version.

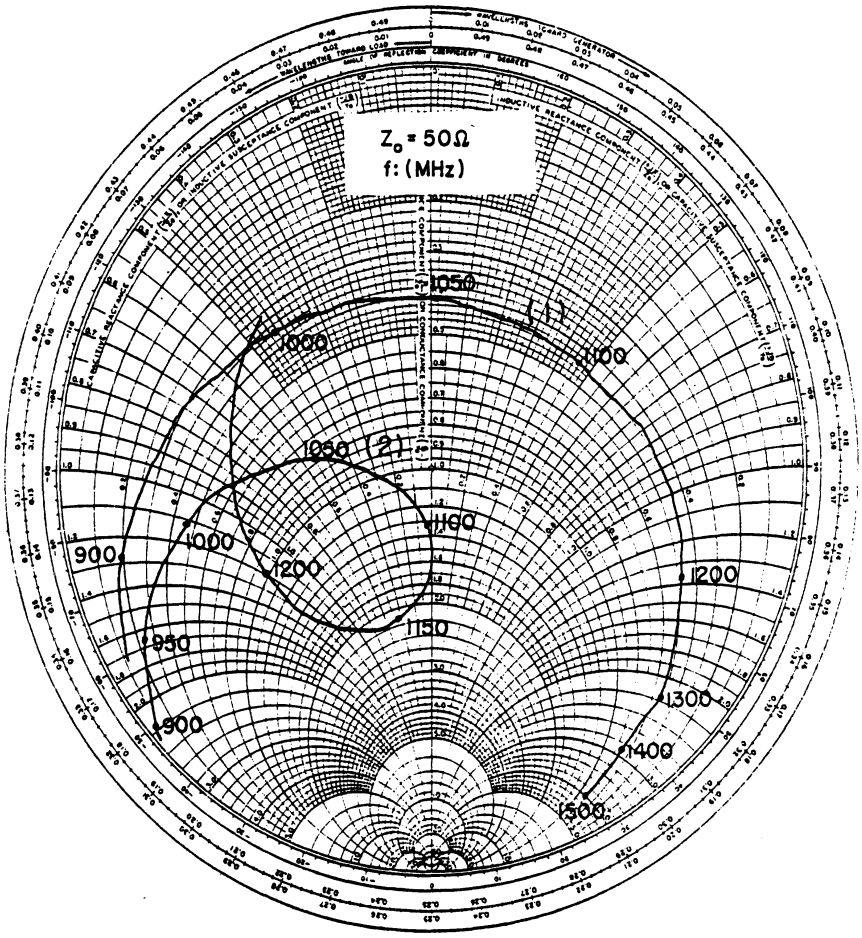

(b) Impedance curves

Fig. 4.7: Meander monopoles (N = 4) and their impedances.

Table 4.1

Comparison of the meander monopole and the folded meander monopole, N = 4, w ≃ 0.2 cm, ℓ = 4.5 cm and 2a = 0.8 mm

Type of meander antenna	f_o (MHz)	≃ ($\Delta f/f$) (%)	R_{res} (Ω)
(1) monopole	1050	6	20
(2) folded monopole	1105	11	75

that although the geometry of the meander folded monopole seems to be too complicated for a theoretical analysis, one can anticipate its properties based on the characteristics of the simple meander monopole version. In fact the relationship between a meander monopole and the folded meander monopole is the same as the relation between an ordinary monopole and a conventional folded monopole. The characteristics of the meander version of a structure can therefore, be predicted on the basis of the results now known for the original structure.

4.3 A Meander Self-Complementary Antenna

Two different concepts are known for frequency independent structures:

(a) structures dependent on angles only, and

(b) self-complementary structures.

The first class was introduced by Rumsey [64]. In terms of wavelength, the shapes of these structures are the same at all frequencies. In practice the antenna cannot be ideally frequency independent because of its finite dimension. The lower frequency end of the band is determined by the truncation of the structure, which, in practice, is intended to prevent an enormous physical size. At the high frequency end the feeding system and the feed point are the limiting factors. This group of antennas is also called "continuously scaled" by Mittra and Jones [65] as to be distinguished from the log-periodically scaled antennas previously introduced.

The second class of frequency independent antennas are the self-complementary structures based on Booker's relation [66]:

$$Z_d Z_s = \frac{\eta^2}{4} , \qquad (4.1)$$

where Z_s = input impedance of a slot,

Z_d = input impedance of the complementary strip and

η = the free space characteristic impedance.

By complementary, we refer to two structures which, when superimposed, make a complete plane without overlapping. If a structure has the same shape as its complement, its input impedance will always be constant and equal to 60π at all frequencies. Such a structure is called a self-complementary structure. This property was pointed out by Uda and Mushiake [67] and was later extended to the formation of many new antennas [68,69,70]. In two-port, three-dimensional complementary antennas the second port is terminated by a load impedance, Z_ℓ, equal to the characteristic impedance Z_c of the antenna. In these antennas the directivity is reduced by the presence of several main lobes due to structure symmetry and finite size of the antenna planes. A modified self-complementary structure with improved directional properties is introduced by Ishizone et al., [71], which consists of only half of a complementary structure.

The geometry of a modified self-complementary antenna with a meander strip (N = 2) is shown in Fig. 4.8(a). The load impedance,

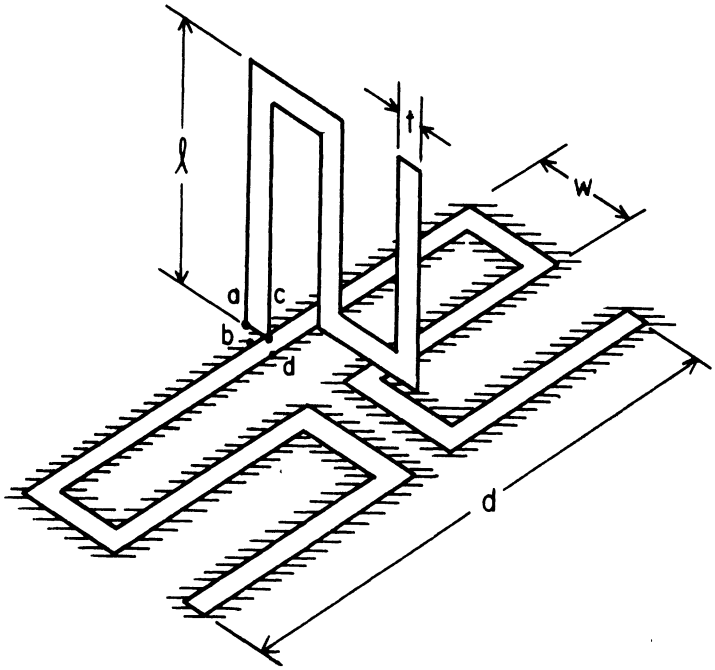

(a) Geometry of the antenna, w = 7 mm, t = 1.5 mm, d = 3 cm and $\ell \simeq 14$ mm.

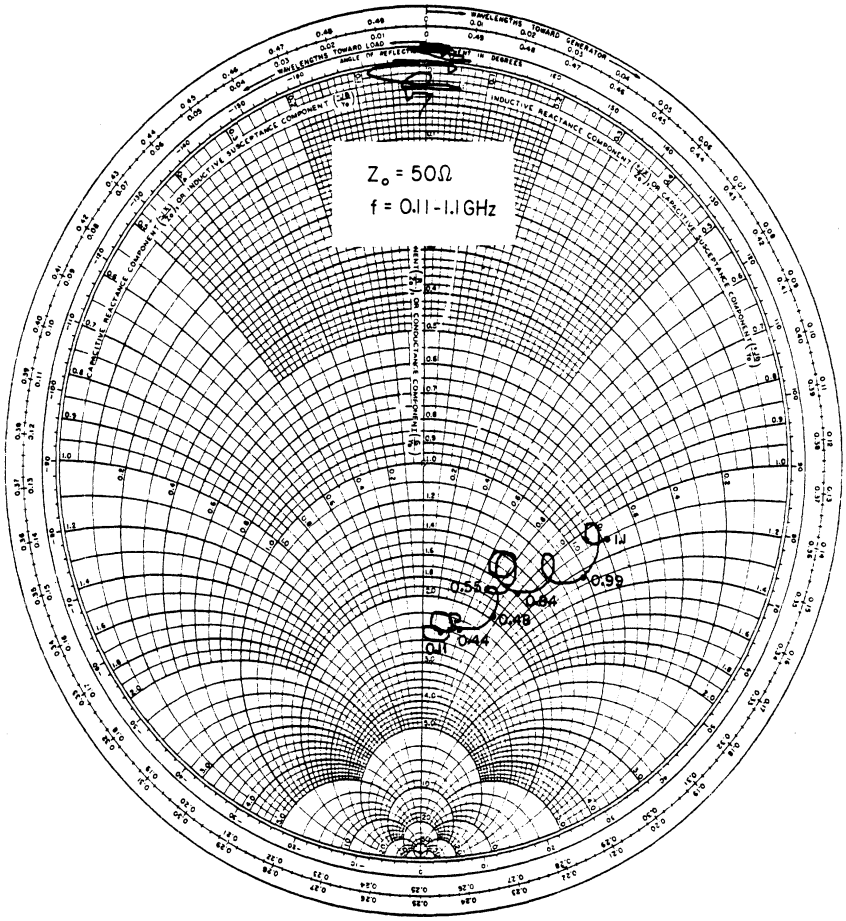

(b) Impedance of the antenna over a 10:1 bandwidth.

Fig. 4.8: Modified self-complementary antenna with a meander strip.

$Z_\ell = Z_c$ is connected between 'c' and 'd' with 'a' and 'b' as the excitation terminals. The feeding system consists of a thin coaxial cable with outer and inner conductor diameters of 0.22 cm and 0.51 mm, respectively. The outer conductor is grounded on the back of the plane and the inner conductor is connected to the meander strip at 'a' trhough a small notch at the edge of the slot. The aluminum ground plane has a dimension of 91.5 cm x 91.5 cm. The characteristic impedance Z_c, and the efficiency of this modified self-complementary antenna can be calculated by considering the equivalent network for these antennas suggested by Tai (Appendix B). This method yields a characteristic impedance of $Z_c \simeq 133\ \Omega$ for this structure. The load is constructed from a small ceramic cylinder 6 mm in height covered by a resistive paint. Since this load is not sufficiently small in height, the distance of the meander strip from the plane is more than necessary and this results in the lack of an accurate complementary structure creating some impedance changes over a wide frequency range. In addition, the nature of the load itself deviates from a pure 133 ohm resistor and exhibits a reactive part as the frequency is increased. The impedance of the antenna is shown in Fig. 4.8(b) over a 10:1 bandwidth (0.11 to 1.1 GHz). The locus of a short circuit is also shown on the chart as a reference over the same frequency band. It is seen that the impedance starts from a value of $Z_{in} \simeq 133$ ohms and remains relatively constant in the lower portion of the band. As the frequency increases, a reactive component appears shifting the impedance from its initial value on the chart. The constant impedance property, as anticipated,

is attributed to the formation of the modified self-complementary structure (combination of a strip and the complementary slot) and not to the meander structure. Other complementary structures with similar impedance properties can be constructed. For example, a triangular strip version with excellent impedance properties is reported over a 20:1 bandwidth [71].

Since the meander strip shows a resonant resistance of 9.5 ohms, i.e., $Z_a = 19$ ohms, the efficiency of the self-complementary antenna with this meander strip (N = 2), using (B.5) is found to be only 44 percent. A modified self-complementary antenna with a monopole strip [71,72] has a better gain due to its higher resonant resistance. At frequencies other than resonance, the efficiency becomes lower and lower. To improve the efficiency of the modified self-complementary antennas, one can think of increasing Z_a up to the value of Z_c, but this is equivalent to an increase of the input impedance of the strip. A shift of the feeding point is not a simple task since in that case the slot should be fed differently to preserve the complementary structure. To increase Z_a, one can increase the input impedance of the strip by changing its shape. A monopole strip has a higher resonant resistance than a meander strip but it still can be increased using folded monopoles or folded circular strips.

Generally speaking, the complementary structures, while having good impednace properties, have the disadvantage of low efficiency and the necessity of providing a large plane. In

addition, the pattern of these antennas are disturbed by the finite size of the ground plane.

CHAPTER V. STRUCTURES RELATED TO MEANDER ANTENNAS

Thus far, we were restricted to threefold meander elements which were simply called "meanders." In this chapter other meander antennas without this limitation will be illustrated.

5.1 Fivefold Meander Antennas

The threefold meander antennas discussed in previous chapters were used to reduce the resonant length of a monopole up to approximately 40 percent. For a constant wire radius, more reduction is possible by increasing the separation of the folded arms, w. This method, however, is not acceptable to any degree because of the resulting side effects. Some versions of meander antennas such as fivefold or sevenfold are possible to construct with similar properties. In these versions the size reduction is greater than the previous threefold meanders.

Figure 5.1(a) shows one possible fivefold meander section. The impedance curves for some fivefold meander monopoles made from one, two or three of these sections (N = 4,8,12) are shown in Fig. 5.1(b). The impedance of a monopole of the same length is also given as a reference. The antennas are 6.5 cm in height with a wire diameters, 2a = 0.8 mm and a separation w ≃ 0.25 cm. The experimental data is tabulated in Table 5.1. For small wire separations, w, the approximate radiation resistance, R_{rad}, can be found from the

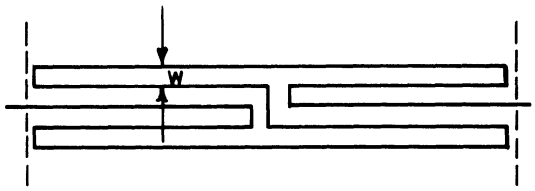

(a) A fivefold meander section.

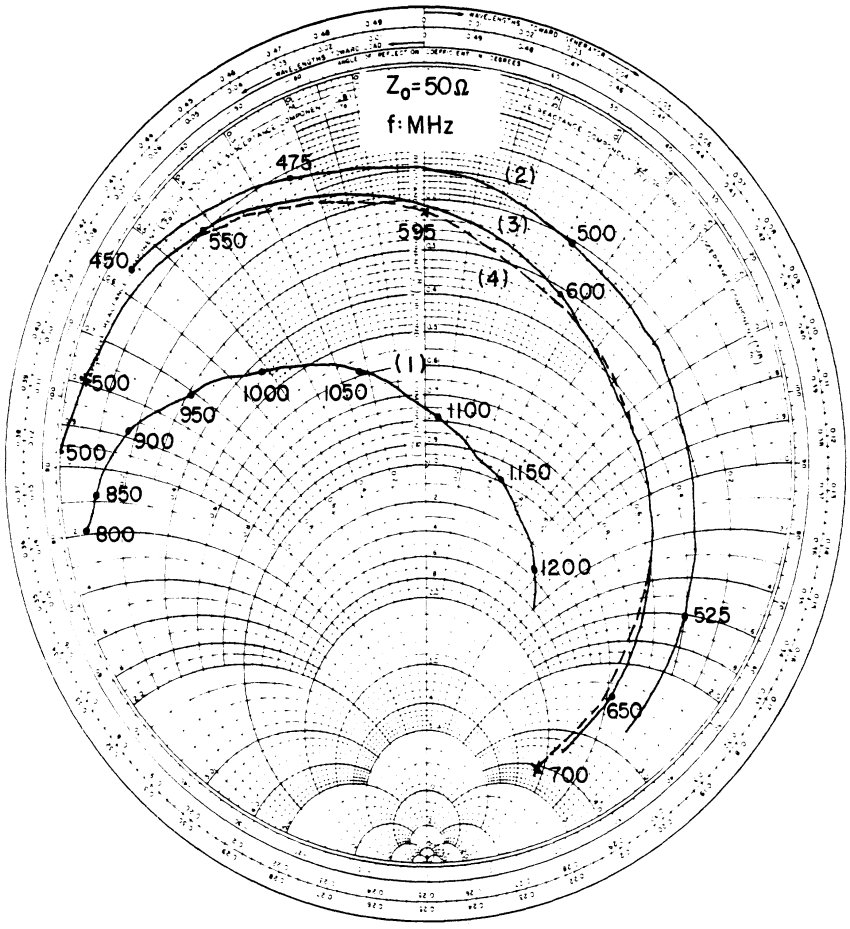

(b) Impedance curves (N = 4,8,12).

Fig. 5.1: A Fivefold Meander Section and the Impedance of the Corresponding Meander Antennas (N = 4,8.12).

Table 5.1

Data Table for Fivefold Meander Antennas with a length, ℓ = 6.5 cm and w $\simeq$ 0.25 cm. A monopole of the Same Length Is Given as a Reference

Antenna Type	N	f_o(MHz)	$\simeq (\Delta f/f_o)$ (%)	β	$R_{res}(\Omega)$	$R_{rad}(\Omega)$
monopole: (1)	-	1095	12.8	1.0	37.5	36.5
meander: (2)	4	488	1.9	0.45	7.2	8
(3)	8	582	3.2	0.53	10.5	11
(4)	12	595	3.6	0.54	11.0	11.5

approximate current distribution (Eq. 2.1) by inserting the appropriate reduction factor. In these structures, the net current is z-directed as in all other meander antennas. From Table 5.1, the characteristics of the fivefold meanders is seen to be similar to the threefold antennas. An increase in N results in an increase in the reduction factor β. The bandwidth is seen to be reduced at the expense of the size reduction. The antennas with a higher number of meander cells have a better bandwidth. The efficiency of the antenna, however, is not affected except for the ohmic losses of the wire.

As an application, a fivefold meander monopole and the corresponding folded version are compared. The N = 4 case is selected. The impedance curves are shown in Fig. 5.2 with the experimental data given in Table 5.2. The first resonance of the meander version of the folded monopole occurs at 523 MHz. This frequency deviates about 7 percent from the expected value of 488 MHz. The resonant resistance of the folded monopole (31.25 ohms) is also in close agreement with the expected value of 28.8 ohm. This example confirms the earlier statement that the characteristics of the meander version of an antenna can be anticipated by the study of a simple meander monopole.

5.2 Other Meander Antennas

5.2.1 Modified Meander Antennas. The antennas presented in the foregoing chapters all had similar geometries with a different number of meander cells per wavelength, N. The

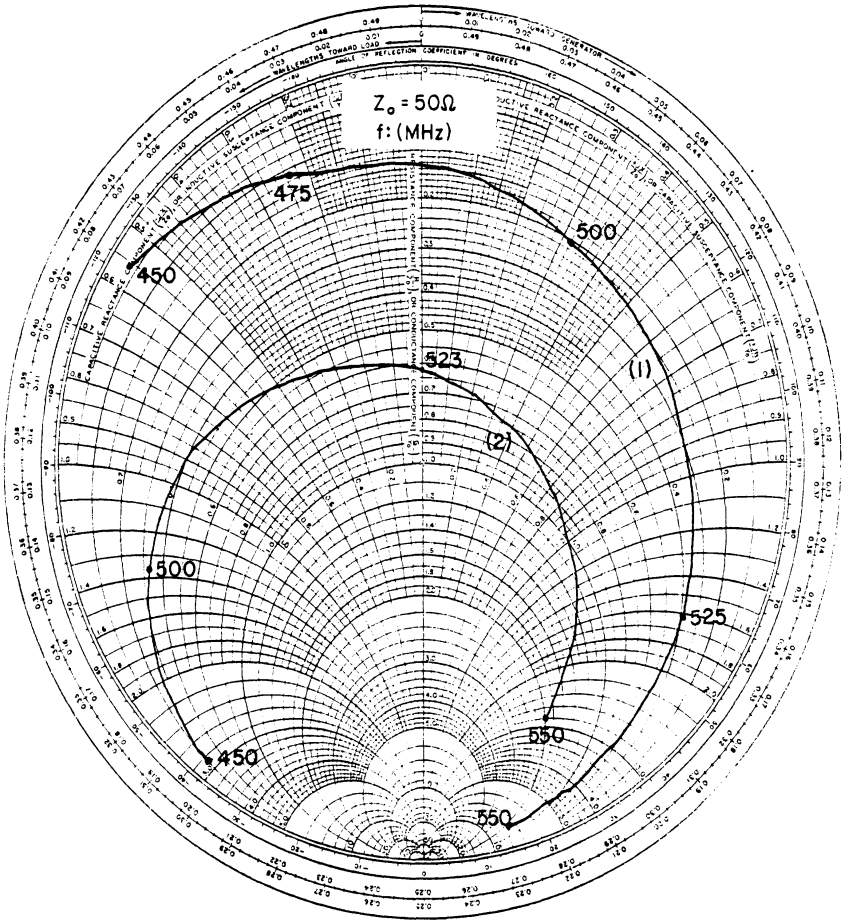

Fig. 5.2: Impedance of the Fivefold Meander Monopole and the Corresponding Folded Monopole Version (N = 4).

Table 5.2

Comparison of a Monopole and a Folded Monopole Made from Fivefold Meander Sections (N = 4)

fivefold meander antenna type	f_o(MHz)	$\simeq(\Delta f/f_o)$ (%)	R_{res} (Ω)
monopole: (1)	488	1.9	7.2
folded monopole: (2)	523	2.2	31.25

geometry of these antennas can be changed, however, without increasing the height of the antenna and yet with different characteristics. This can be achieved by spatial versions of meander antennas. For example, based on the N = 2 meander monopole, which is in fact one half of a meander section, one can build different antenna configurations by changing the relative positions of the folded arms while preserving the same physical length ℓ, and the total wire length L. By twisting the third arm of the antenna about a vertical axis, we can find different spatial antennas (Fig. 5.3a). The antennas shown in Fig. 5.3(b) and (c) are two versions completely placed in the yz plane. Although it seems that a big difference may not exist between these two configurations, the proximity of the two co-directed currents in Fig. 5.3(c) changes the coupling from that of Fig. 5.3(b) and hence the entire picture. Experimental results and numerical analysis both verify the differences between the two structures. These results are summarized in Table 5.3. Both antennas were made from the same wire (2a = 0.8 mm) with ℓ = 4.5 cm, L = 13.5 cm and w less than 0.3 cm (w $\simeq$ 7a). A monopole with L = 13.5 cm, 2a = 0.8 mm and f_0 = 540 MHz is used for calculating the reduction factor. It is clear that a substantial improvement in the reduction factor is obtained by the new N = 2 version in exchange for a lower bandwidth. The bandwidth, according to the experimental results shows a considerable decrease from an approximate value of 2.5 percent to about 1.2 percent. The current distribution at resonance for the two N = 2 meander monopoles (with w = 0.3 cm) are compared in

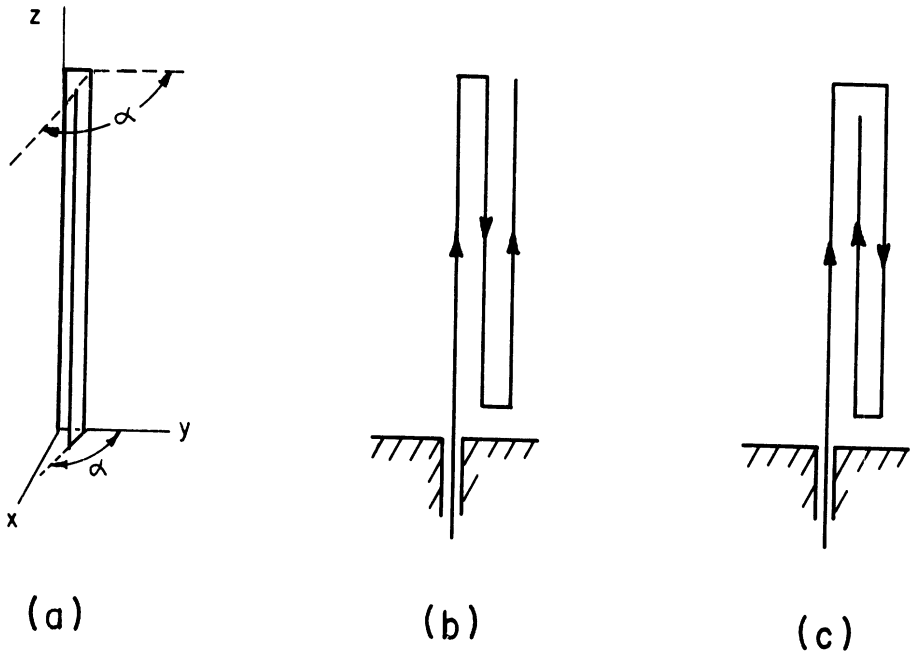

Fig. 5.3: Some Modified Meander Antennas (N = 2).

Table 5.3

Experimental and Numerical Results for Antennas Shown in Fig. 5.3(b) and (c). L = 13.5 cm, ℓ = 4.5 cm and 2a = 018 mm

Antenna type	Experimental			Numerical (w = 0.3 cm)		
	f_o(MHz)	β	R_{res}(Ω)	f_o(MHz)	β	R_{res} (Ω)
N = 2 meander, (1): Fig. 5.3(b)	920	0.57	8.5	918	0.57	11.5
N = 2 meander (2): Fig. 5.3(c)	765	0.47	8.0	794.4	0.49	7.7

Fig. 5.4. The higher input current in the new version is an indication of the decrease in the input resonant resistance. The phase of the new version is almost constant with less fluctuation. The general shape of the current is however about the same with a marked peak near the feeding point. The net current introduced in Chapter III, is contained in the interval $0 \leq z \leq \ell$ and has its greatest magnitude at the feeding point for both antennas (Fig. 5.5).

Preliminary experiments show similarity between the characteristics of the spatial antenna (Fig. 5.3a) and those of Fig. 5.3(b) and (c). An antenna with α = 120 degrees shows a resonant frequency of $f_0 \simeq$ 890 MHz corresponding to a reduction factor of β = 0.55.

5.2.2 Structures Related to Meander Elements. Although meander antennas themselves have a variety of combinations in geometry by changing the number of sections per wavelength N, separation of folded arms w, and even the shape of each meander cell, a variety of other structures related to these antennas can be obtained. These structures offer more flexibility to the antenna characteristics pending the designer's preference. In the previous section we introduced some modified N = 2 antennas with reduction factors, typically in the range of 0.5 to 0.6. By making a partially meander antenna we can adjust for a reduction factor over a wide range up to β = 1. Some of the structures related to the N = 2 meander antenna are shown in Fig. 5.6. The geometry of the antennas shown in Fig. 5.6(a) through (f) can vary from a

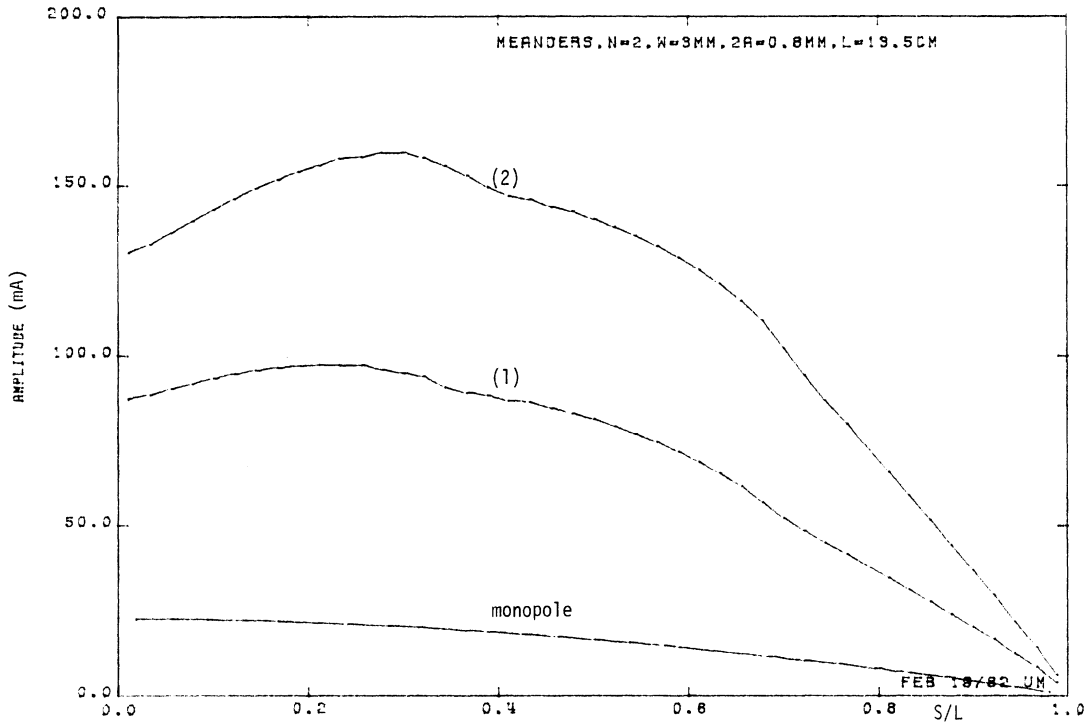

(a) Amplitude.

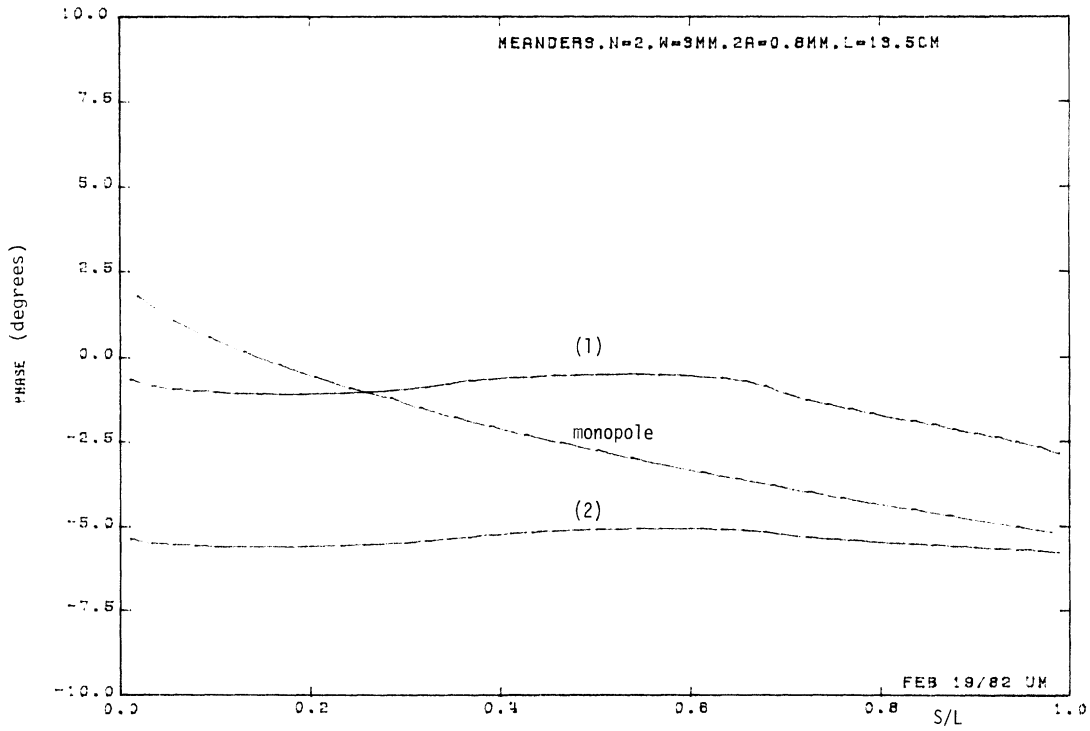

(b) Phase.

Fig. 5.4: Current Distribution for N = 2 Meanders.

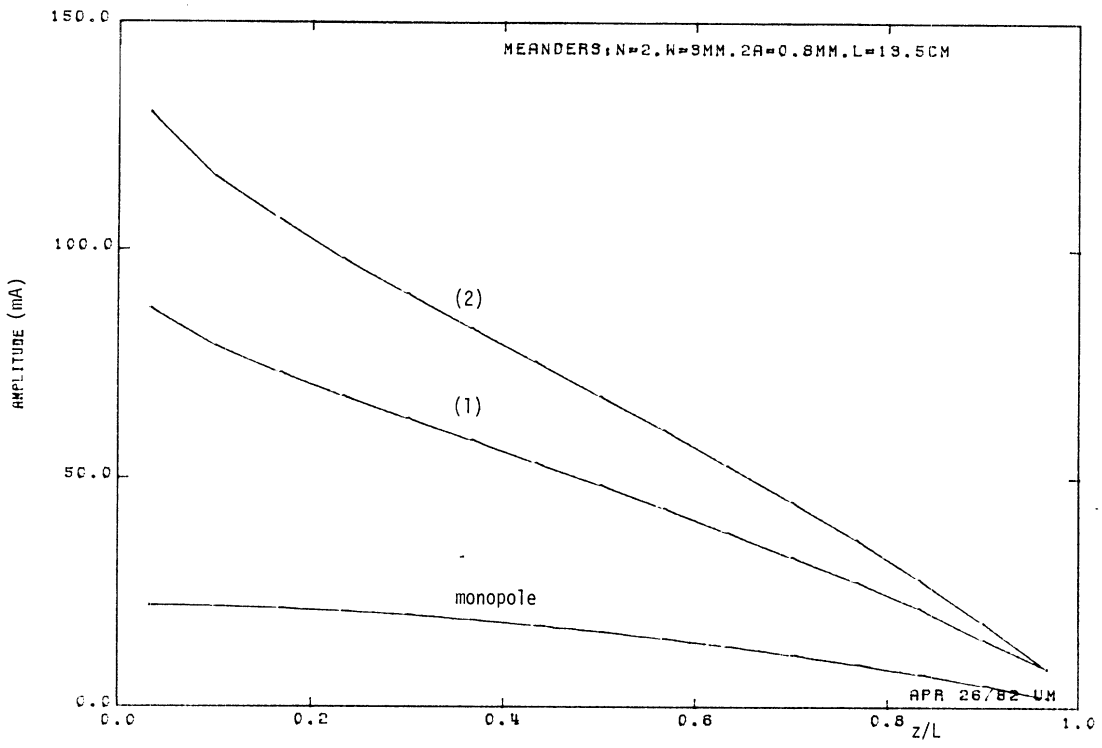

(a) Amplitude.

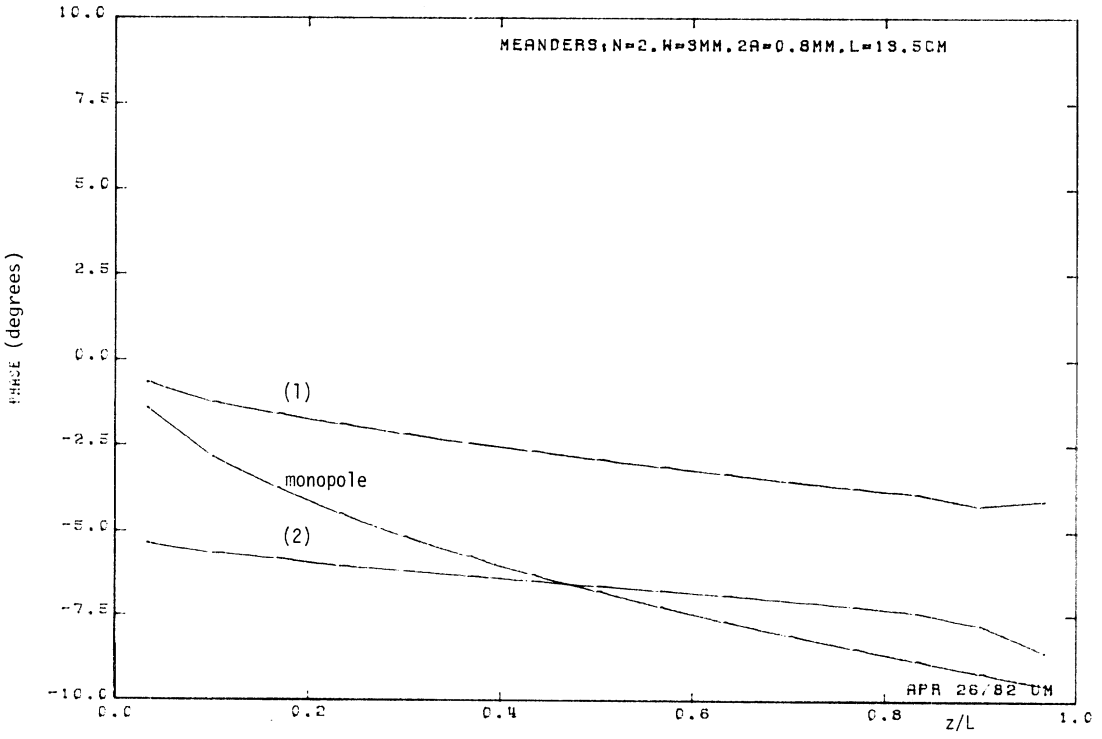

(b) Phase.

Fig. 5.5: Effective Current Distribution for N = 2 Meanders.

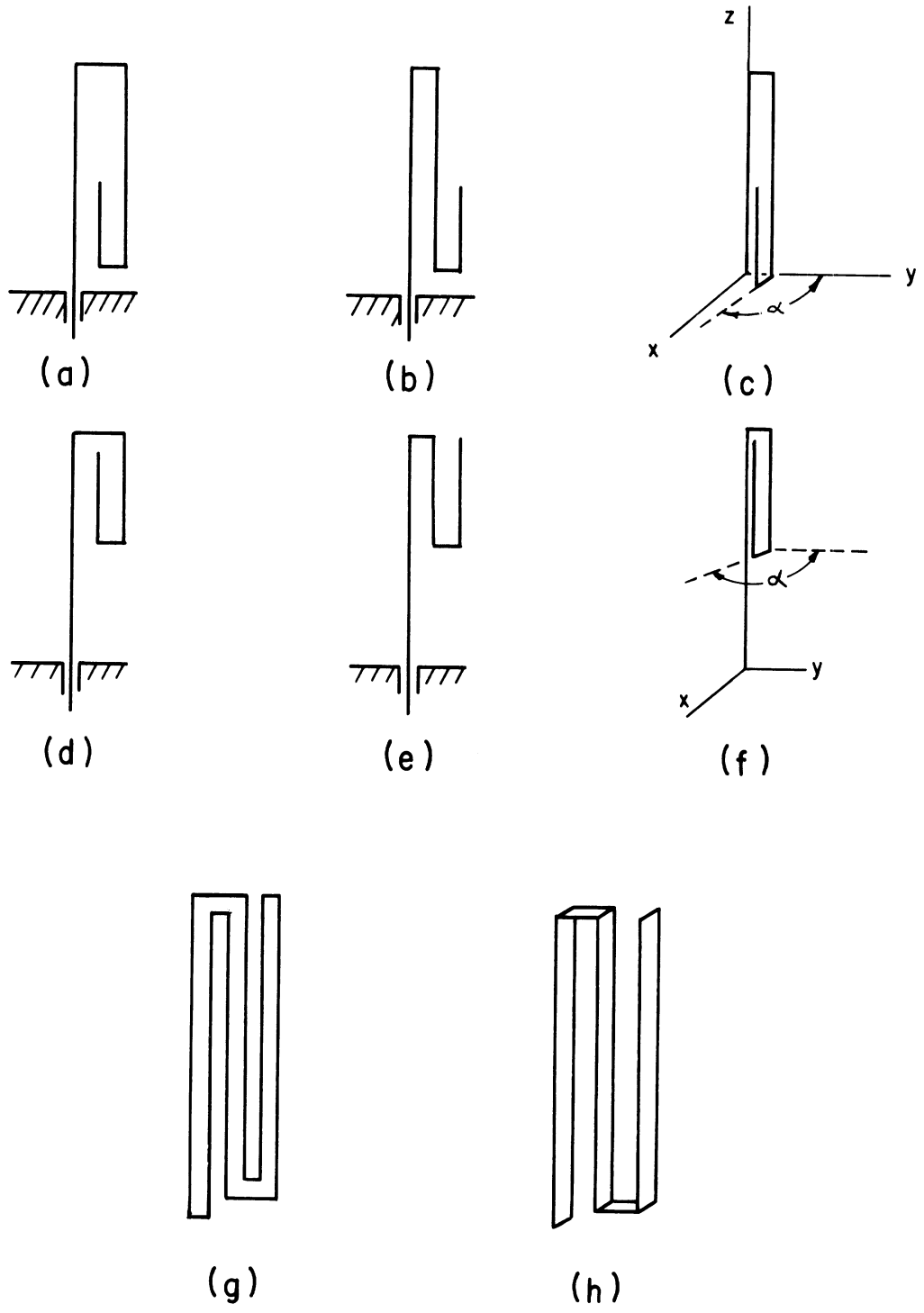

Fig. 5.6: Some Structures Related to N = 2 Meander Antennas.

complete N = 2 meander antenna to a conventional monopole. They presumably have similar properties and their reduction factors depend on the extent of the "meandering" of the antenna. Figure 5.6(a) is reportedly tested with satisfactory results [73]. Two meander strips are shown in Fig. 5.6(g) and (h). These strips can be covered by a dielectric or other materials not only for protection but also for further size reduction. However in this case, losses in the material will decrease the efficiency of the antenna.

When the number of meander cells increases, the number of possible geometries become much higher than the N = 2 case. Each antenna differs from the other because of the different relative position of the folded arms which affects the current distribution along the folded wire.

CHAPTER VI. CONCLUSIONS

Meander antennas introduced during the course of this work have modest size reduction ranging typically from 25 to 50 percent. The efficiency of the antenna is affected only by the ohmic losses in the wire. The bandwidth is generally narrower when compared to a conventional monopole but comparable to that of other size reduction techniques such as base loaded antennas. Since there is very little lateral expansion in a meander antenna, the undesirable radiation is negligible. The effect of increasing the width of the meander cells on the antenna characteristics has been considered both experimentally and numerically. These studies show that when the width of the meander sections w increases, the size reduction improves but at the same time the bandwidth deteriorates. The asymmetry of the radiation pattern is not significant as long as the width of the meander cells are small in comparison to the physical length of the antenna.

The analysis shows that the size reduction also depends on the radius of the wire. When all other dimensions are held constant, a decrease in radius effectively enhances the size reduction.

The number of meander cells per wavelength N has a crucial role in determining the characteristics of a meander antenna. When the number of meander sections increases, the reduction factor increases (which is equivalent to less size reduction) and so does the resonant resistance. The bandwidth of the antenna however improves for

higher values of N. Therefore the antennas with a higher number of sections per wavelength N, (such as N = 4,6 and 10) are preferrable since they are reduced in size and yet maintain favorable characteristics.

The resonant frequency, the resonant resistance and the reduction factor for meander antennas with several different geometries are examined both experimentally and numerically. Close agreement exists between these results. The low resonant resistance can be matched to any desirable impedance level by shifting the feeding point to a point of lower current along the structure.

The current distribution for different meander antennas is obtained and the dependence of the current distribution, as well as the reduction factor and the resonant resistance on the wire radius and the separation of the wires is studied. It is observed that the current distribution on a meander antenna is different from that of a conventional monopole with a marked peak near the feeding point while the phase of the current remains relatively constant.

Meander antennas introduce a moderate size reduction in the resonant length and can be used in the existing wire antennas especially large arrays with long elements. Log-periodic dipole arrays and folded monopoles using meander elements have been investigated experimentally with satisfactory results as an illustration of the application.

On the basis of these studies, other meander antennas are also suggested with similar characteristics. These antennas range

from partial meandering of the wire to a complete folded version. The possibility of using an antenna with meander cells, different in both length and shape greatly increases the number of possible combinations. For example, some structures such as fivefold meander antennas are examined for even further reduction in size. This miniaturization can be achieved at the expense of the bandwidth reduction.

Similar to all other size reduction methods, this technique has its own limitations if miniaturization is attempted to a great degree [74]. For modest size reductions, however, the method can be used successfully in the existing wire antennas.

For further study, the effects of a dielectric coating on the antenna characteristics and the improvement of the bandwidth for lower reduction factors can be investigated. Meander slots and their characteristics can be studied in conjunction with meander antennas.

APPENDICES

APPENDIX A. THE DESIGN OF LPDA AND LPMDA

From the standard constant directivity contours [75], a scaling factor, $\tau = 0.865$ and a spacing factor, $\sigma = 0.16$ are selected for a 9 dB directivity. Figure A.1 shows the terminology of the LPDA in which we have

$$\tau = \frac{R_{i+1}}{R_i} = \frac{L_{i+1}}{L_i} = \frac{d_{i+1}}{d_i} \qquad (A.1)$$

and

$$\sigma = \frac{d_i}{4L_i} = \frac{1 - \tau}{4 \tan \alpha} \quad . \qquad (A.2)$$

Following Smith [63], we find:

Half angle of the structure, $\alpha = 12$ degrees,

Boom length (the feeder length) = 12.57 cm

Length of the longest element, $2L_1 = 7.47$ cm

Distance of the longest element to the apex, $R_1 = 17.7$ cm

Number of element, N = 10

E-plane beamwidth > 50 degrees

The half length of all other dipoles, $L_2, L_3, \ldots$, and their distance from the virtual apex can be readily obtained from

$$L_n = \tau^{n-1} L_1 \qquad (A.3)$$

and

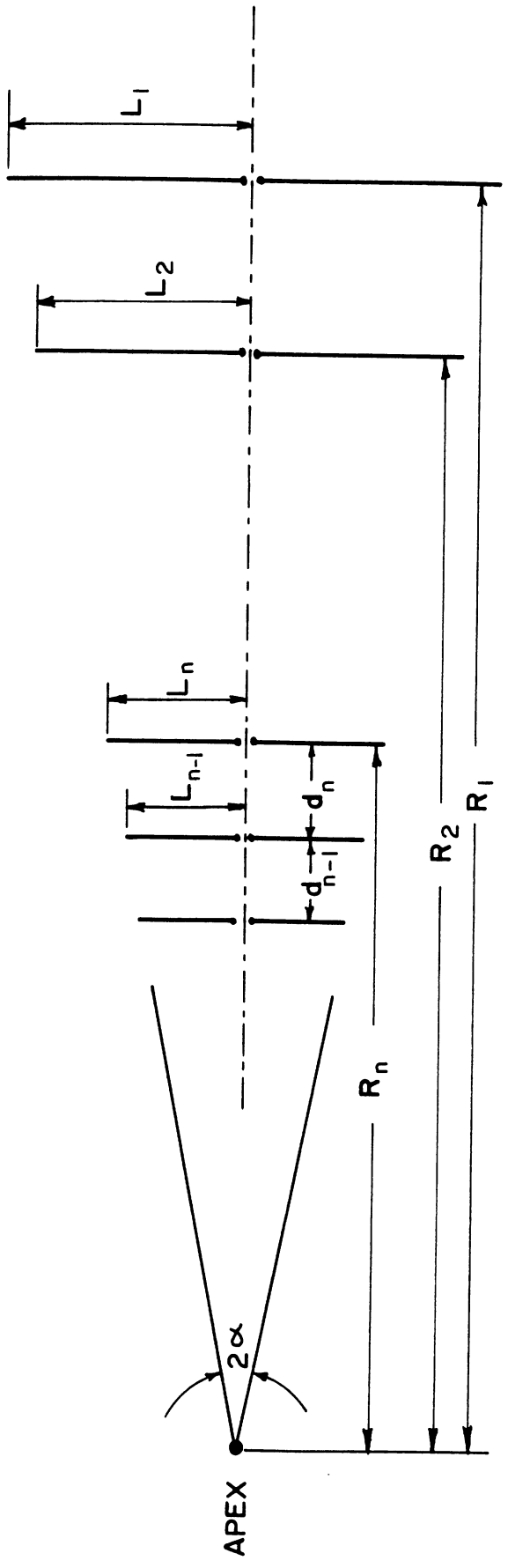

Fig. A.1: A Log-Periodic Dipole Array.

$$R_n = \frac{4\sigma}{1-\tau} L_1 , \quad (n = 2,3,\ldots,10) . \quad (A.4)$$

To find an input resistance of $R_o \simeq 50\ \Omega$ for the antenna, an average value of L/a = 75 for the elements is assumed, where a(= 0.31 mm) is the radius of the elements.

The average characteristic impedance, Z_a of the elements, is given by [76]

$$Z_a = 120 \left(\ell n \frac{L}{a} - 2.25\right) . \quad (A.5)$$

The characteristic impedance of the unloaded feeder, Z_o is therefore obtained to be 57.8 ohm from [75]

$$R_o = Z_o \left(1 + \frac{Z_o}{4\sigma Z_a}\right)^{-1/2} \quad (A.6)$$

or equivalently,

$$Z_o = \frac{R_o^2}{8\sigma Z_a} + \sqrt{1 + \frac{R_o^2}{(8\sigma' Z_a)}} , \quad (A.7)$$

where σ' is the mean spacing factor given by

$$\sigma' = \frac{\sigma}{\sqrt{\tau}} . \quad (A.8)$$

For the antenna to be fed from a balanced system, the inner conductor of a coaxial cable is connected to the outer conductor at the high frequency side producing a balanced feeding system with a conductor diameter, 2b = 0.22 cm and a separation s = 0.36 cm to produce the desired characteristic impedance, $Z_o \simeq 57.8\ \Omega$ for the unloaded feeder. With this value, the impedance curve will cluster around the approximate expected value of $R_o \simeq 50\ \Omega$.

A simple graphical method for finding the length of the elements and their spacing, is shown in Fig. A.2. In this figure the angle ϕ is obtained from

$$\tan \phi = \frac{d_n}{L_n} = \frac{1 - \tau}{\tan \alpha}$$

$$= 4\sigma .$$

Hence

$$\phi = \tan^{-1} 4\sigma \quad . \tag{A.9}$$

Having the angle ϕ to be 32.6 degrees in our example, we construct the angle α = 12 degrees and find the point A where the perpendicular line A_1O_1 is the length of the longest monopole and AO_1 is its distance from the apex. Constructing the angle ϕ on A_1O_1 and following the direction of the arrow the length of all other elements, A_2O_2, A_3O_3 and their spacing, O_1O_2, O_2O_3,..., can be readily obtained. This process continues until the number of dipole elements, N, is completed.

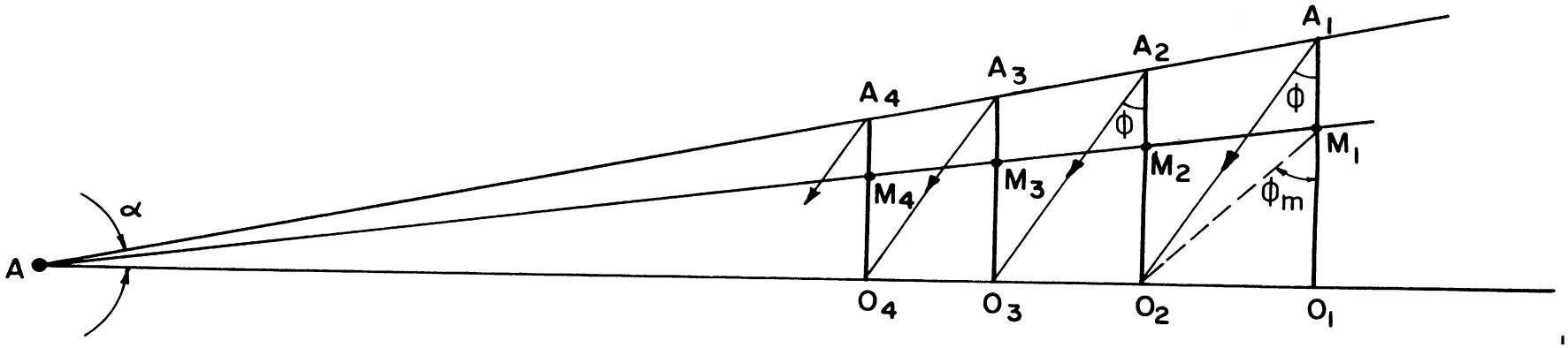

Fig. A.2: A Graphical Method for Finding the Length and the Position of the Array Elements.

A line emanating from the virtual apex and dividing one of the dipoles by a ratio of β to one, gives the length of the meander versions, $O_1M_1, O_2M_2, \ldots$. The angle ϕ_m corresponding to the meander version is,

$$\phi_m = \tan^{-1} \frac{4\sigma}{\beta} \quad . \tag{A.10}$$

APPENDIX B. THE EQUIVALENT NETWORK OF THE COMPLEMENTARY ANTENNAS

The input impedance and the efficiency of the self-complementary antennas based on their equivalent circuits are discussed by Tai [77].

The voltages and currents in a two-port symmetrical network made of passive antennas (Fig. B.1a) can be decomposed into two pairs such that

$$V_1 = V_a + V_b \quad , \quad I_1 = I_a + I_b \quad , \tag{B.1}$$

$$V_2 = V_a - V_b \quad , \quad I_2 = I_a - I_b \quad . \tag{B.2}$$

This decomposition is shown in Fig. B.1(b).

We now define two active impedances Z_a and Z_b:

$Z_a = (V_a/I_a)$ = symmetrical impedance,

$Z_b = (V_b/I_b)$ = anti-symmetrical impedance.

Based on these definitions, an equivalent circuit for the original symmetrical network is shown in Fig. B.1(c). In the general case, if Z_a and Z_b are linearly proportional to the input impedances Z_d and Z_s of an arbitrary strip and its complementary slot respectively, then $Z_a = mZ_d, Z_b = nZ_s$, and according to Booker's relation [66]

$$Z_a Z_b = \frac{mn}{4} \eta^2 \quad . \tag{B.3}$$

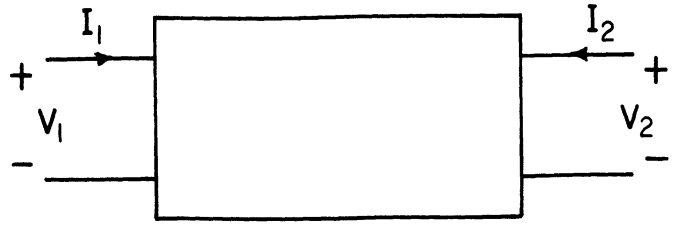

(a) A Two-Port Network.

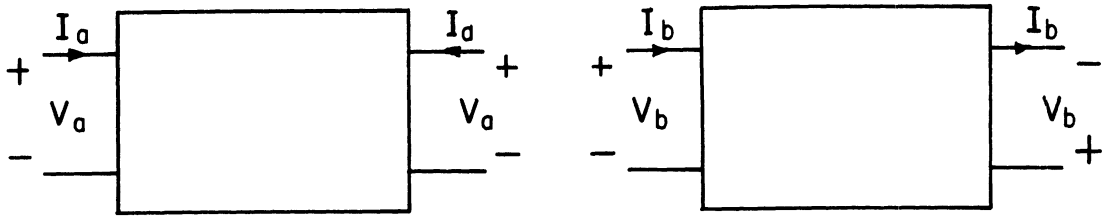

(b) Symmetrical and Antisymmetrical Decomposition.

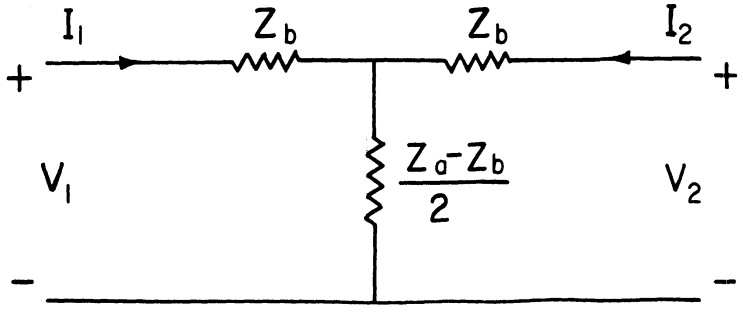

(c) Equivalent Network.

Fig. B.1: The Equivalent Networks for a Two-Port Symmetrical Network.

It can be readily shown that if a load impedance Z_ℓ is selected in Fig. B.1(c) such that

$$Z_\ell = \frac{1}{2} \sqrt{mn}\, \eta$$

then we also will have,

$$Z_{in} = \frac{1}{2} \sqrt{mn}\, \eta \qquad \text{(B.4)}$$

which is the characteristic impedance of the antenna denoted by Z_c. When a self-complementary antenna is terminated by Z_c is has a constant input impedance, $Z_{in} = Z_c$. The radiation efficiency in the transmitting mode can be found from the equivalent network. The result is

$$\eta = 1 - \left| \frac{Z_a - Z_c}{Z_a + Z_c} \right|^2 \quad . \qquad \text{(B.5)}$$

The same factor is present in the receiving cross section of a self-complementary antenna when it is operated in the receiving mode.

For the modified self-complementary antenna with the meander monopole strip (Fig. 4.6) we have, m = 1 and n = 1/2. The characteristic impedance, Z_c, of the antenna is therefore equal to $30\, \pi\, \sqrt{2}\ \Omega \simeq 133\ \Omega$.

REFERENCES

LIST OF REFERENCES

1. Brown, G. H., "A Critical Study of the Characteristics of Broadcast Antennas as Affected by Antenna Current," Proc. of IRE, Vol. 24, No. 1, January 1936, pp. 48-81.
2. Williams, H. P., Antenna Theory and Design, Vol. II, Chapters II and III, Sir Isaac Pitman and Sons, Ltd., London, 1950.
3. Wells, N., "Aerial Characteristics," Journal of IEE, Vol. 89, Part III, 1942, pp. 76-95.
4. Pierce, G. W., Electric Oscillations and Electric Waves, Chapter IX, New York: McGraw-Hill, 1920.
5. Josephson, B., "The Quarter Wave Dipole," 1957 IRE WESCON Convention Record, Vol. 1, Part 1, August 1957, pp. 77-90.
6. King, R.W.P., The Theory of Linear Antennas, Harvard University Press, MA., 1958.
7. Prasad, S., King, R.W.P., "Experimental Study of Inverted L-T-, and Related Transmission-Line Antennas," Journal of Res., NBS, Vol. 65D, No. 5, September-October, 1961, pp. 449-454.
8. Kitsuregawa, T., Takeichi, Y. and Mizusowa, M., "A One-Eighth-wave Broadband Folded Unipole Antenna," Proc. of Symp., at Copenhagen, Denmark, June 1962, Electromagnetic Theory and Antennas, Part 2, Jordan, E. C., Editor, pp. 1201-1205.

9. Harrison, C. W., "Monopole with Inductive Loading," IEEE Trans. on Antennas and Propagation, Vol. AP-11, No. 4, July 1963, pp. 394-400.

10. King, R.W.P., Mimno, H. R., Wing, A. H., Transmission Lines, Antennas and Wave Guides, Chapter II, Dover Publications, New York, 1965.

11. Czerwinski, W. P., "On optimizing efficiency and bandwidth of inductively loaded antennas," IEEE Trans. on Antennas and Propagation, Vol. AP-13, pp. 811-812, September 1965.

12. Fujimoto, K., "A loaded antenna system applied to VHF Portable Communication Equipment," IEEE Trans. Vehicular Technology, Vol. VT-17, pp. 6-12, October 1968.

13. Simpson, T. L., "The Theory of Top-Loaded Antennas: Integral Equation for the Currents," IEEE Trans. on Antennas and Propagation, Vol. AP-19, No. 2, March 1971, pp. 186-190.

14. Hansen, R. C., "Efficiency and Matching Tradeoffs for Inductively Loaded Short Antennas," IEEE Trans. on Communication, Vol. COM-23, No. 4, April 1975, pp. 430-435.

15. Do-Boi-Hoan, "Efficiency Improvement Computation of HF Short Ground Antennas Provided with Inductive Loading," International Conference on Antennas and Propagation, London 1978, Part 1, Antennas, pp. 345-349.

16. ARRL, The A.R.R.L. Antenna Book, 11th Ed., The American Radio Relay League, pp. 59-66; 292-296, Newington, Connecticut, 1968.

17. Altschuler, E. E., "The Traveling-Wave Linear Antenna," IRE Trans. on Antennas and Propagat., Vol. AP-9, pp. 324-329, July 1961.

18. Wu, T. T., King, R.W.P., Correction to "The Cylindrical Antenna with Nonreflecting Resistive Loading," IEEE Trans. on Antennas and Propagation, Vol. AP-13, p. 998, November 1965.

19. Motohisa Kanda, "The Characteristics of a Relatively Short Broadband Linear Antenna with Tapered Resistive Loading," Digest of International Symposium, Antennas and Propagation Society, pp. 230-234, Stanford Univ., Stanford, CA, 1977.

20. Grimes, D. M., "A Resonant Miniaturized Antenna," Technical Memorandum No. 45, Engineering Research Institute, The University of Michigan, Ann Arbor, June 1957.

21. James, J. R., Burrows, R. M., "Resonance Properties of Dielectric-Loaded Short Unipoles," Electronics Letters, Vol. 9, No. 14, pp. 300-302, July 1973.

22. James, J. R., Schuler, A. J., Binham, R. F., "Reduction of Antenna Dimensions by Dielectric Loading," ibid., Vol. 10, No. 13, pp. 263-265, June 1974.

23. James, J. R., Henderson, A., "Electrically Short Monopole Antennas with Dielectric or Ferrite Coatings," Proc. IEE, pp. 793-803, September 1978.

24. James, J. R., Henderson, A., "Investigation of Electrically Small VHF and HF Cavity-Type Antennas," International Conference on Antennas and Propagation, Part 1, pp. 322-326, London, 1978.

25. Wilson, W. R., "A Solenoid-Whip Aerial," Electronics, Vol. 14, pp. 56-64, January 1941.

26. Czerwiski, W. P., "On a Foreshortened Center-Fed Whip Antenna," IEEE Trans. Vehicular Comm., Vol. VC-15, pp. 33-39, October 1966.

27. Wheeler, H. A., "A Helical Antenna for Circular Polarization," Proc. IRE, Vol. 35, pp. 1484-1488, December 1947.

28. Li, T., "The Small-Diameter Helical Antenna and Its Input Impedance Characteristics," Ph.D. Dissertation, Northwestern University, Evanston, Illinois, June 1958.

29. Li, T., Beam, R. E., "Helical Folded Dipoles and Unipoles," Proc. NEC, Vol. 13, pp. 89-105; 1947.

30. Kandoian, A. G., Sichak, W., "Wide-Frequency-Range Tuned Helical Antennas and Circuits," IRE National Convention Record, Part 2, pp. 42-47, 1953.

31. Moore, R. A., Beam, R. E., "Small Antenna Arrays Utilizing Distributed Loading," WESCON, Technical Papers, Part 1/ Antennas, August 1963.

32. Stephenson, D. T., Mayes, P. E., "Log-Periodic Helical Dipole Arrays," ibid, August 1963.

33. Chatterjee, J. S., Roy, M. N., "Helical Log-Periodic Array." IEEE Trans. Antennas and Propagation, Vol. AP-16, pp. 592-593, September 1968.

34. Roy, M. N., Das, G. C., "Design of Two New Types of Plane-Polarized Log-Periodic Dipole Antennas," International Conference on Antennas and Propagation, Part 1, pp. 336-340, London, 1978.

35. Elfving, C. T., "Foreshortened Log Periodic Dipole Array," WESCON, Technical Papers, Part 1/Antennas, August 1963.

36. DiFonzo, D. F., "Reduced Size Log Periodic Antennas," Microwave Journal, Vol. 7, No. 12, pp. 37-42, December 1964.

37. Kuo. S. C., "Size-Reduced Log-Periodic Dipole Array Antenna," ibid., Vol. 15, No. 12, pp. 27-33, December 1972.

38. Roland, E. T., Patterson, W. F., "A Slow-Wave Flat Spiral Antenna," prepared for the Seventeenth USAF Antenna Symp., Monticello, Illinois, November 1967.

39. Hong, S., Rassweiler. G., "Size Reduction of a Conical Log-Spiral Antenna by Loading with Magneto-Dielectric Material," IEEE Trans. Antennas and Propagat., Vol. AP-14, No. 5, pp. 650-651, September 1966.

40. Anders, R. W., Wohlleben, R., "Phase Velocity on a Conical Two-Armed Logarithmic Foil-Type Spiral Antennas," ibid, Vol. AP-17, No. 2, pp. 233, 234, March 1969.

41. Storer, J. E., King., R., "Radiation Resistance of a Two-Wire Line," Proc. of IRE, pp. 1408-1412, November 1951.

42. Tai, C. T., "The Theory of Terminated Folded Monopole," Technical Report, RL 698, Radiation Laboratory, The University of Michigan, Ann Arbor, MI., August 1981.

43. Poggio, A. J., Miller, E. K., "Integral Equation Solutions of Three-Dimensional Scattering Problems," Chapter 4, Computer Techniques for Electromagnetics, ed. R. Mittra, Pergamon Press, New York, 1973.

44. Tai, C. T., "Eigen Function Expansion of Dyadic Green's Function in Electromagnetic Theory," Math. Notes No. 28, Weapons Laboratory, Kirtland Air Force Base, Albuquerque, NM, 1973.

45. Hallén, E., "Theoretical Investigations into the Transmitting and Receiving Qualities of Antennas," Nova Acta, Royal Society of Sciences of Uppsala, Ser. IV, Vol. 11, No. 4, pp. 1-44, November 1938.

46. Tai, C. T., "A New Interpretation of the Integral Equation Formulation of Cylindrical Antennas," IRE Trans. on Antennas and Propag., Vol. AP-3, pp. 125-127, July 1955.

47. Richmond, J. H., "Digital Computer Solutions of the Rigorous Equations for Scattering Problems," Proc. of IEEE, Vol. 53, No. 8, pp. 796-804, August 1965.

48. King, R.W.P., "The Linear Antennas--Eighty Years of Progress," Proc. of IEEE, Vol. 55, No. 1, pp. 2-16, January 1967.

49. Mei, K. K., "On the Integral Equations of Thin Wire Antennas," IEEE Trans. on Antennas and Propagat., Vol. AP-13, No. 3, pp. 374-378, May 1965.

50. Harrington, R. F., "Matrix Methods for Field Problems," Proc. of IEEE, Vol. 55, No. 2, pp. 136-149, February 1967.

51. Harrington, R. F., Field Comptuation by Moment Methods, Macmillan, New York, 1968.

52. Wu, C. P., "Variational and Iterative Methods for Waveguide and Arrays," Chapter 5, Computer Techniques for Electromagnetics, ed. R. Mittra, Pergamon Press, New York, 1973.

53. Anders, R., "Criteria for the Choice of Optimal Basis Functions," International Conference on Antennas and Propagation, Part 1, pp. 170-173, London, 1978.

54. Wilton, D. R., Glisson, A. W., "Some Recent Developments in the Numerical Modeling of Wires and Surfaces," ibid, pp. 179-183.

55. Yeh, Y. S., Mei, K. K., "Theory of Conical Equiangular-Spiral Antennas Part I-Numerical Technique," IEEE Trans. on Antennas and Propagat., Vol. AP-15, No. 5, pp. 634-639, September 1967.

56. Neureuther, A. R. et al., "A Comparison of Numerical Methods for Thin Wire Antennas," presented at the 1968 Fall URSI Meeting.

57. Poggio, A. J., Mayes, P. E., "Numerical Solution of Integral Equations of Dipole and Slot Antennas Including Active and Passive Loading," Tech. Report AFAL-TR-69-180, University of Illinois, Antenna Lab., August 1969.

58. Burke, G. J., Poggio, A. J., "Numerical Electromagnetic Code (NEC)--Method of Moments," Parts I and III, Technical Document 116, Naval Ocean Systems Center, Revised January 1980, California.

59. Adams, R. W., Poggio, A. J., Miller, E. K., "Study of a New Antenna Source Model," UCRL-51693, Lawrence Livermore Laboratory, CA, October 28, 1974.

60. Poggio, A. J., Adams, R. W., "Approximations for Terms Related to the Kernel in Thin-Wire Integral Equations," UCRL-51985, Lawrence Livermore Laboratory, CA, December 19, 1975.

61. Isbell, D. E., "Log-Periodic Dipole Arrays," IRE Trans. on Antennas and Propagat., Vol. AP-8, pp. 260-267, May 1960.

62. DuHamel, R. H. and Isbell, D. E., "Broadband Logarithmically Periodic Antenna Structures," IRE National Convention Record, Part I, pp. 119-128, 1957.

63. Smith, C. E., Editor, Log Periodic Antenna Design Handbook, Smith Electronics Inc., Ohio, 1966.

64. Rumsey, V. H., "Frequency Independent Antennas," IRE National Convention Record, Part I, pp. 114-118, 1957.

65. Mittra, R., Jones, K. E., "On Continuously Scaled and Log-Periodic Structures," Technical Report No. 73, Contract No. AF33(657)-10474, Antenna Laboratory, University of Illinois, September 1963.

66. Booker, H. G., "Slot Aerials and Their Relation to Complementary Wire Aerials (Babinet's Principle)," Journal of IEE (London), Vol. 93, Part IIIA, pp. 620-626, April 1946.

67. Uda, S. and Mushiake, Y., "The input impedance of a slit antenna," Technical Report, No. 1, Vol. XIV, Technology Reports, Tohoku University, Sendai, Japan, 1949.

68. Ishizone, T., Mushiake, Y., "A Self-Complementary Antenna Composed of Notch Antenna," Digest of International Symposium, Antenna and Propagation Society, Stanford University, 1977.

69. Inagaki, N., Isogai, Y. and Mushiake, Y., "Ichimatsu Moyou Antenna-Self-Complementary Antenna with Periodic Feeding Points," The Transaction of IECE of Japan, Vol. E62, No. 4, pp. 267-268, April 1979.

70. Mushiake, Y. and Saito, H., "On three-dimensional self-complementary antennas," Joint Conference of Electrical Engineering of Japan, p. 1212, 1963 (in Japanese).

71. Ishizone, T., Kasahara, T. and Mushiake, Y., "Modified Two Planes Self-Complementary Antennas and Propagation, Summary of Papers," International Symposium on Antennas and Propagat., pp. 145-148, Sendai, Japan, 1978.

72. Ishizone, T. and Mushiake, Y., "The gain of modified self complementary antennas consisting of unipole and a slot," Proc. of the National Conference on Optics and Electromagnetic Waves, p. 54, IECE of Japan, 1978 (in Japanese).

73. Dilley, D. M., "NOSC Wideband VHF Whip Antenna," Technical Report 299, Naval Ocean Systems Center, September 1978, California.

74. Hansen, R. C., "Microminiature Antennas," Microwave Journal, Vol. 9, No. 7, July 1966, pp. 22 and 24.

75. Carrel, R. L., "The Design of Log-Periodic Dipole Antennas," IRE International Convention Record, Part 1, pp. 61-75, 1961.

76. Jordan, E. C., Balmain, K. G., Electromagnetic Waves and Radiating Systems, N.J. Prentice-Hall, 1968.

77. Tai, C. T., Private Communication.